



FACULTY OF SCIENCE AND TECHNOLOGY

MASTER THESIS

Study programme / specialisation:

Marine and Offshore Technology

The spring semester, 2022

Author:

Laksri Tharanga Jayathilake
Jayathilake Hitihami Appuhamilage

Open / ~~Confidential~~

.....
(signature author)

Course coordinator: Prof. Yihan Xing

Supervisor(s): Prof. Daniel Karunakaran

Thesis title:

Parametrization of Steel Lazy Wave Riser Configuration for Fatigue Considerations
at the Touch Down Point

Credits (ECTS): 30

Keywords:

Santos Basin, Offshore Brazil
Deepwater, FPSO, Parametric Study,
Steel Lazy Wave Riser (SLWR),
Fatigue Analysis, Fatigue Life,
Touch Down Point (TDP)

Pages: 125

+ appendix: 37

Stavanger, 14th June 2022
date/year

Parametrization of Steel Lazy Wave
Riser Configuration for Fatigue
Considerations at the Touch Down Point

by

Laksri Jayathilake

Master Thesis

Marine and Offshore Technology



subsea 7

Department of Mechanical and Structural Engineering and Materials Science

Faculty of Science and Technology

University of Stavanger

June 2022

Abstract

With the advancement of technologies, deepwater oil and gas exploration has shown promising results worldwide. Production risers are integral in offshore hydrocarbon exploration because they transfer oil and gas from the subsea wells to the topsides. Steel Catenary Riser (SCR) is a favourable riser solution for deepwater developments due to its low cost and less complexity in implementation. With the increasing water depths and large floater motions, SCR has raised major concerns about fatigue performance at the touch down zone (TDZ). This can be solved by introducing buoyancy modules to the SCR, forming the Steel Lazy Wave Riser (SLWR) configuration. SLWR has shown better fatigue performance near the TDZ due to their ability to decouple vessel motion from TDZ.

The initial phase of the thesis presents static, dynamic and fatigue analysis and design of an SLWR connected to a Floating Production and Storage and Offloading (FPSO) vessel in 2000m water depth in Santos basin in Offshore Brazil. The riser has an internal diameter of 254mm and a wall thickness of 25mm and is made of API 5L X65 Carbon steel with a coating thickness of 70mm. Analyses are performed using OrcaFlex software, and the design is based on Load Resistance Factor Design (LRFD) guidelines as per DNV-OS-F201: Dynamic Risers.

The latter part of the thesis presents the parametric study on fatigue life near the Touch Down Point (TDP) for different SLWR configurations. Four different water depths (1500m, 2000m, 2500m, 3000m) and two different coating thicknesses (70mm: production riser, 3mm: injection riser) are considered, creating eight different scenarios. Each scenario considers 25 different SLWR configurations by changing the riser's wave height (D_B : distance between sag bend and hog bend) and distance from sag bend to the seabed (D_S). In total, 200 different SLWR configurations are analysed during the research. Results show that fatigue life always increases with the increase of D_B value irrespective of the D_S value, water depth and coating thickness. In contrast, increasing the D_S value does not always yield high fatigue life, and the rate of fatigue life change is marginal.

Keywords: Santos Basin, Offshore Brazil, Deepwater, FPSO, Steel Lazy Wave Riser (SLWR), Parametric Study, Fatigue Analysis, Fatigue Life, Touch Down Point (TDP)

Preface and Acknowledgements

This thesis is a partial requirement of the Master Programme in Marine and Offshore Technology at the Department of Mechanical and Structural Engineering and Material Science, Faculty of Science and Technology, University of Stavanger.

First, I would like to extend my sincere gratitude to Professor Daniel Karunakaran for allowing me to write the thesis under his guidance. His continuous guidance pushed me in the right direction to successfully complete the thesis. I am thankful to Subsea7 AS Stavanger for providing me with the necessary resources to carry out my thesis work on their premises. I also appreciate the support given by everyone at the Hydrodynamics and Ocean Technology Group and the Pipeline Group at Subsea7. A big thank goes to Vinicius Vileti and Danilo Lima at Subsea7 Brazil for their continuous support throughout the thesis. My sincere gratitude goes to Adekunle Peter Orimolade at Subsea7 Norway for his support during the period.

A big thank goes to my good friends at UiS, Andre Eltervaag and Anuraj Karuvathil, for motivating me to complete the thesis on time. I am thankful to Professor Sudath Siriwardane for giving valuable advice while writing the thesis. I would also remind my thesis colleagues from UiS, Marina Silva and Jonathan Byman, for sharing their knowledge with me during the thesis work. Finally, I would like to thank my wife, Sachini and my whole family for standing tall all the time to see me achieve goals in life.



.....
Laksri Jayathilake

On 14th June 2022 at Stavanger, Norway

Table of Contents

Abstract.....	i
Preface and Acknowledgements	ii
Table of Contents	iii
List of Abbreviations	viii
List of Figures.....	x
List of Tables	xiii
1 Introduction.....	1
1.1 Background.....	1
1.2 Research Objective	3
1.3 Scope and the Structure of the Thesis.....	3
1.4 Limitations	4
2 Platform Selection for Deepwater Developments	5
2.1 Introduction.....	5
2.2 Deepwater Floating Platforms	6
2.2.1 Floating Production Storage and Offloading vessels (FPSO).....	6
2.2.2 Semi-submersible platforms (SS)	7
2.2.3 Tensioned Leg Platforms (TLP)	8
2.2.4 Spar Platforms.....	8
2.3 Drivers for Platform Selection	9
2.3.1 Reservoir Depletion Drivers	9
2.3.2 Regional Drivers	10
2.3.3 Business Drivers	11
2.4 Selection of FPSO Concept for the Research	11
3 Deepwater Riser Systems	13
3.1 Classification of Risers	13

3.1.1	Top Tensioned Risers (TTR)	13
3.1.2	Compliant Riser	13
3.1.3	Hybrid Riser.....	15
3.2	Riser Material Selection.....	16
3.2.1	Flexible Risers	16
3.2.2	Rigid Risers.....	18
3.3	Production Risers	18
3.3.1	Steel Catenary Riser Configuration (SCR).....	19
3.3.2	Steel Lazy Wave Riser Configuration (SLWR).....	20
3.3.3	Initial Static State Solution for SLWR Configuration	21
3.4	Selection of SLWR over SCR for Deepwater Applications	23
4	Codes and Standards for Riser Design	27
4.1	Introduction.....	27
4.2	Overview of Codes and Standards for Riser Design	27
4.3	DNV-OS-F201 LRFD Approach.....	29
4.3.1	Load Effects	32
4.3.2	Resistance	33
4.3.3	Serviceability Limit State (SLS).....	33
4.3.4	Ultimate Limit State (ULS)	34
4.3.5	Accidental Limit State (ALS)	39
4.3.6	Fatigue Limit State (FLS)	39
4.4	DNV-OS-F201 WSD Approach	41
4.5	Selection of LRFD Approach over WSD Approach.....	42
5	Riser Fabrication and Installation	44
5.1	Introduction.....	44
5.2	Riser Fabrication.....	44
5.3	Riser Installation	46
5.3.1	S-Lay Method	47
5.3.2	J-Lay Method.....	48

5.3.3	Reel-Lay Method	50
6	Design Basis and Input Data.....	52
6.1	Introduction.....	52
6.2	Analysis Method	52
6.2.1	Global Analysis.....	52
6.2.2	Analysis Software – OrcaFlex 11.2	54
6.3	Environmental Data	55
6.3.1	Location	55
6.3.2	Water Depth	56
6.3.3	Waves.....	56
6.3.4	Currents.....	57
6.3.5	Hydrodynamic Coefficients and Marine Growth	58
6.3.6	Riser-Soil Interaction	59
6.4	Vessel Data	59
6.4.1	FPSO Dimensions, RAOs and Orientation.....	59
6.4.2	FPSO Offsets and Motion.....	60
6.5	Riser Properties.....	62
6.5.1	Design Life.....	62
6.5.2	Internal Fluid Data	62
6.5.3	Riser Properties.....	63
6.5.4	Riser Coatings.....	63
6.5.5	Buoyancy Modules	64
6.5.6	Riser End Terminations	65
6.6	SLWR Acceptance Criteria.....	66
7	Extreme Response Analysis	68
7.1	Introduction.....	68
7.2	Design Load Cases.....	68
7.2.1	Environmental Direction.....	68
7.2.2	Load Case Matrix for SLWR.....	68

7.3	SLWR Static Analysis	69
7.3.1	Optimum SLWR Configuration.....	69
7.3.2	Static Analysis Results.....	71
7.3.3	Discussion on Static Analysis.....	73
7.4	SLWR Dynamic Analysis.....	74
7.4.1	Importance of Random Simulation (Seed Number Selection)	74
7.4.2	Analysis Procedure	75
7.4.3	Dynamic Analysis Results	78
7.4.4	Discussion on Dynamic Analysis	80
7.5	Summary of Extreme Response Analysis.....	81
8	Fatigue Response Analysis	82
8.1	Introduction.....	82
8.2	Fatigue Analysis Methodology	82
8.3	Sources of Riser Fatigue	84
8.3.1	Wave Induced Fatigue	84
8.3.2	VIV Induced Fatigue.....	84
8.3.3	Slug Induced Fatigue	85
8.3.4	Fatigue During Riser Installation.....	86
8.4	Wave Induced Fatigue	87
8.4.1	Introduction to DNV Approach	87
8.4.2	Analysis Procedure	90
8.4.3	Fatigue Analysis Results.....	94
8.5	Discussion on Fatigue Analysis	95
9	Parametric Study on Fatigue Life near TDP	97
9.1	Introduction.....	97
9.2	Selection of Different SLWR Configurations.....	99
9.3	Analysis Results.....	101
9.3.1	Analysis for 1500m Water Depth with 70mm Coating [SET1]	101
9.3.2	Analysis for 1500m Water Depth with 3mm Coating [SET2]	103

9.3.3	Analysis for 2000m Water Depth with 70mm Coating [SET3]	105
9.3.4	Analysis for 2000m Water Depth with 3mm Coating [SET4]	107
9.3.5	Analysis for 2500m Water Depth with 70mm Coating [SET5]	109
9.3.6	Analysis for 2500m Water Depth with 3mm Coating [SET6]	111
9.3.7	Analysis for 3000m Water Depth with 70mm Coating [SET7]	113
9.3.8	Analysis for 3000m Water Depth with 3mm Coating [SET8]	115
9.4	Summary of Fatigue Life Variation near TDP (Outer Wall).....	117
9.4.1	Summary of Fatigue Life Variation Against D_B for 70mm Coating.....	117
9.4.2	Summary of Fatigue Life Variation Against D_B for 3mm Coating.....	118
9.4.3	Summary of Fatigue Life Variation Against D_S for 70mm Coating.....	119
9.4.4	Summary of Fatigue Life Variation Against D_S for 3mm Coating.....	120
9.5	Discussion on Fatigue Life Variation near TDP	121
10	Conclusions and Recommendations for Future Work.....	122
10.1	Conclusions.....	122
10.1.1	Extreme Response Analysis.....	122
10.1.2	Fatigue Analysis.....	123
10.1.3	Parametric Study on Fatigue Life near TDP	123
10.2	Recommendations for Future Work.....	125
	Bibliography	126
	Appendix A: Riser Wall Thickness Calculations.....	133
	Appendix B: Riser Configurations for Fatigue Analysis.....	135
	Appendix C: Fatigue Analysis Results (Inner Wall)	143
	Appendix D: Summary of Fatigue Life Variation near TDP (Inner Wall).....	159

List of Abbreviations

GoM	Gulf of Mexico
FPSO	Floating Production Storage and Offloading
TDZ	Touch Down Zone
TLP	Tension-Leg Platform
SCR	Steel Catenary Riser
SLWR	Steel Lazy Wave Riser
SPM	Single Point Mooring
SS	Semi-Submersible
BOP	Blow Out Preventers
MODU	Mobile Offshore Drilling Unit
DNV	Det Norske Veritas
TTR	Top Tensioned Risers
FSHR	Free Standing Hybrid Riser
HRT	Hybrid Riser Tower
SLOR	Single Line Offset Riser
HDPE	High Density Polyethylene
XLPE	Cross Linked Polyethylene
PA	Polyamide/ Nylon
PVDF	Polyvinylidene Fluoride
PP	Polypropylene
PVC	Polyvinylchloride
PU	Polyurethane
API	American Petroleum Institute
TDP	Touch Down Point
ISO	International Standards Organization
WSD	Working Stress Design
LRFD	Load Factor Resistance Design
SLS	Serviceability Limit State

ULS	Ultimate Limit State
FLS	Fatigue Limit State
ALS	Accidental Limit State
TRB	Three Roll Bending
VIV	Vortex Induced Vibrations
DFF	Design Fatigue Factor
AISC	American Institute of Steel Construction
CAPEX	Capital Expenditure
CRA	Corrosion Resistant Alloys
NDT	Non-Destructive Test
LF	Low Frequency
WF	Wave Frequency
RAO	Response Amplitude Operator
FEA	Finite Element Analysis
JONSWAP	Joint North Sea Wave Project
PM	Pierson-Moskowitz
FEM	Finite Element Model
SCF	Stress Concentration Factor
ET	Effective Tension
BM	Bending Moment
UF	Utilization Factor
HCF	High Cycle Fatigue
LCF	Low Cycle Fatigue

List of Figures

Figure 1-1: Global deepwater basins [1].....	1
Figure 2-1: Deepwater field development process [8].....	5
Figure 2-2: Different floating platforms for deepwater developments [8].....	6
Figure 2-3: Number of active FPSOs by year [13].....	12
Figure 3-1: Top tensioned riser (TTR) [16].....	14
Figure 3-2: Typical compliant riser configurations [16].....	14
Figure 3-3: A typical hybrid riser configuration [14].....	15
Figure 3-4: A flexible riser configuration and the layers [19].....	17
Figure 3-5: Hierarchy of risers of interest.....	19
Figure 3-6: A schematic of SCR [22].....	20
Figure 3-7: A typical SLWR configuration [24].....	21
Figure 3-8: SLWR parameters [4].....	22
Figure 3-9: TDP movement of SCR and SLWR [4].....	24
Figure 3-10: Static effective tension variation of different risers [25].....	24
Figure 3-11: Fatigue performance at TDP for SCR and SLWR [21].....	25
Figure 3-12: Utilization vs downward velocity at riser hang-off point [25].....	25
Figure 3-13: Static bending moment variation along risers [25].....	26
Figure 4-1: DNV's framework for riser design [29].....	28
Figure 4-2: Riser design approach as described in DNV-OS-F201 [29].....	31
Figure 4-3: AISC's WSD and LFRD approach [34].....	43
Figure 5-1: Mechanized PGTAW weld in clad pipes [3].....	45
Figure 5-2: PGMAW in operation [3].....	46
Figure 5-3: S-lay configuration [16].....	47
Figure 5-4: Seven Borealis, Subsea 7 [37].....	48
Figure 5-5: A schematic of J-lay operation [38].....	49
Figure 5-6: Saipem 7000 [39].....	49
Figure 5-7: A schematic of Reel-lay operation [41].....	50
Figure 5-8: Seven Oceans owned by Subsea 7 [40].....	51
Figure 6-1: Global analysis approach [29].....	53
Figure 6-2: FEA model formulation in OrcaFlex [42].....	54
Figure 6-3: Basins of the Brazilian South and Southeast coasts [47].....	55

Figure 6-4: Orientation of soil springs [52]	59
Figure 6-5: Vessel orientation.....	60
Figure 6-6: Vessel offsets [48].....	62
Figure 6-7: A typical buoyancy module [55].....	64
Figure 6-8: Equivalent buoyancy module.....	65
Figure 6-9: A typical riser flex joint [56].....	66
Figure 7-1: SLWR strength calculation load matrix.....	69
Figure 7-2: SLWR configuration from OrcaFlex.....	70
Figure 7-3: Effective Tension variation in static state	71
Figure 7-4: Bending Moment variation in static state.....	72
Figure 7-5: DNV LRFD Utilization Factor variation in static state.....	72
Figure 7-6: Irregular wave realizations for various seed numbers.....	74
Figure 7-7: Gumbel Distribution for the downward velocity at hang-off point.....	76
Figure 7-8: Time and simulation stages	77
Figure 7-9: 3-hour time history of downward velocity	77
Figure 7-10: Effective Tension variation in dynamic state.....	78
Figure 7-11: Bending Moment variation in dynamic state	78
Figure 7-12: DNV LRFD Utilization Factor variation in dynamic state	79
Figure 7-13: Hang-off angle variation in dynamic state	79
Figure 8-1: Fatigue life statistical behaviour [61].....	82
Figure 8-2: Fatigue in welded joints [62].....	83
Figure 8-3: VIV suppressing strakes [63].....	85
Figure 8-4: A slug unit followed by a gas pocket [65]	86
Figure 8-5: S-N curves in seawater with cathodic protection [32]	89
Figure 8-6: S-N curves in the air [32].....	89
Figure 8-7: Subdivision of sea states in sector 60°	91
Figure 8-8: Fatigue life of SLWR against arc length.....	94
Figure 8-9: Fatigue life near the TDP	95
Figure 9-1: SLWR notations for fatigue analysis	97
Figure 9-2: Different SLWR analysis scenarios	98
Figure 9-3: SLWR configuration matrix for fatigue analysis [SET1]	99
Figure 9-4: Different SLWR configurations for S1-A1 to S1-A5 [SET1].....	100
Figure 9-5: Fatigue life variation against D_B (outer wall) [SET1].....	101
Figure 9-6: Fatigue life variation against D_S (outer wall) [SET1]	101

Figure 9-7: Fatigue life variation against D_B (outer wall) [SET2]	103
Figure 9-8: Fatigue life variation against D_S (outer wall) [SET2]	103
Figure 9-9: Fatigue life variation against D_B (outer wall) [SET3]	105
Figure 9-10: Fatigue life variation against D_S (outer wall) [SET3]	105
Figure 9-11: Fatigue life variation against D_B (outer wall) [SET4]	107
Figure 9-12: Fatigue life variation against D_S (outer wall) [SET4]	107
Figure 9-13: Fatigue life variation against D_B (outer wall) [SET5]	109
Figure 9-14: Fatigue life variation against D_S (outer wall) [SET5]	109
Figure 9-15: Fatigue life variation against D_B (outer wall) [SET6]	111
Figure 9-16: Fatigue life variation against D_S (outer wall) [SET6]	111
Figure 9-17: Fatigue life variation against D_B (outer wall) [SET7]	113
Figure 9-18: Fatigue life variation against D_S (outer wall) [SET7]	113
Figure 9-19: Fatigue life variation against D_B (outer wall) [SET8]	115
Figure 9-20: Fatigue life variation against D_S (outer wall) [SET8]	115
Figure 9-21: Summary of fatigue life variation against D_B for 70mm coating (outer wall)	117
Figure 9-22: Summary of fatigue life variation against D_B for 3mm coating (outer wall)	118
Figure 9-23: Summary of fatigue life variation against D_S for 70mm coating (outer wall)	119
Figure 9-24: Summary of fatigue life variation against D_S for 3mm coating (outer wall)	120
Figure 10-1: Upper and lower bound fatigue life variation against D_B (70mm coating)	124
Figure 10-2: Upper and lower bound fatigue life variation against D_S (70mm coating)	124

List of Tables

Table 2-1: Comparison between turret and spread moored FPSOs [11].....	7
Table 2-2: Comparison of floating platform capabilities [8]	12
Table 3-1: Flexible pipe layer properties [19].....	17
Table 3-2: API 5L material strength properties [20].....	18
Table 4-1: Classification of safety classes [29]	29
Table 4-2: Categorization of loads (load effects) [29]	32
Table 4-3: Load effect factors [29]	32
Table 4-4: γ_{SC} Safety class resistance factors [29].....	33
Table 4-5: γ_m Material resistance factors [29].....	33
Table 4-6: γ_c Simplified check for Accidental loads [29]	33
Table 4-7: Fabrication factor α_{fab} [29].....	37
Table 4-8: Design fatigue factors DFF [29].....	41
Table 4-9: Usage factor η for combined loading [29].....	42
Table 6-1: 100-year H_s and T_p values	57
Table 6-2: 10-year current profile.....	57
Table 6-3: Hydrodynamic coefficients of riser sections	58
Table 6-4: Soil parameters	59
Table 6-5: FPSO details	60
Table 6-6: Summary of vessel offsets.....	61
Table 6-7: Summary of fluid properties.....	62
Table 6-8: Summary of riser properties	63
Table 6-9: Buoyancy module properties.....	64
Table 6-10: Partial Safety Factors for ULS, ALS and Design.....	67
Table 7-1: SLWR static configurations (Nominal, ULS, ALS).....	69
Table 7-2: SLWR nominal static configuration.....	70
Table 7-3: Summary of static analysis results	73
Table 7-4: Seed numbers and the maximum downward velocity	75
Table 7-5: Summary of dynamic analysis.....	80
Table 7-6: Summary of static and dynamic analysis	81
Table 8-1: Directional frequency of waves.....	90
Table 8-2: Representative sea states and their lumped probabilities	92

Table 8-3: Fatigue damage near the TDP	95
Table 9-1: Summary of fatigue life (outer wall) [SET1]	102
Table 9-2: Summary of fatigue life (outer wall) [SET2]	104
Table 9-3: Summary of fatigue life (outer wall) [SET3]	106
Table 9-4: Summary of fatigue life (outer wall) [SET4]	108
Table 9-5: Summary of fatigue life (outer wall) [SET5]	110
Table 9-6: Summary of fatigue life (outer wall) [SET6]	112
Table 9-7: Summary of fatigue life (outer wall) [SET7]	114
Table 9-8: Summary of fatigue life (outer wall) [SET8]	116

1 Introduction

1.1 Background

Offshore oil and gas exploration is dated back to the 19th century (1859) when the first offshore oil field was drilled by Colonel Edwin Drake in the Santa Barbara Channel in California at a few meters in depth [1]. With the advancement of technologies, oil and gas exploration further expanded to the deepwater areas. In 1975, Shell discovered the first deepwater oil field, Cognac, with a water depth of 313m in the Gulf of Mexico (GoM). In the 21st century, 50% of offshore developments are located deepwater [2]. Until 1998, water depths greater than 300m were considered deepwater, but at present, 500m is mainly regarded as deepwater [1]. Depths over 1500m are considered ultra-deepwater. The existing deepwater oil fields are primarily located in the Atlantic deepwater basin of Brazil, the GoM, and West Africa. The existing deepwater gas fields are located in the North Sea, Barents Sea, East Africa, Eastern Mediterranean and Northwest shelf of Australia. These locations are shown in Figure 1-1 [1].



Figure 1-1: Global deepwater basins [1]

Deepwater oil and gas fields developments are always associated with technical and economic difficulties due to the extreme environmental conditions. A few of these limitations are the increased payload in the vessel and large environmental loads due to waves, currents and ice conditions. Robust and expensive mooring systems are required to overcome these limitations [3]. The Floating Production Storage and Offloading systems (FPSO) are one of the most desired solutions for those environmental conditions. During the past decades, FPSOs have successfully deployed production risers in shallow to ultra-deepwater field developments in areas with harsh environmental conditions [4].

Production risers are mainly categorized as rigid and flexible risers depending on the type of conduit used. Flexible risers have been traditionally used in most FPSO solutions since they are more compliant and less sensitive to vessel motions, thus eliminating fatigue issues in the touch down zone (TDZ) [5]. On the other side, the rigid risers have been extensively used in fixed platform solutions, Spar solutions and Tension-Leg Platform (TLP) solutions [6]. Compared with the flexible risers, a rigid riser type called Steel Catenary Riser (SCR) offers a simple and cost-effective method for deepwater developments under high pressure, temperature and sour service conditions [4]. Despite the advantages of the SCRs, it is almost impossible to utilize this method from FPSOs due to excessive stresses caused by vessel heave and pitch motions [7]. SCRs in deepwater also cause a large payload on the vessel. Not being able to isolate the riser motion from the vessel motion is another drawback of the SCRs [3].

Steel Lazy Wave Riser (SLWR) is a compliant form of SCR with the buoyancy modules inserted in the middle section of the riser, thus isolating the TDZ from the vessel motion and largely improving the fatigue performance of the riser [3]. This method was initially proposed by Karunakaran et al. in 1996 [7]. SLWR was called “Low Long Wave Configuration” during its inception. SLWRs were first implemented in the BC10 field in Brazil at 1780m water depth in the year 2008 [5]. Since its inception, SLWRs have gained popularity in deepwater oil and gas developments. They have been successfully deployed in GoM, the North Sea and Offshore Brazil projects.

1.2 Research Objective

The thesis aims to establish an SLWR configuration that can be deployed by a spread moored FPSO in ultra-deepwater conditions in Offshore Brazil. Assessment of SLWR is carried out in two different phases as mentioned below.

- Evaluate the static and dynamic behaviour of the SLWR in 2000m water depth under extreme environmental loading conditions to determine the strength of the riser.
- Evaluate the fatigue performance of the SLWR. Study the parametric relationship between the fatigue life at the touch down point (TDP) and the height between sag and hog bend (D_B), and the distance between sag bend and seabed (D_S). Four different water depths (1500m, 2000m, 2500m, 3000m) and two different coating thicknesses (70mm: production riser and 3mm: injection riser) are considered in the analysis.

1.3 Scope and the Structure of the Thesis

- Chapter 1: Introduction
Background of the deepwater riser concept and its applicability.
- Chapter 2: Platform Selection for Deepwater Developments
Discuss different deepwater floaters and their applicability and justification for selecting FPSO for the thesis work.
- Chapter 3: Deepwater Riser Systems
Classification of risers and their applicability to deepwater developments and justification for the selection of SLWR.
- Chapter 4: Codes and Standards for Riser Design
Discuss different standards used in the riser design and the two different design concepts, LRFD (Load Factor Resistance Design) and WSD (Working Stress Design). Justification of the selection of the LRFD approach for the thesis.
- Chapter 5: Riser Fabrication and Installation
Discuss different riser materials and fabrication methods. Discuss the three different offshore pipe installation methods used in the riser installation.

- Chapter 6: Design Basis and Input Data

Discuss the analysis method and the relevant design guidelines and tools. Introduce the design input data used in the analysis.

- Chapter 7: Extreme Response Analysis

Introduction to extreme response analysis and analysis procedure. Carry out static and dynamic analysis and discuss analysis results on Effective tension and compression, bending moment and LRFD utilization.

- Chapter 8: Fatigue Response Analysis

Introduction to riser fatigue and analysis procedure. Discuss the long-term fatigue response of the SLWR.

- Chapter 9: Parametric Study on Fatigue Life near TDP

The parametric study focuses on the fatigue life near TDP for different SLWR configurations in 1500m, 2000m, 2500m and 3000m water depths. The analysis also uses two different coating thicknesses (70mm with a density of 700kg/m^3 and 3mm with a density of 900kg/m^3).

- Chapter 10: Conclusions and Recommendations for Future Work

Discuss the findings of the thesis and recommendations based on them. Propose future work.

1.4 Limitations

- Extreme response analysis is only carried out for 2000m water depth in the Santos basin (Offshore Brazil). Input data are referred to the project's relevant met-ocean reports, which are not fully disclosed due to confidentiality.
- Optimization of SLWR is only based on strength calculation and fatigue performance. Consideration is only given to wave induced fatigue. Fatigue damage due to vortex-induced vibrations (VIV) is not a part of the thesis.
- This thesis does not address riser optimization based on the cost of the riser, interference with other risers and installation methods.

2 Platform Selection for Deepwater Developments

2.1 Introduction

A deepwater field development process following the discovery of hydrocarbons usually involves five significant phases. The "select" phase is carried out after a discovery has been adequately appraised for further development [8]. This phase requires the evaluation of multiple development concepts and selecting the one that satisfies the commercial and strategic goals. The selection of a floating platform is an essential subset of the "select" phase and the overall field development [8]. The entire process of deepwater field development is shown in Figure 2-1.

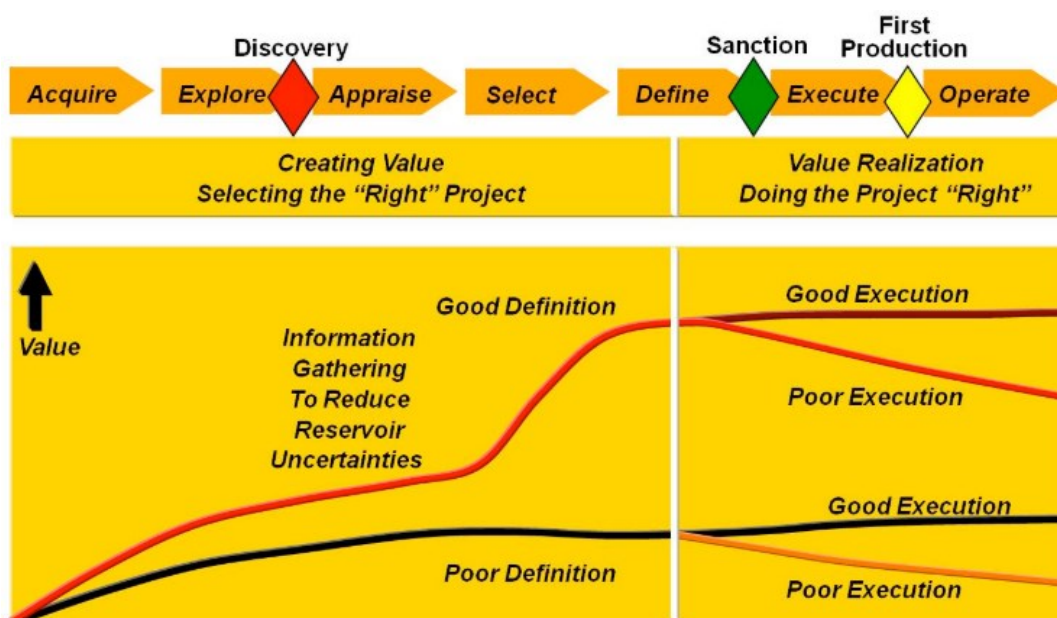


Figure 2-1: Deepwater field development process [8]

Deepwater developments are capital intensive, and consequences are severe if a poor development concept is selected. In the select phase, considerations should be given to platform type and its functionalities such as type of tree (wet or dry tree), reservoir depletion plan (well count, placement, intervention, production profile), site characteristics (water depth, met-ocean conditions, seabed topography) and topside payload while satisfying the commercial and strategic goals [8]. In the following sections, different types of deepwater floating platforms are discussed.

2.2 Deepwater Floating Platforms

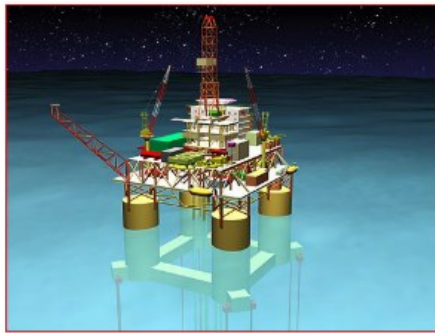
Four different floating platform concepts are typically used in deepwater developments. They are FPSO (Floating Production Storage and Offloading vessels), TLP (Tension Leg Platforms), Semi-submersible vessels and Spar platforms [8]. Figure 2-2 shows above mentioned concepts.



**FPSO
(Wet Trees)**



**Semisub
(Wet Trees)**



**TLP
(Dry/Wet Trees)**



**Spar
(Drv/Wet Trees)**

Figure 2-2: Different floating platforms for deepwater developments [8]

2.2.1 Floating Production Storage and Offloading vessels (FPSO)

FPSOs are constructed mainly by converting liquid cargo vessels. FPSOs have been successfully deployed in shallow to ultra-deepwater environments worldwide and can be used in any water depth [9]. FPSOs are ideal for large fields like Offshore Brazil and small, marginal and isolated reservoirs away from pipeline grid infrastructures and located in deepwater with no possibility of installing fixed platforms [10]. There are two main categories of FPSOs based on their mooring systems. A spread moored FPSO uses anchor legs from the bow and stern of the vessel in a four-group arrangement. A turret moored FPSO is designed as a single point

mooring (SPM) system to weathervane about the mooring system to respond to the changing weather conditions. Thus, most FPSOs in extreme weather conditions are designed with a disconnectable turret to sail away during extreme cyclones [11]. A comparison between these two concepts is shown in Table 2-1.

Table 2-1: Comparison between turret and spread moored FPSOs [11]

	Turret-Moored	Spread-Moored
Vessel Orientation	360 degree weathervaning	Fixed orientation, can impact flare
Environment	Mild to extreme, directional to spread	Mild to moderate, uni- to fairly directional
Field Layout	Fairly adaptable, partial to distributed flowline arrangements	Prefers flowline arrangement to approach beam-on
Riser Number & Arrangement	Requires commitment, moderate expansion capability	Can be designed for flexibility, additional tie-ins
Riser Systems	Location of turret (bow) requires robust riser design	Adapts to various riser systems, combinations of various types
Stationkeeping Performance	Number of anchor legs, offsets minimized	Larger number of anchor legs, offsets variable
Vessel Motions	Weathervaning capability reduces motions	Dependent on relative vessel/ environment directionality
Vessel Arrangement	Turret provides "compact" load and fluid transfer system	Components spread on deck, requires extensive interfaces
Offloading Performance	FPSO typically aligned with mean environment	Dependent on vessel/ environment orientation

FPSO is also an ideal early production system for deepwater reservoirs to acquire reservoir performance data while generating cash flow [8]. FPSOs are currently operating in many projects worldwide, such as West Africa, Offshore Brazil, the Gulf of Mexico (GoM) and the North Sea.

2.2.2 Semi-submersible platforms (SS)

For field developments with no need for oil and condensate storage, semi-submersible platforms are more suitable than FPSOs due to their better motion performance in heave. Typical semi-submersibles have four wide-spaced columns and a ring pontoon at the base [8]. These are typically anchored to the seabed with spread mooring lines. The pontoon and the four columns have sufficient buoyancy to let the structure float and keep the platform upright.

They can be ballasted depending on the wave condition and can be towed from place to place [10].

These floaters use wet trees, but dry tress can also be used. These are easily scalable for large topsides and different water depths than TLPs and Spars. These can accommodate many flexible risers and allow for quayside topside hull integration. A few disadvantages are high maintenance cost, fatigue issues if SCRs are used for production and the requirement of Blow Out Preventers (BOP) if drilling needs to be done [10]. SSs have been successfully deployed in water depths of more than 2000m in the Gulf of Mexico, the North Sea and Offshore Brazil.

2.2.3 Tensioned Leg Platforms (TLP)

A conventional TLP has four columns and a ring pontoon configured into a truss deck. The heave motion of the hull is restrained by steel tendons attached with flexible joints to the porches in the column base at the seabed. TLPs can utilize both wet trees and dry trees. Production risers are clustered into a central well bay and attached to the topside with tensioners. Since the heave motion is restricted, the fatigue performance of SCRs is better compared to FPSOs and SSs. Thus, SCRs with a higher diameter and higher thickness can reduce the number of SCRs. Installation of tendons and foundations and mating operations are weather-sensitive and challenging compared to other concepts [8].

TLPs are cost-effective in water depths between 600m to 1200m. But they have been used in water depths between 460m to 2130m despite their increased costs. The conventional TLP looks similar to a semi-submersible but is relatively low cost and incurs low maintenance costs. TLPs have disadvantages such as sensitivity to payload change, not being friendly to offshore drilling, tendon fatigue and increased tendon diameter with water depth [10]. TLPs have been successfully installed in the Gulf of Mexico (GoM), West Africa and the North Sea.

2.2.4 Spar Platforms

The Spar platform was designed to enable drilling with surface BOPs and allow for dry trees. There are three commonly used configurations, and the truss Spar is the most widely used configuration. It consists of four major components: hull, topside, moorings and risers. Spars

have favourable motion characteristics in heave compared to other floating platforms. The vertical cylinder provides the buoyancy, while the truss with heave plates and ballast provides stability. Production risers are clustered inside the moonpool and tensioned by air cans (also hydro-pneumatic dampers), providing the decoupled motion between the risers and the hull. Wet trees and SCRs can also be implemented due to the low heave motion of Spars [8].

Spars have been used in water depths between 550m to 3050m. Initially, Spars were used as marker buoys and oil storages, but now they are used for drilling and production. Some advantages of Spars are low maintenance costs, passive hull system, offshore drilling and workover friendliness and accommodate for payload changes. One disadvantage is that it requires large derrick barges to install the topside [10]. Spars have been successfully deployed in GoM, the North Sea and West Africa.

2.3 Drivers for Platform Selection

Drivers for floating platform selection can be discussed under three main topics. They are reservoir depletion characteristics, regional drivers, and business drivers. All the explanations below refer to the study carried out by Xia et al. [8].

2.3.1 Reservoir Depletion Drivers

- Reservoir geology and geometry

The ultimate goal of a development plan is to achieve the highest recovery rate with fewer wells. The number and the seabed location of the wells are significant when selecting a floating platform. When selecting the floater, the depth of the reservoir below the mud line and reservoir pressure also need to be considered.

- Reservoir fluid property

This will determine how the wells flow and help define the measures for flow assurance. These significantly impact the cost and complexity of subsea and platform topside components. The presence of CO₂ and H₂S can cause severe corrosion, especially under high pressure.

-
- Drilling, completion and intervention

Drilling and completion wells can consume 50% of the development. Well performance is directly linked to the type and effectiveness of the completions. Thus, future interventions to stimulate well flow can significantly reduce operating costs. Drilling from a dry tree costs less than subsea wells drilled from MODU (Mobile Offshore Drilling Unit).

- Process requirements

The location needs to be considered for process requirements such as acid gas removal, liquefaction and condensate stabilization. The deck space should fit those facilities, or subsea solutions should be implemented.

2.3.2 Regional Drivers

- Water depth

Water depth is one key factor that decides the cost of drilling, design and installation of moorings and the type and material of pipelines and risers.

- Met-ocean conditions

Both operational and extreme weather conditions such as wind, waves, and current at the site significantly impact the cost of the floating platform hull and its applicability to the weather conditions.

- Geotechnical conditions

The type of foundation and mooring depends on the type of platform. Poor soil conditions in the seabed lead to higher foundation costs which can be significant. Typical foundations used in deepwater developments are suction anchors, drilled and grouted piles and gravity foundations.

- Remoteness

Distance to existing pipeline infrastructure and processing facilities can determine whether the platform needs storage and processing facilities. Platform fabrication locations also need to be considered since long-distance transportation is normally involved.

-
- Regulatory conditions

Local and environmental rules and regulations must be addressed during the platform selection. These cover health and safety, technical and workplace safety, environmental protection and pollution prevention.

2.3.3 Business Drivers

- Investment strategies

It is essential to differentiate between gas development and oil development as gas is a low-priced and less fungible commodity requiring high capital investment. Hence reservoir development plan for gas and oil is different.

- Standardization

Many oil companies agree with vendors and contractors to ensure the equipment and services supply chain. This enhances execution certainty and operational efficiencies.

- Market influence

Some platform concepts are more preferred among fabricators. That means the platform is delivered in a shorter period. Other factors that need to be considered are the availability of MODUs, installation vessels, fabrication yards, and engineering contractors.

A comparison among floating platform (FPSO, TLP, SS, SPAR) concepts are presented in Table 2-2 [8].

2.4 Selection of FPSO Concept for the Research

The location of the study is the Santos basin in Offshore Brazil. Since the field in consideration is located 300km away from the shore, the floater needs to have storage capacity. Due to this, FPSOs are a favourable option over SSs. Santos basin is a benign environment where the presence of hurricanes or extreme weather conditions are not yet characterized [12]. Therefore, the need for turret moored FPSOs in this region is less. Instead, the spread moored FPSOs are a preferred solution for Offshore Brazil [12]. Currently, FPSOs are in operation across Santos and Campos basin Pre-Salt areas in ultra-deepwater from 1800m to 2400m, 300km away from Rio de Janeiro and São Paulo coasts, southeast of Brazil. Petrobras led the industry effort to

approve FPSO international standards and local regulations. At present, 18 third-generation FPSOs are operating in Offshore Brazil. Out of them, 50% are conversions, and 50% are new builds. Globally, there are around 200 FPSOs are in operation [13]. Figure 2-3 shows the global presence of FPSOs by the end of the year 2020.

Table 2-2: Comparison of floating platform capabilities [8]

		Spar	TLP	Semisubmersible	FPSO
Variants		Classic, Truss or Cell	Classic, Extended, New Generation	Conventional or Deep-draft	Shipshape or Cylindrical
Functionality		Dry/Wet Trees; Surface BOP drilling, completion, intervention	Dry/Wet Trees; Surface BOP drilling, completion, intervention	Wet Trees; Subsea BOP drilling, completion, intervention	Wet Trees; Subsea BOP drilling in mild conditions; Integrated liquid product storage
Constraints	Water Depth	Not for shallow water	Tendons to ~1,500 m; Not for shallow water	None	None
	Topside Payload	< 20,000 tons dry weight	None	None	None
Riser Types		SCR, TTR and flexible risers; (Dual Barrier HP production riser to ~1,500 m)	SCR, TTR and flexible risers	Flexible risers, hybrid riser towers and SCRs for deepwater	Flexible risers and hybrid riser towers; very limited SCR applicability
Offshore Installation, Integration, Commissioning		Complex offshore operations; high execution risk	Relatively complex offshore operations; moderate execution risk	Relatively simple offshore operations; low execution risk	Simple offshore operations; low execution risk
Decommissioning, Relocation and Expansion		Difficult and costly	Difficult and costly	Simple	Simple

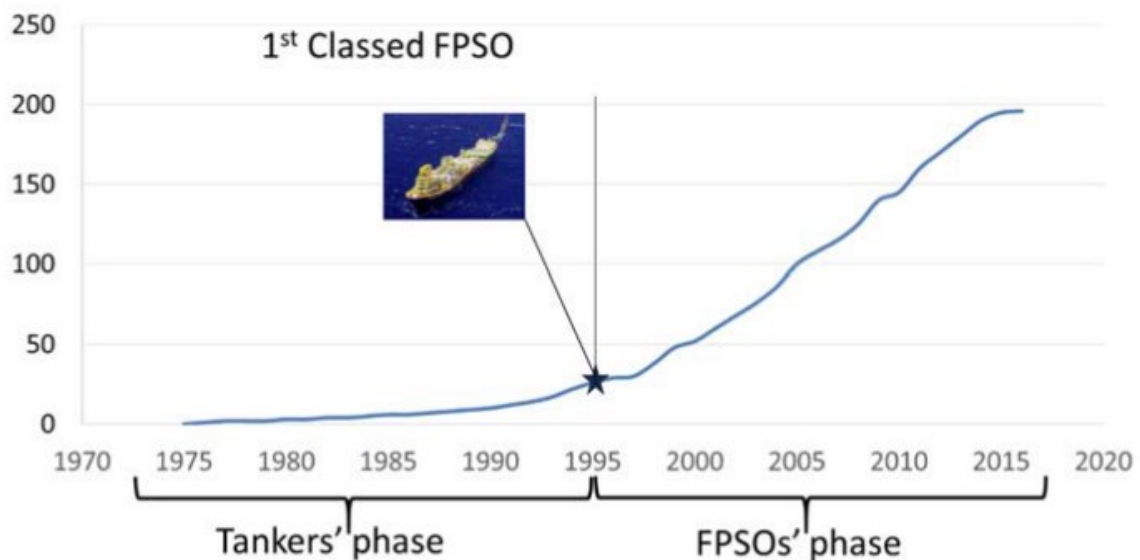


Figure 2-3: Number of active FPSOs by year [13]

3 Deepwater Riser Systems

3.1 Classification of Risers

The primary function of offshore riser systems is to act as a conduit for the safe transportation of hydrocarbons between the seafloor and the host facility. Risers are used during the whole lifetime of a project [14]. As per the DNVGL-SE-0476 Specification [15], hydrocarbon exploration risers are mainly categorized into three groups. They are Top Tensioned Risers (TTR), Compliant Risers and Hybrid Risers.

3.1.1 Top Tensioned Risers (TTR)

TTRs are vertical risers supported by top tension, which allows for relative motion between riser and floater motion in the vertical direction using heave compensation. These are used in all functional areas of hydrocarbon exploration [15]. TTRs are mainly used for drilling, although they can be used as production, injection, and export risers. TTRs are primarily deployed from platforms with relatively small heave motion, such as Spar and Tensioned Leg Platform (TLP). Avoiding compressive forces along the riser is the governing design criterion. Figure 3-1 shows a schematic of a TTR [16].

3.1.2 Compliant Riser

Compliant risers can absorb floater motions by changing their geometry without the use of heave compensation systems. These are mainly used in production, export/import, and injection risers [15]. These risers are flexible to move horizontally. Riser material can be either flexible pipe or rigid pipe. The connection between riser and vessel is a crucial design consideration in compliant risers. The selection of a compliant riser depends on several factors such as water depth, vessel type, cost, and environmental loading conditions. The free-hanging catenary riser is the widely used configuration. Also, compliant risers can be configured into different shapes, as shown in Figure 3-2 [16].

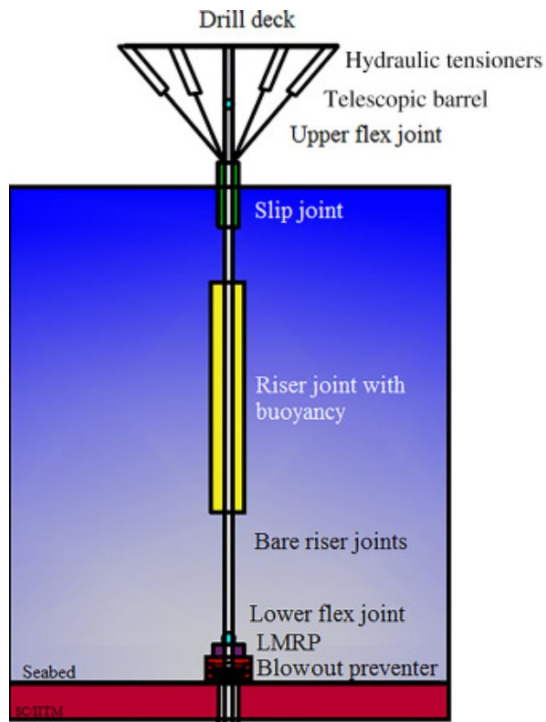


Figure 3-1: Top tensioned riser (TTR) [16]

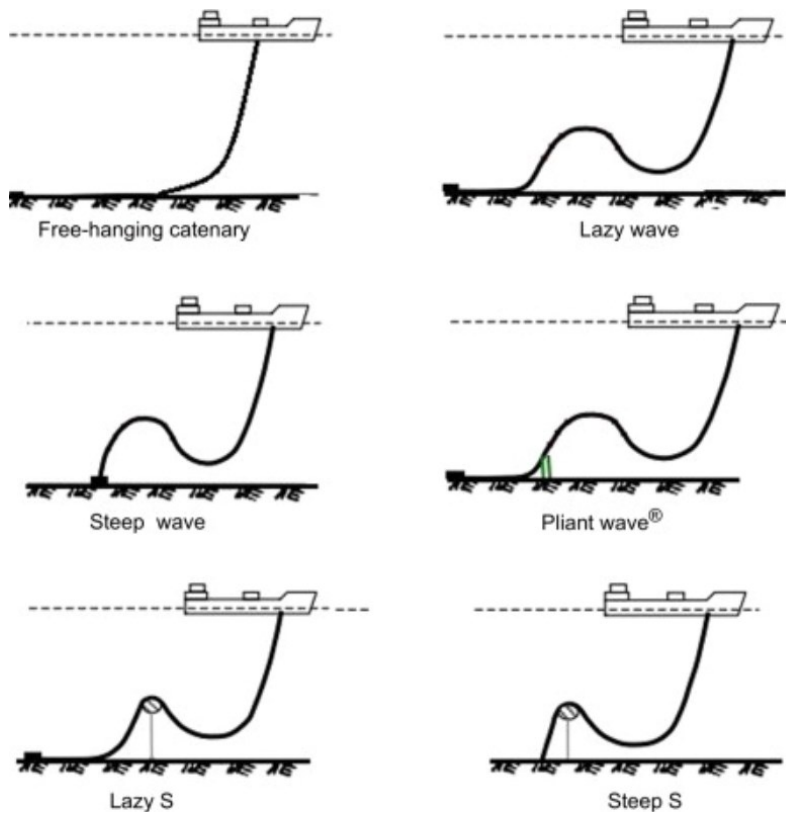


Figure 3-2: Typical compliant riser configurations [16]

3.1.3 Hybrid Riser

This configuration is a combination of tensioned and compliant risers. The typical setup is a vertical/free-hanging riser from a submerged buoy to the seabed with a compliant riser from the buoy to the vessel [15]. These risers can be installed before or after the host vessel is installed. The vertical riser section starts from the base established on the seabed and extends to the submerged buoy. The tension provided by a buoy holds the vertical portion. The flexible jumper goes from the buoy to the host platform. Buoy also carries a part of the flexible jumper [16]. Commonly used hybrid risers are Hybrid Riser Tower (HRT), Free Standing Hybrid Riser (FSHR), and Grouped Single Line Offset Riser (SLOR) [16]. A typical hybrid riser configuration is shown in Figure 3-3.

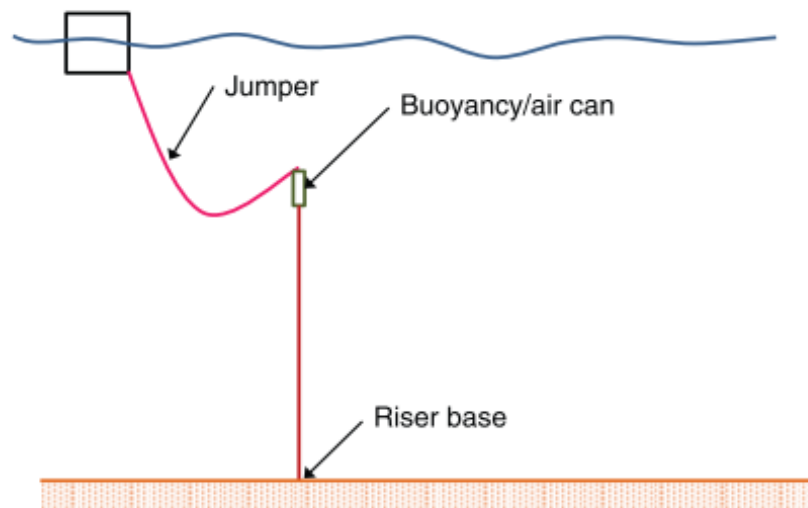


Figure 3-3: A typical hybrid riser configuration [14]

Commonly used risers associated with hydrocarbon exploration are mentioned below [15].

- Production riser
- Injection riser
- Gas lift riser
- Service riser
- Export/import riser
- Completion//workover riser
- Marine drilling riser

-
- Subsea control umbilical
 - Integrated production umbilical

3.2 Riser Material Selection

Material selection is a crucial step in riser design. As per Norsok M-001: Material Selection [17], assessing the below-mentioned criteria is required for an optimized design while providing acceptable safety and reliability. Further, risers can be classified as flexible and rigid depending on the material used.

- Corrosivity during operations, including start-up and shut-down conditions
- Design life and system availability requirements
- Failure probabilities, failure modes and associated consequences to humans, environment, safety, and assets
- Corrosion inspection and monitoring possibilities
- Market availability of materials and documented service and fabrication performance
- Associated costs of materials, interchangeability, and availability of Spare parts

3.2.1 Flexible Risers

Flexible pipes are constructed using a polymeric sealing material that holds the well fluid, multiple helical armouring layers that give the required strength for external and internal loads, and a polymer outer sheath that prevents the interaction between seawater and armour wires. Flexible pipes enable the design of pipelines with a lower bending radius than rigid pipes, which typically require a 25 times higher bending radius. There are two main reasons to select flexible risers over rigid steel pipes [18].

- The compliant structure can be used to permanently connect the riser with the floating support vessel with large motions and subsea installations.
- Transportation and installation are simplified due to the possibility of prefabrication in long lengths stored into reels.

However, reeling is also possible with steel pipes, but the process involves plastic yielding and ovalization of the pipes. This requires special equipment in the installation process. Hence, flexible pipes have been extensively used to permanently connect subsea systems to vessels. They are also used to connect subsea installations with topside facilities and as flowlines and jumpers connecting subsea equipment [18]. Alternatives such as SCRs may replace flexible pipes in several situations like deepwater riser systems for TLPs, Spar buoys, and floating vessels with higher motion due to increased external pressure and limited production bore size [18]. Figure 3-4 shows a flexible riser arrangement and the layers. Table 3-1 shows the flexible pipe's layer properties and the purpose of each layer [19].

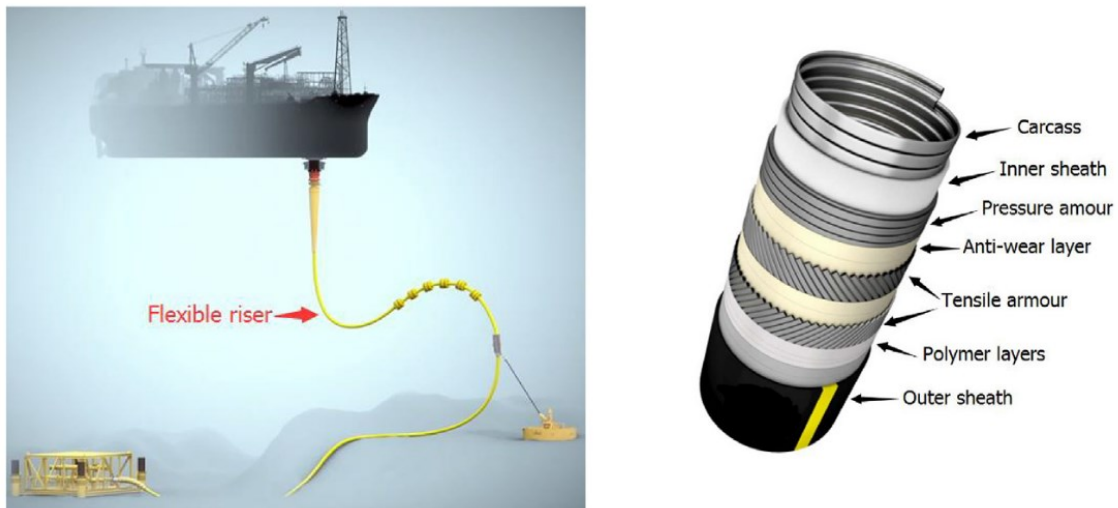


Figure 3-4: A flexible riser configuration and the layers [19]

Table 3-1: Flexible pipe layer properties [19]

Layer	Material	Function
Carcass	Duplex steel	External pressure resistance
Pressure armour	Carbon steel	Hoop stress resistance
Tensile armour	Carbon steel	Axial load and torsion resistance
Inner sheath	HDPE, XLPE, PA, PVDF	Well fluid containment
Outer sheath	HDPE	External fluid barrier
Anti-wear layer	PA, PVDF, HDPE	Abrasion resistance
Insulation layer	PP, PVC, PU	Thermal insulation

3.2.2 Rigid Risers

Rigid risers are mainly made from Carbon steel, Aluminium alloys or Titanium. Due to the low costs, low Carbon steel risers are the widely used material in the current offshore industry [16]. Low Carbon steels come in different grades, such as API 5L X60, X65, and X70. These risers are available in different diameters and different wall thicknesses. Rigid risers also have higher tensile strength than flexible pipes, favouring them in deepwater applications [16]. Table 3-2 shows the commonly used API 5L material strength properties.

Table 3-2: API 5L material strength properties [20]

Grade	Yield Strength (ksi / MPa)	Tensile Strength (ksi / MPa)	Elongation %
API 5L X60	60 / 414	75 / 517	19
API 5L X65	65 / 448	77 / 531	18
API 5L X70	70 / 483	82 / 565	17

Rigid steel risers can be adopted to different riser configurations, but this study focuses mainly on the Steel Lazy Wave Risers (SLWR).

3.3 Production Risers

Production risers are conduits for the produced oil and gas from a well. They mainly transport unprocessed oil and gas to a processing facility or a vessel. Their functional requirements are mentioned below [14].

- Safely contain the well fluids
- Facilitate safe and efficient production during the life of the well
- Prevent the development of wax and hydrates, which can reduce the flow
- Facilitate pipe pigging operations for wet-tree wells
- Facilitate completion/workover operations for vertical TTRs.

Production risers can be mainly categorized into three groups, as mentioned in Chapter 3.1. They can be further subdivided into two groups depending on the riser material. The main emphasis of this research is based on rigid production risers. The following chapters briefly

introduce two main rigid production risers; Steel Catenary Riser (SCR) and Steel Lazy Wave Riser (SLWR). The hierarchy of risers of interest is also shown in Figure 3-5.

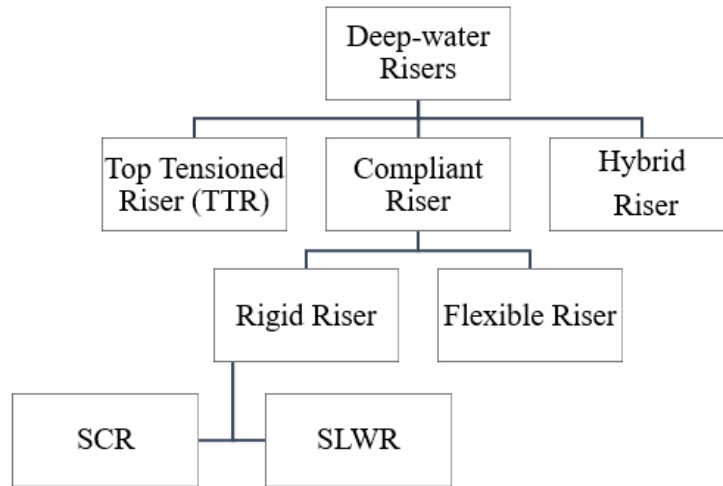


Figure 3-5: Hierarchy of risers of interest

3.3.1 Steel Catenary Riser Configuration (SCR)

Catenary risers are riser systems that take the shape of a catenary when deployed. Catenary risers can be made of either rigid or flexible pipes. When the riser is made from steel pipes, it is called a steel catenary riser (SCR). They are a favourable solution for deepwater developments due to the less complexity in installation and low cost [14]. The top tension of the riser is a function of the riser suspended length above the seabed and the total submerged weight of the riser. These risers are typically hung from the platform without motion-compensating systems. Typical hang-off arrangements are flex-joint/basket, stress-joint/basket and pull-tube arrangement. Hence, the riser's top angle fluctuates due to the wind, wave, and current generated motion [14].

The major drawbacks of SCR are the poor dynamic and fatigue performance when connected to vessels with high dynamic motion (FPSO) in deepwater applications [21]. Hang-off region and the TDZ are the two most vulnerable locations of the SCR. The hang-off region's high damage can be eliminated by using particular hang-off arrangements or tapered Titanium stress joints [21]. But design for fatigue near the TDZ is difficult with the conventional SCR arrangement due to the complex soil-riser interaction, especially under large floater motions [22].

The study by Karunakaran et al. [22] showed that these design-related issues could be successfully addressed by varying the weight of the riser along the length. This variation can be achieved by applying heavy and light coatings along the riser length. Further research has shown that applying weight distributed risers can achieve robust riser designs for FPSOs [23]. Weight distribution is achieved using readily available ballast and buoyancy wraps [23]. The first SCR was installed in the year 1993 on the TLP “Shell Auger”. SCRs have been extensively used in deepwater applications in the Gulf of Mexico (GoM), West Africa, and Brazil [21]. A schematic of the typical SCR configuration is shown in Figure 3-6 [22].

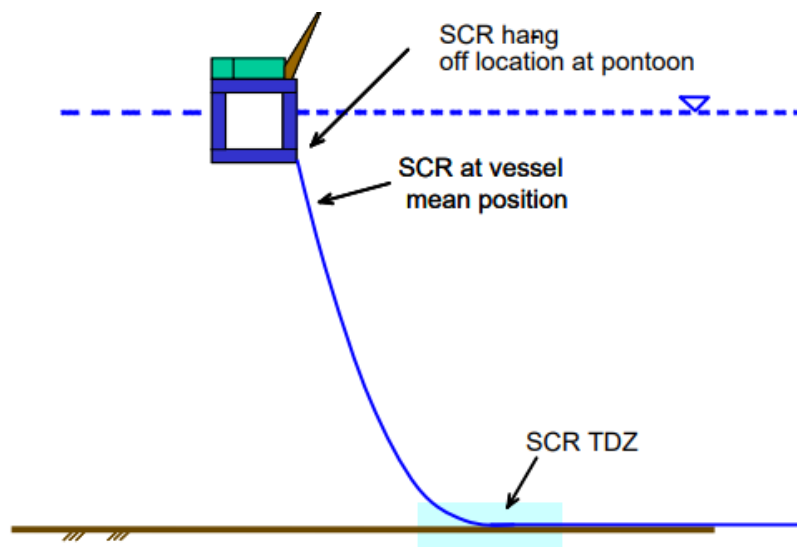


Figure 3-6: A schematic of SCR [22]

3.3.2 Steel Lazy Wave Riser Configuration (SLWR)

The traditional SCR configuration deployed from an FPSO is almost impossible to utilize in deepwater developments due to large floater motion, which causes high fatigue damage near the TDP [7]. In 1996, Karunakaran et al. [7] proposed an efficient configuration to overcome this problem which was then named “Low Long Wave Configuration”. This configuration is now called the Steel Lazy Wave Riser (SLWR). An SLWR configuration is achieved by adding buoyancy elements along the length in a traditional SCR. The buoyancy section separates the motion between the riser and floater and acts as a damper [5]. The first SLWR was installed in 2008 at the BC-10 field in Brazil, and the fabrication and installation were carried out by Subsea7 [3]. Since then, SLWRs have been successfully deployed in deepwater projects in

GoM, Offshore Brazil and several other projects [4]. Figure 3-7 shows the typical SLWR configuration [24].

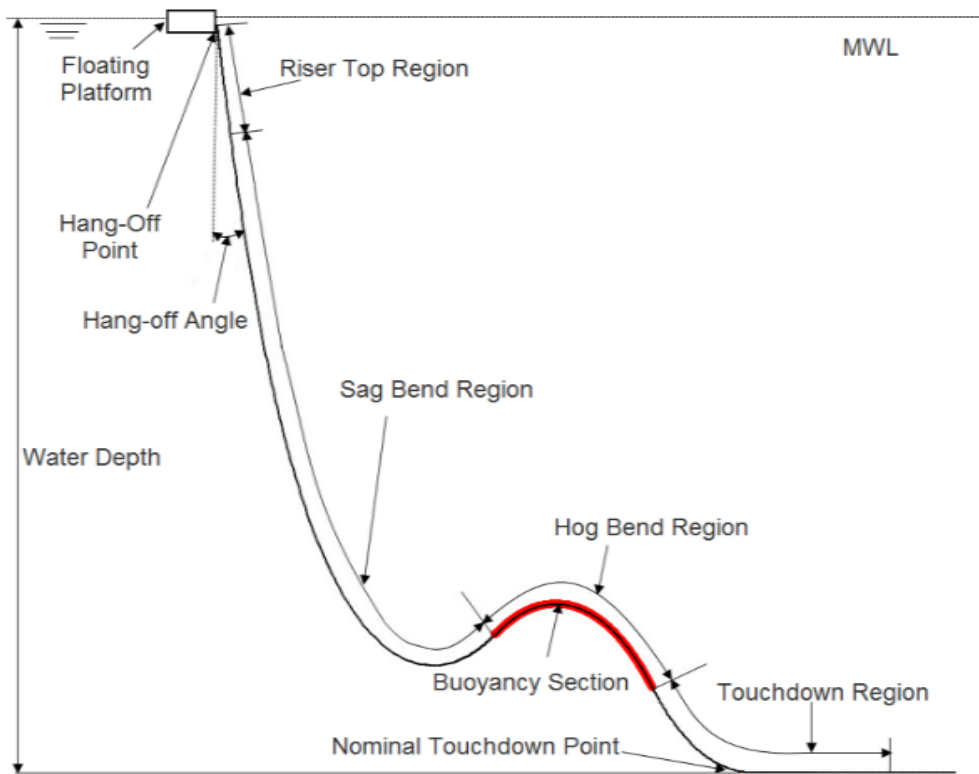


Figure 3-7: A typical SLWR configuration [24]

3.3.3 Initial Static State Solution for SLWR Configuration

A typical SLWR has four sections: an upper catenary, a buoyant middle section, a lower catenary, and a bottom section. Due to the complex geometry and number of parameters, SLWR has attracted several professionals to develop a method that defines its configuration. In 2013, Cheng et al. [4] proposed a method based on intuitive observations. Another method is to use the catenary theory to describe the SLWR configuration proposed in OC2017 A-001; Handbook on the design and operation of flexible risers [18]. The method proposed by Cheng et al. [4] is described below. Figure 3-8 shows the relevant parameters used to form the static state solution for SLWR.

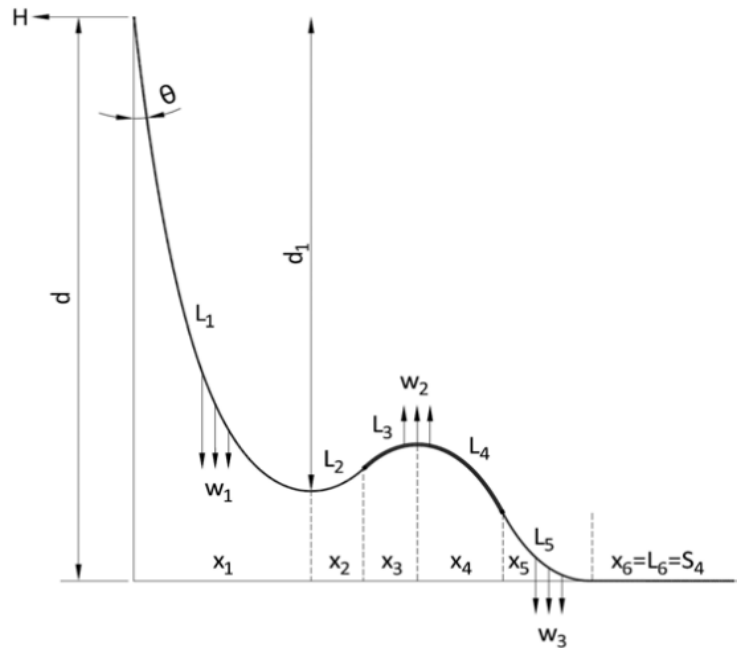


Figure 3-8: SLWR parameters [4]

Parameters:

- d : Water depth
- H : Horizontal component of tension at hang-off point
- w_1 : Submerged weight of L_1
- w_2 : Submerged weight of L_2
- w_3 : Submerged weight of L_3
- $L_1, L_2, L_3, L_4, L_5, L_6$: Segment lengths
- $x_1, x_2, x_3, x_4, x_5, x_6$: Horizontal projection of each segment length
- $S_1 = L_1 + L_2$
- $S_3 = L_5$

Variables:

- θ : Departure angle
- d_1 : Equivalent payload water depth
- $S_2 = L_3 + L_4$

The static state solution can be derived as follows.

$$a_1 \sinh\left(\frac{x_1}{a_1}\right) + a_1 \sinh\left(\frac{x_3}{a_2}\right) = L_1 + L_2 = S_1 \quad 1$$

$$a_2 \sinh\left(\frac{x_3}{a_2}\right) + a_2 \sinh\left(\frac{x_5}{a_3}\right) = L_3 + L_4 = S_2 \quad 2$$

$$a_1 \cosh\left(\frac{x_1}{a_1}\right) - (a_1 + a_2) \cosh\left(\frac{x_3}{a_2}\right) + (a_2 + a_3) \cosh\left(\frac{x_5}{a_3}\right) = a_3 + d \quad 3$$

$$\text{Buoyancy ratio} = 1 + \frac{w_2}{w_1} = 1 + \frac{a_1}{a_2} \quad 4$$

$$\text{Where; } a_1 = \frac{H}{w_1}, \quad a_2 = \frac{H}{w_2}, \quad a_3 = \frac{H}{w_3} \quad 5$$

The static state solution can be obtained using equations 1, 2, 3, 4, and 5. a_1 , a_2 , and a_3 are the minimum bending radii at the sag bend, hog bend and touch down locations. The above system has a determinate solution for known departure angle θ , equivalent payload water depth d_1 , and buoyancy section length S_2 [4].

3.4 Selection of SLWR over SCR for Deepwater Applications

Several studies have been done to find the pros and cons of SCR and SLWR. Cheng et al. [4] have compared the Touch Down Point (TDP) movement of deepwater SLWR and SCR operated from FPSOs. Their findings show that SCR has a higher TDP movement compared to SLWR. The less TDP moves, the more efficient the riser system is. Another observation is that the TDP movement is more influenced by the heave (vertical) motion than the surge (horizontal) motion [4]. Figure 3-9 further illustrates their findings.

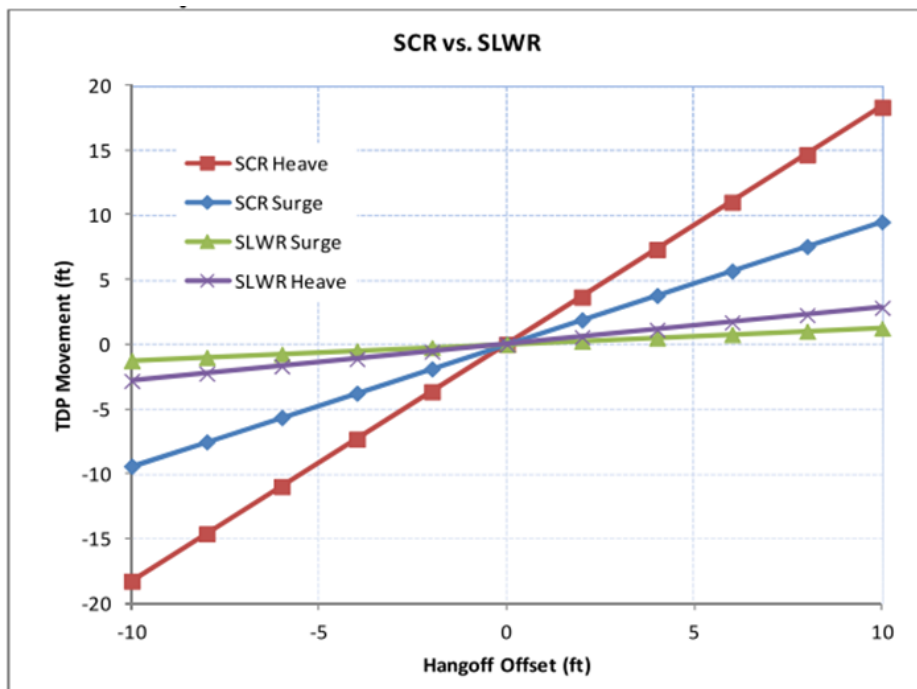


Figure 3-9: TDP movement of SCR and SLWR [4]

Gemilang et al. [25] have compared three different riser concepts' static state effective tension for deepwater conditions in a separate study. These three different risers are SCR, SLWR and WDSCR (Weight Distributed Steel Catenary Riser). SLWR has the lowest effective tension variation along the riser. This is also valid for the dynamic state as well. This implies that the payload at the riser hang-off is also less for the SLWR. This is mainly due to the upward buoyancy provided by the buoyancy modules in the riser [25]. Figure 3-10 further illustrates this.

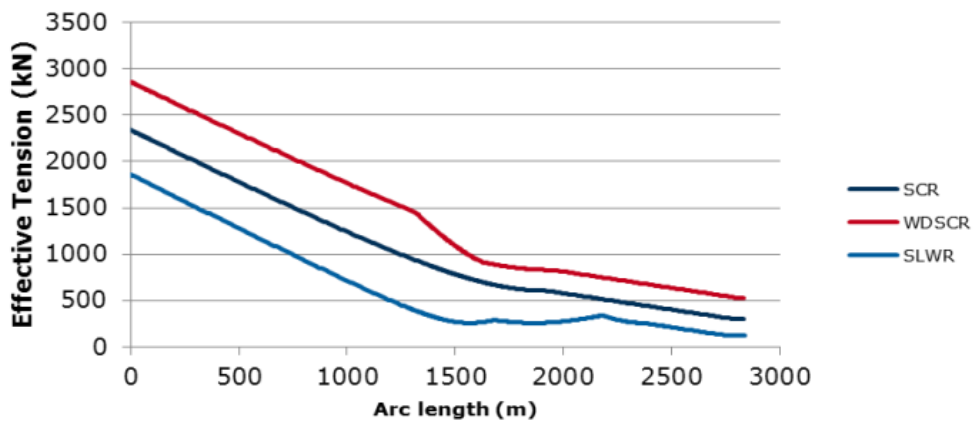


Figure 3-10: Static effective tension variation of different risers [25]

A separate study by Yue et al. [21] compares the fatigue performance of TDP for SCR and SLWR. SLWR has a much higher fatigue life than an SCR at the TDP. Their findings are illustrated in Figure 3-11. Hence SLWRs are more suitable for deepwater applications due to their fatigue performance at the touch down point [21].

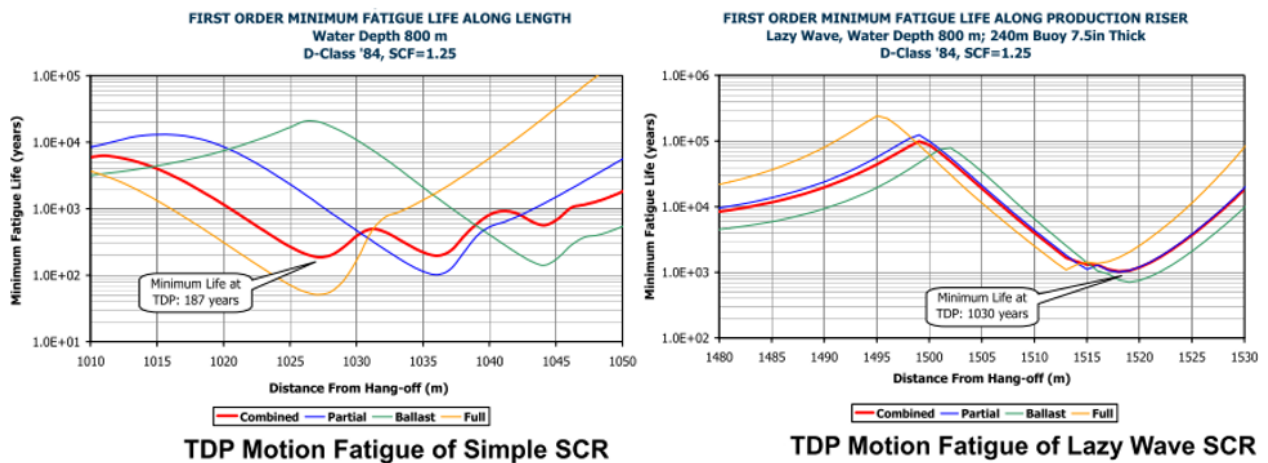


Figure 3-11: Fatigue performance at TDP for SCR and SLWR [21]

The fatigue life at the TDP is governed by the floater motion [7]. Gemilang et al. [25] further show that the SLWRs can handle large downward velocities at the riser hang-off point caused by floater motion. This makes SLWRs a more preferred solution for deepwater developments. Their finding is illustrated in Figure 3-12 [25].

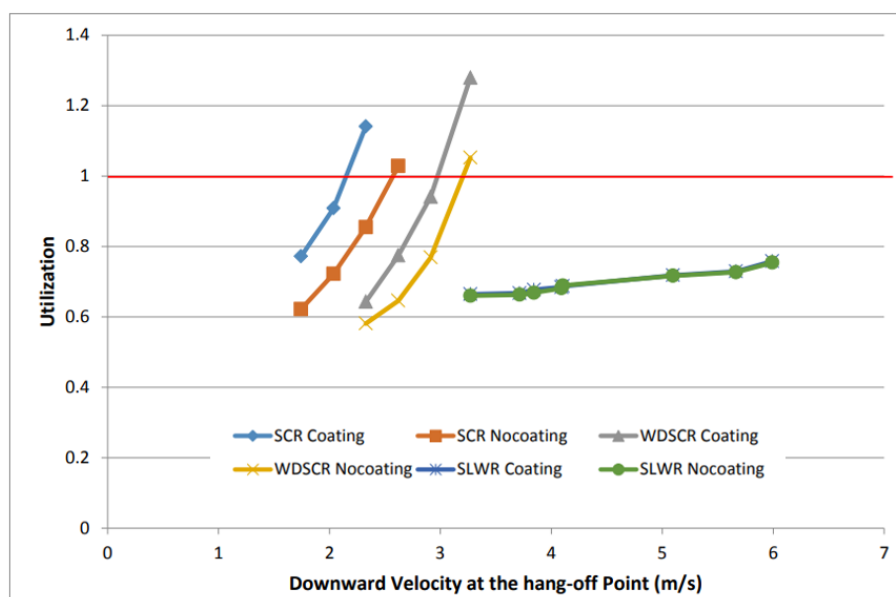


Figure 3-12: Utilization vs downward velocity at riser hang-off point [25]

Higher bending moment in the sag and hog bends and touch down point (both in the static and dynamic state) is one of the disadvantages of the SLWR. Gemilang et al. [25] have shown this in their research work. This is illustrated in Figure 3-13.

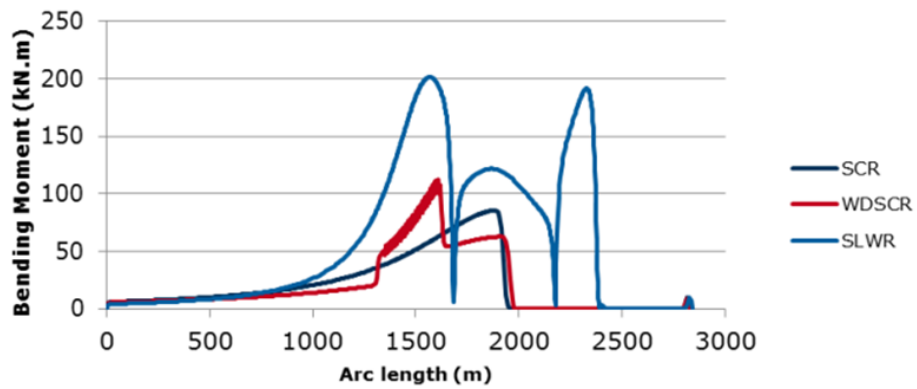


Figure 3-13: Static bending moment variation along risers [25]

4 Codes and Standards for Riser Design

4.1 Introduction

The terms “code of practice”, “standards”, and “specifications” are used differently in different parts of the world. One must need to understand the hierarchy of the applicability of the particulars depending on the region [26]. As per the International Standards Organization (ISO), a standard is “a set of documented agreements containing technical specifications or other precise criteria as guidelines, definitions, or characteristics to ensure that the materials, products, processes, and services fit their purpose”. When government bodies adopt a standard, it becomes a code of practice or simply a code. Codes will serve as legal documents when a jurisdiction process is involved. Specifications are the specifier's means of conveying particular requirements to the constructor, supplier or producer. They can be standard specifications or tailor-made to suit the client's requirements [26].

4.2 Overview of Codes and Standards for Riser Design

Industry-leading riser design codes and standards are mentioned below [27].

- API RP 2RD: Design of Risers for Floating Production Systems (FPSs) and Tension-Leg Platforms (TLPs) by the American Petroleum Institute [28]
- DNV-OS-F201: Dynamic Risers by DNV [29]
- DNV-OS-F101: Submarine Pipeline Systems by DNV [30]
- API RP 1111: Design, Construction, Operation, and Maintenance of Offshore Hydrocarbon Pipelines (Limit State Design) by American Petroleum Institute

Generally, there are two different design methods adopted in the riser design. They are Working Stress Design (WSD) and Load Factor Resistance Design (LRFD), also known as Limit State Design (LSD). API RP 2RD follows WSD methodology and the design criterion uses one safety factor on Von Mises stress. This single safety factor covers uncertainties and inaccuracies due to loads and materials. DNV-OS-F201 has two design approaches. They are WSD and LRFD. The LRFD methodology uses partial safety factors for each load effect and resistance [31].

It is essential to be consistent when using design codes and standards. This means that one design code should be used during the whole design process. Since DNV-OS-F201 provides design guidelines for WSD and LRFD approaches, it is selected as the design standard for this research. Figure 4-1 shows DNV's framework for riser design.

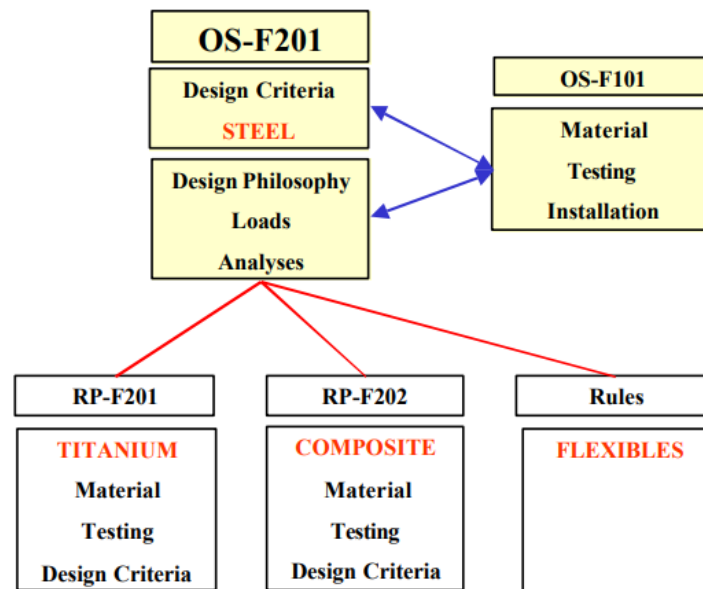


Figure 4-1: DNV's framework for riser design [29]

DNV-OS-F201 mentions three safety classes that need to be considered during the design. These safety classes are based on the potential failure consequences. Safety classes depend on the following factors.

- The type of fluid in the riser
- The location of the riser
- Status of the riser (i.e., whether in the operational state or temporary state)

The classification of safety classes is shown in Table 4-1.

Table 4-1: Classification of safety classes [29]

<i>Safety class</i>	<i>Definition</i>
Low	Where failure implies low risk of human injury and minor environmental and economic consequences.
Normal	For conditions where failure implies risk of human injury, significant environmental pollution or very high economic or political consequences.
High	For operating conditions where failure implies high risk of human injury, significant environmental pollution or very high economic or political consequences.

4.3 DNV-OS-F201 LRFD Approach

DNV-OS-F201: Dynamic Riser [29] provides an LRFD design approach as described in this chapter. The fundamental approach of the LRFD method is to verify that the factored design loads are below the factored design resistance for any limit state. The general LRFD safety format is expressed as:

$$g(S_P; \gamma_F \cdot S_F; \gamma_A \cdot S_A; R_k; \gamma_{SC}; \gamma_m; \gamma_C; t) \leq 1 \quad 6$$

where:

- S_P – Pressure loads
- S_F – Load effect from functional loads
- γ_F – Functional load effect factor
- S_E – Load effect from environmental loads
- γ_E – Environmental load effect factor
- S_A – Load effect from accidental loads
- γ_A – Accidental load effect factor
- R_K – Generalized resistance
- γ_{SC} – Resistance factor for safety class
- γ_m – Resistance factor for material uncertainty

-
- γ_c – Resistance factor for special conditions
 - t – Time

To have a safe design, the above equation should be satisfied. If not, there is a possibility of failure. Hence design process is an iterative process until it satisfies the above requirement. This is illustrated in Figure 4-2.

Code specifies different limit states a riser can experience during its design life. These limit states are associated with different failure modes. The four different limit states as per DNV-OS-F201 are mentioned below. These limit states are further explained in detail in this chapter.

- Serviceability Limit State (SLS)
- Ultimate Limit State (ULS)
- Accidental Limit State (ALS).
- Fatigue Limit State (FLS)

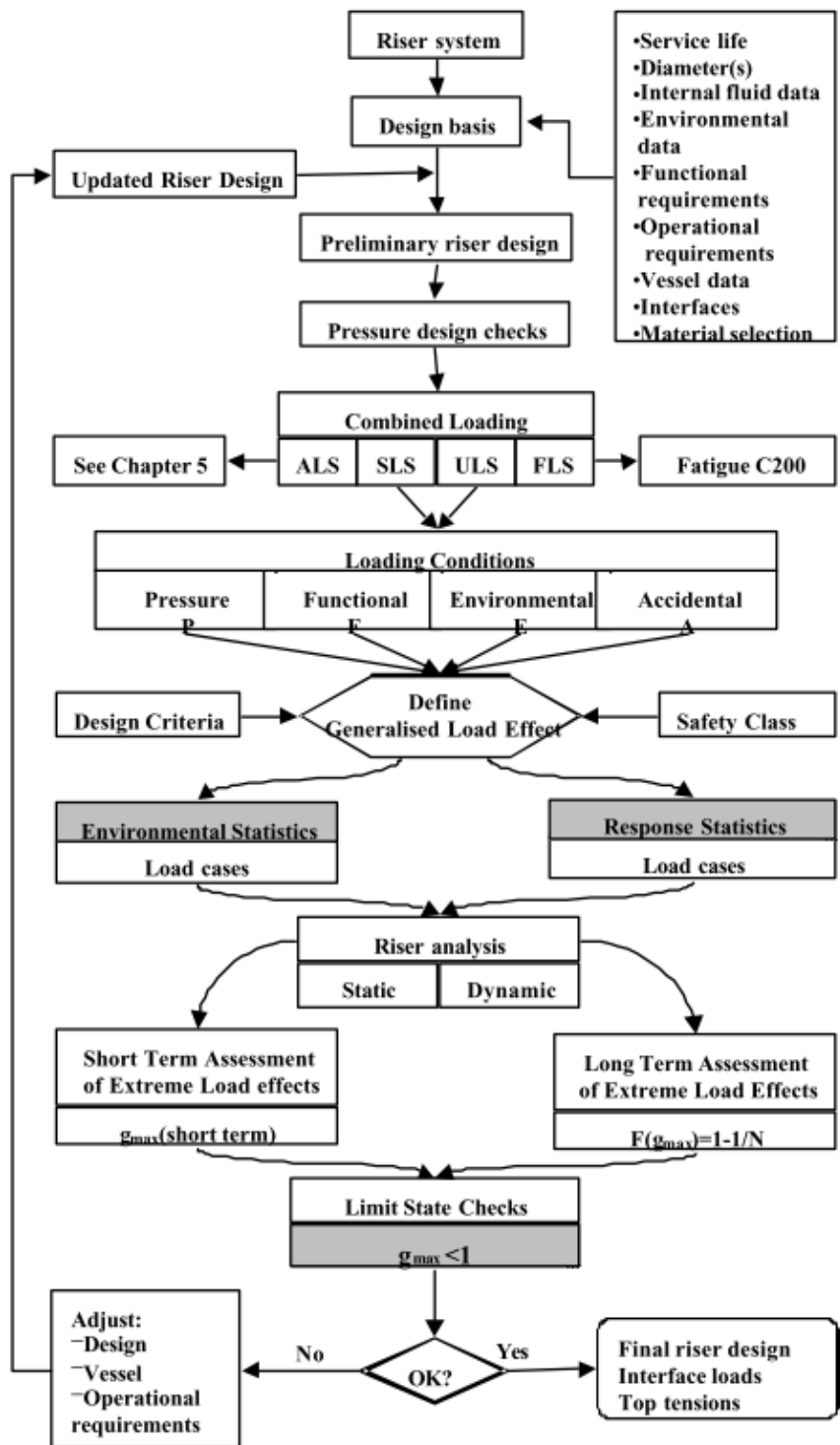


Figure 4-2: Riser design approach as described in DNV-OS-F201 [29]

4.3.1 Load Effects

Design load effects are obtained by multiplying them with their corresponding load effect factor. Load effects are classified into four different classes.

- Functional loads (F-loads)
- Environmental loads (E-loads)
- Pressure loads (P-loads)
- Accidental loads (A-loads)

Examples of different load effects are shown in Table 4-2. When several load effects enter into one design check, several load combinations need to be checked. The corresponding load effect factors are shown in Table 4-3. These load effect factors are relevant to all four limit states.

Table 4-2: Categorization of loads (load effects) [29]

<i>F-loads</i>	<i>E-loads</i>	<i>P-loads</i> ⁷⁾
Weight and buoyancy ⁶⁾ of riser, tubing, coatings ⁶⁾ , marine growth ²⁾ , anodes, buoyancy modules, contents and attachments Weight of internal fluid Applied tension for top-tension risers Installation induced residual loads or pre-stressing Pre-load of connectors Applied displacements and guidance loads, including active positioning of support floater Thermal loads Soil pressure on buried risers Differential settlements Loads from drilling operations Construction loads and loads caused by tools	Waves Internal waves and other effects due to differences in water density. Current Earthquake ⁴⁾ Ice ³⁾ Floater motions induced by wind, waves and current, i.e.: — Mean offset including steady wave drift, wind and current forces — Wave frequency motions — Low frequency motions	External hydrostatic pressure Internal fluid pressure: hydrostatic, static and dynamic ³⁾ contributions, as relevant Water Levels

Table 4-3: Load effect factors [29]

<i>Limit state</i>	<i>F-load effect</i>	<i>E-load effect</i>	<i>A-load effect</i>
	γ_F	γ_E	γ_A
ULS	1.1 ¹⁾	1.3 ²⁾	NA
FLS	1.0	1.0	NA
SLS & ALS	1.0	1.0	1.0
NOTES			
1) If the functional load effect reduces the combined load effects, γ_F shall be taken as 1/1.1.			
2) If the environmental load effect reduces the combined load effects, γ_E shall be taken as 1/1.3.			

4.3.2 Resistance

DNV-OS-F201 provides resistance factors to be applied on three different levels. These factors account for model uncertainties and tolerances. These resistance factors should be applied for all limit states unless specified.

- γ_{SC} is linked to the safety class and accounts for failure consequences
- γ_m accounts for material uncertainties
- γ_c account for special conditions which applies to different limit states

Relevant resistance factors extracted from DNV-OS-F201 are shown in the below tables.

Table 4-4: γ_{SC} Safety class resistance factors [29]

<i>Low</i>	<i>Normal</i>	<i>High</i>
1.04	1.14	1.26

Table 4-5: γ_m Material resistance factors [29]

<i>ULS & ALS</i>	<i>SLS & FLS</i>
1.15	1.0

Table 4-6: γ_c Simplified check for Accidental loads [29]

<i>Prob. of occurrence</i>	<i>Safety Class Low</i>	<i>Safety Class Normal</i>	<i>Safety Class High</i>
$>10^{-2}$	Accidental loads may be regarded similar to environmental loads and may be evaluated similar to ULS design check		
$10^{-2} \cdot 10^{-3}$	To be evaluated on a case by case basis		
$10^{-3} \cdot 10^{-4}$	$\gamma_c = 1.0$	$\gamma_c = 1.0$	$\gamma_c = 1.0$
$10^{-4} \cdot 10^{-5}$		$\gamma_c = 0.9$	$\gamma_c = 0.9$
$10^{-5} \cdot 10^{-6}$	Accidental loads or events		$\gamma_c = 0.8$
$<10^{-6}$	may be disregarded		

4.3.3 Serviceability Limit State (SLS)

The SLS mentions that the riser should remain in service and properly operate during regular operations (functional state). Consideration should be given to four failure modes as below.

- Clearance – no contact between risers, mooring lines and other system components

-
- Excessive angular response – Angular deflection should be within specified limits
 - The excessive top displacement between riser and floater
 - Mechanical function during make-up/ break-out

DNV Code suggests a few design controls that need to be carried out to have a safe design.

- Weather limitations shall be followed during the installation to avoid interference with other system components
- Ovalization limit due to bending – To avoid premature local buckling, the total out-of-roundness should be limited to 3%, as stated in the equation below.

$$f_0 = \frac{D_{max} - D_{min}}{D} \leq 0.03 \quad 7$$

where:

f_0 – Ovality

D_{max} – Maximum outer diameter

D_{min} – Minimum outer diameter

D – Initial pipe outer diameter

- The riser system needs to have sufficient stroke to avoid damage to the riser, components, and equipment. Here, the stroke refers to the travel of the tensioner, where the top tensioner maintains a constant tension on the riser to limit bending.

4.3.4 Ultimate Limit State (ULS)

The ULS mentions that the riser should remain intact and avoid rupture during its design life but not necessarily be able to operate. ULS corresponds to maximum resistance to applied loads for operating conditions with an annual exceedance probability of 10^{-2} . Relevant failure modes are as follows.

- Bursting
- Hoop bucking (collapse)
- Propagating buckling

-
- Gross plastic deformation and associated local buckling
 - Gross plastic deformation and associated local and hoop buckling
 - Unstable fracture and gross plastic deformation
 - Liquid tightness
 - Global buckling

DNV states a few design checks to be carried out in ULS to achieve a safe design.

- Bursting criterion

Pipes subjected to net internal overpressure must be designed to satisfy the following conditions.

$$(p_{li} - p_e) \leq \frac{p_b(t_1)}{\gamma_m \cdot \gamma_{SC}} \quad 8$$

The burst resistance is given by,

$$p_b(t_1) = \frac{2 \cdot 2 \cdot t_1}{\sqrt{3} \cdot (D - t_1)} \cdot \min\left(f_y; \frac{f_u}{1.15}\right) \quad 9$$

The following equation gives the minimum required wall thickness (t_1) for a straight pipe without allowances.

$$t_1 = \frac{D}{1 + \frac{4}{\sqrt{3}} \cdot \frac{\min\left(f_y; \frac{f_u}{1.15}\right)}{\gamma_m \cdot \gamma_{SC} \cdot (p_{li} - p_e)}} \quad 10$$

where:

p_{li} – Local incidental pressure ($p_{inc} + \rho_i \cdot g \cdot h$)

ρ_i – Internal fluid density

p_{inc} – Incidental pressure ($1.1 \cdot p_{design}$)

p_e – External pressure

f_y – Material yield strength

f_u – Material tensile strength

- Hoop buckling (Collapse) criterion

If the external overpressure is dominant, hoop buckling can occur. To avoid failure, the following criteria should be met.

$$(p_e - p_{min}) \leq \frac{p_c(t_1)}{\gamma_m \cdot \gamma_{SC}} \quad 11$$

The resistance for external pressure $p_c(t)$ is given by the following equation and can be found in DNV-ST-F101 [30].

$$(p_c(t) - p_{el}(t)) \cdot (p_c^2(t) - p_p^2(t)) = p_c(t) \cdot p_{el}(t) \cdot p_p(t) \cdot f_0 \cdot \frac{D}{t} \quad 12$$

The pipe's elastic collapse pressure $p_{el}(t)$ is given by the following equation.

$$p_{el}(t) = \frac{2 \cdot E \cdot \left(\frac{t}{D}\right)^3}{1 - \nu^2} \quad 13$$

The plastic collapse pressure $p_p(t)$ is given by:

$$p_p(t) = \frac{2 \cdot t \cdot f_y \cdot \alpha_{fab}}{D} \quad 14$$

where:

t – Should be substituted with t_1 or t_2 where necessary

p_{min} – Minimum internal pressure

f_0 – Initial ovality as described in Eq. 7

α_{fab} – Fabrication factor as shown in Table 4-7

E – Young's modulus of material

ν – Poisson's ratio

Table 4-7: Fabrication factor α_{fab} [29]

<i>Tensile strength or seamless pipe</i>	<i>Compressive strength for welded pipe</i>	
	<i>UOE/</i>	<i>UO/TRB</i>
1.00	0.85	0.925

UOE, UO and TRB (Three Roll Bending) are three different cold-forming processes used to manufacture pipes.

- Propagating buckling criterion

Even though the hoop buckling criterion mentioned above is satisfied, hoop buckling can be initiated due to accidental pressures. To avoid this, the riser design should satisfy the criterion mentioned below.

$$(p_e - p_{min}) \leq \frac{p_{pr}}{\gamma_c \cdot \gamma_m \cdot \gamma_{SC}} \quad 15$$

The resistance against propagation buckling p_{pr} is calculated as,

$$p_{pr} = 35 \cdot f_y \cdot \alpha_{fab} \cdot \left(\frac{t_2}{D}\right)^{2.5} \quad 16$$

$$t_2 = t_{nom} - t_{corr} \quad 17$$

where:

$\gamma_c = 1.0$ if no buckling is allowed

$\gamma_c = 0.9$ if buckling is allowed to travel a short distance where the neighbouring pipe section acts as a buckle arrestor.

t_{nom} – Nominal pipe wall thickness

t_{corr} – Corrosion allowance

All the other symbols have similar meanings as mentioned above.

- Combined loading criterion

The following criterion needs to be checked when a pipe is subjected to bending moment, effective tension, and net internal overpressure.

$$(\gamma_m \cdot \gamma_{SC}) \cdot \left[\left\{ \left(\frac{|M_d|}{M_k} \right) \cdot \sqrt{1 - \left(\frac{p_{ld} - p_e}{p_b(t_2)} \right)^2} \right\} + \left(\frac{T_{ed}}{T_k} \right)^2 \right] + \left(\frac{p_{ld} - p_e}{p_b(t_2)} \right)^2 \leq 1 \quad 18$$

The following criterion needs to be checked when a pipe is subjected to bending moment, effective tension, and net external overpressure.

$$(\gamma_m \cdot \gamma_{SC})^2 \cdot \left\{ \left(\frac{|M_d|}{M_k} \right) + \left(\frac{T_{ed}}{T_k} \right)^2 \right\}^2 + (\gamma_m \cdot \gamma_{SC})^2 \cdot \left(\frac{p_e - p_{min}}{p_c(t_2)} \right)^2 \leq 1 \quad 19$$

The design bending moment M_d is:

$$M_d = \gamma_F \cdot M_F + \gamma_E \cdot M_E + \gamma_A \cdot M_A \quad 20$$

where M_F , M_E , M_A are the bending moments due to different load effects

The plastic bending moment resistance M_k is:

$$M_k = f_y \cdot \alpha_c \cdot (D - t_2)^2 \cdot t_2 \quad 21$$

The design effective tension is given by:

$$T_{ed} = \gamma_F \cdot T_{eF} + \gamma_E \cdot T_{eE} + \gamma_A \cdot T_{eA} \quad 22$$

where T_{eF} , T_{eE} , T_{eA} are the effective tensions due to different load effects

The plastic axial force resistance T_k is,

$$T_k = f_y \cdot \alpha_c \cdot \pi \cdot (D - t_2) \cdot t_2 \quad 23$$

where:

p_{ld} – Local internal design pressure

α_c – Parameter accounting for strain hardening as provided in the DNV code

4.3.5 Accidental Limit State (ALS)

DNV-OS-F201 defines the ALS as a limit state due to accidental loads which occur due to accidental incidents. Events of such nature have an annual probability of occurrence less than 10^{-2} . A few typical accidental events are mentioned below.

- Fires and accidents
- Impact or collisions with risers, anchors, floaters and dropped objects
- Hook or snag loads
- Support system failures such as heave compensators, mooring lines and loss of buoyancy
- Exceedance of incidental internal pressure
- Environmental events such as earthquakes, tsunamis, and icebergs

Before performing the ALS, the riser should be checked for ULS. DNV-OS-F201 provides simplified design guidelines to check for ALS.

4.3.6 Fatigue Limit State (FLS)

FLS is an ultimate limit state where the riser system needs to have adequate safety against fatigue damage during the service life. All the cyclic loadings the riser experiences during the design life needs to be considered in the evaluation, including temporary phases like transportation and installation. The primary reasons for fatigue damage in risers are mentioned below.

- Waves
- Currents (Vortex-Induced Vibration – VIV)
- Vessel motion
- Slugging

The stress to be used for fatigue damage accumulation is the cyclic principal stress. Cyclic nominal stress component (σ) is a linear combination of axial and bending stress given by:

$$\sigma = \frac{T_e}{\pi \cdot (D - t_3) \cdot t_3} + \frac{32 \cdot M \cdot (D - t_3)}{\pi \cdot (D^4 - (D - 2 \cdot t_3)^4)} \quad 24$$

where:

$$t_3 = t_{nom} - 0.5 \cdot t_{corr} \quad 25$$

T_e – Effective tension

M – Bending moment

DNV-OS-F201 specifies two methods that can be used to evaluate fatigue damage. One is based on S-N curves, and the other is based on fatigue crack propagation.

- The method based on S-N curves

This method is commonly used during the design phase for fatigue assessment. The relevant S-N curves should be based on DNV-RP-C203 [32]. When using S-N curves, considerations should be given to the following criteria [32].

- Assessment of the short-term distribution of nominal stress range
- Proper S-N curve selection
- Determination of stress concentration factor (SCF) based on DNV-RP-C203
- Determination of accumulated fatigue damage (D_{fat}) over short-term conditions

The fatigues criterion can be written as below.

$$D_{fat} \cdot DFF \leq 1.0 \quad 26$$

where:

D_{fat} – Accumulated fatigue damage calculated using Palmgren-Minor Rule

DFF – Design fatigue factor as per Table 4-8

Table 4-8: Design fatigue factors DFF [29]

<i>Safety class</i>		
<i>Low</i>	<i>Normal</i>	<i>High</i>
3.0	6.0	10.0

- The method based on crack propagation

Components of the riser should be designed and inspected such that the expected maximum initial defect size should not grow to a critical size during service life or first inspection. DNV-OS-F201 specifies several steps that need to be followed in the assessment.

The fatigue crack growth life should be designed and inspected to satisfy the following criterion.

$$\frac{N_{tot}}{N_{cg}} \cdot DFF \leq 1.0 \quad 27$$

where:

N_{tot} – Total number of stress cycles applied during a service inspection

N_{cg} – Number of stress cycles necessary to increase the defect from the initial to the critical defect size

DFF – As shown in Table 4-8

4.4 DNV-OS-F201 WSD Approach

DNV-OS-F201 suggests an alternative approach that can be used for the combined loading check for pipes with a D/t ratio less than 30. This provides a more conservative design compared to the LRFD approach.

In the WSD method, design load effects are equal to their corresponding characteristic values. That means all the load effect factors and resistance factors are equal to one. Instead of these

factors, a basic usage factor is introduced to the design. Basic usage factors are shown in Table 4-9.

Table 4-9: Usage factor η for combined loading [29]

<i>Low</i>	<i>Normal</i>	<i>High</i>
0.83	0.79	0.75

Two checks need to be performed in the combined loading as described below. The notations have similar meanings as described in previous chapters.

- When pipes are subjected to bending moment, effective tension, and net internal pressure:

$$\left[\left\{ \left(\frac{|M_d|}{M_k} \right) \cdot \sqrt{1 - \left(\frac{p_{ld} - p_e}{p_b(t_2)} \right)^2} \right\} + \left(\frac{T_e}{T_k} \right)^2 \right] + \left(\frac{p_{ld} - p_e}{p_b(t_2)} \right)^2 \leq \eta^2 \quad 28$$

- When pipes are subjected to bending moment, effective tension, and net external pressure:

$$\left\{ \left(\frac{|M_d|}{M_k} \right) + \left(\frac{T_e}{T_k} \right)^2 \right\}^2 + \left(\frac{p_e - p_{min}}{p_c(t_2)} \right)^2 \leq \eta^2 \quad 29$$

4.5 Selection of LRFD Approach over WSD Approach

WSD recommends a design factor that defines the maximum allowable design stress of members as a percentage of the yield strength of the material. These design factors are primarily based on historical criteria rather than any system's structural integrity. No published data suggest any correlation with increased risk between the design factor (0.72~0.8). Hence WSD method is a conservative approach [33].

LRFD method allows for a strain-based design approach where several safety factors are used on loads and resistance. These values are obtained from probabilistic approach methods. This leads to a less conservative design but is still safe for implementation. The LRFD method allows yielding to be reached or exceeded so that the structure can resist further loads and may encounter high levels of deformation without reaching an unstable mechanism [33]. Hence during this thesis, the LRFD approach proposed by DNV is used for all design purposes.

Figure 4-3 shows a comparison between LRFD and WSD when applied to the design of structures utilizing the AISC (American Institute of Steel Construction) steel design code for beam type members. Load conditions a) and b) are: a) functional loads and b) a combination of maximum environmental loads and associated functional loads [34]. AISC 9th stands for AISC Manual of Steel Construction: Allowable Stress Design 9th Edition (1989). AISC 13th Ed. stands for AISC Steel Construction Manual 13th Edition (2005), and AISC 2010 stands for Code of Standard Practice for Steel Buildings and Bridges (2010).

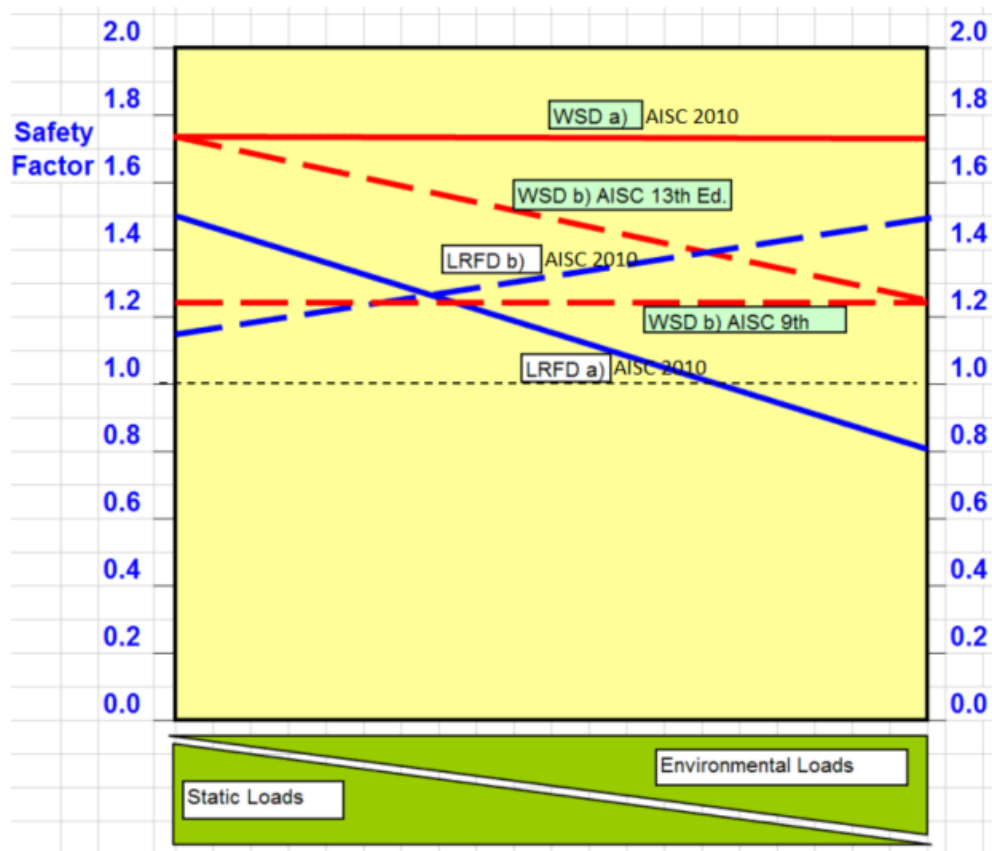


Figure 4-3: AISC's WSD and LFRD approach [34]

5 Riser Fabrication and Installation

5.1 Introduction

This chapter briefly explains the rigid steel riser (SCR and SLWR) fabrication methods and installation methods. The content in this chapter is comprised of relevant experience from the industry. The objective is to understand fabrication and installation methods to give the overall picture of riser concepts.

As per Bai et al. [16], the CAPEX (Capital Expenditure) of a pipeline (or riser) project can be broken down as follows. The following values are indicative and can vary depending on the nature of the project.

- Management and design 5%
- Materials and fabrication 55%
- Installation 29%
- Commissioning 1%
- Insurance 2%
- Miscellaneous 8%

The numbers above clearly show that a project's major cost components are fabrication and installation. Hence, selecting the best possible material and the installation method can save a significant amount of money from the project budget.

5.2 Riser Fabrication

The widely used material for rigid risers is the API X65 Carbon steel. The properties of different steel grades and the criteria for selecting piping material were described in Chapter 3.2. Corrosion Resistant Alloys (CRA) should be used when the well fluid comprises CO₂ and H₂S to avoid the corrosion of the internal surface [22].

Fabrication of rigid steel risers can be carried out either onshore or offshore. Onshore fabrication has an advantage over offshore fabrication since the girth weld inspection can be carried out in a controlled environment. Since steel risers are made up of a series of welded

pipes, the quality of the girth welds directly affects the fatigue performance of risers. These factors are pipe and weld material, joint dimensional tolerance, welding procedure and inspection criteria [23]. Maneschy et al. [35] mention several factors that need to be considered during the welding process.

- The hi/lo joint of two pipes should be controlled within a maximum range of ± 0.5 mm. Counter boring of pipeline ends is required to achieve this.
- Controlled welding to ensure satisfactory weld root and weld cap. This is required to minimize the welding flaw.
- Flush grinding of weld caps is required to ensure high fatigue performance.

Different girth welding techniques used in the industry are listed below [16]. Figure 5-1 shows a typical PGTAW girth weld in clad pipes.

- Gas Metal Arc Welding (GMAW)
- Gas Tungsten Arc Welding (GTAW)
- Flux Core Arc Welding (FCAW)
- Pulsed Gas Tungsten Arc Welding (PGTAW)
- Pulsed Gas Metal Arc Welding (PGMAW)

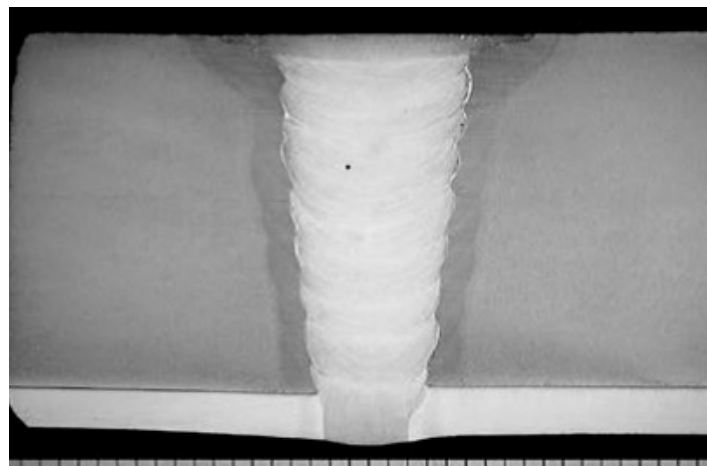


Figure 5-1: Mechanized PGTAW weld in clad pipes [3]

These welding techniques have been successfully applied for X65 line pipes. When welding higher strength grades (X70 and above) pipes, additional measures are required to maintain

weld quality. These measures are proper joint preparation, adequate preheat on pipes, and additional inter-run grinding [16]. The mechanized PGTAW process produces girth welds with high integrity but limited productivity [3]. To overcome this, Subsea 7 developed the PGMAW technique to achieve higher production rates while maintaining acceptable welding integrity for SCRs [3]. Figure 5-2 shows an operation of PGMAW.



Figure 5-2: PGMAW in operation [3]

For post-weld inspection, Non-Destructive Tests (NDT) can be used. Ultrasonic testing and Radiographic testing are two commonly used NDTs [36]. Testing guidelines are available in various design codes and standards.

5.3 Riser Installation

The offshore industry uses three main pipe laying (riser installation) methods. These three concepts are based on principles such as allowable bending stress, allowable axial stress, and the prevention of kicking. These three methods are as follows.

- S-Lay
- J-Lay
- Reel-Lay

5.3.1 S-Lay Method

S-Lay can be carried out from a lay-vessel or semi-submersible vessel. The s-lay vessel is special because of its long ramp extension called "Stinger" at the stern. There is a near-horizontal ramp in the vessel where several workstations such as welding and tension machines are located. Pipelines are cautiously fed into the sea by welding while the vessel moves forward. Pipes move along the rollers placed on both stinger and ramp. The pipeline bends over its curved support on its way to the sea and creates an "overbend". The stinger radius decides the curvature of the overbend [16].

There are several tensioners placed along the ramp. The purpose of applying tension is to control the curvature of the sag bend. The tension capacity of the vessel depends on the number of tensioners and the applied tension. The required tension is a function of water depth, the submerged weight of the pipe, radius of the overbend, departure angle and sag bend radius. These vessels have limitations for both maximum and minimum curvature. This limits the departure angle and the water depth it can operate. The roller supports are built up using some wheels on top and bottom. This method is called "S-lay" because the sag bend and overbend will form a configuration similar to "S" [16]. A schematic of an S-lay vessel and stinger arrangement is shown in Figure 5-3.

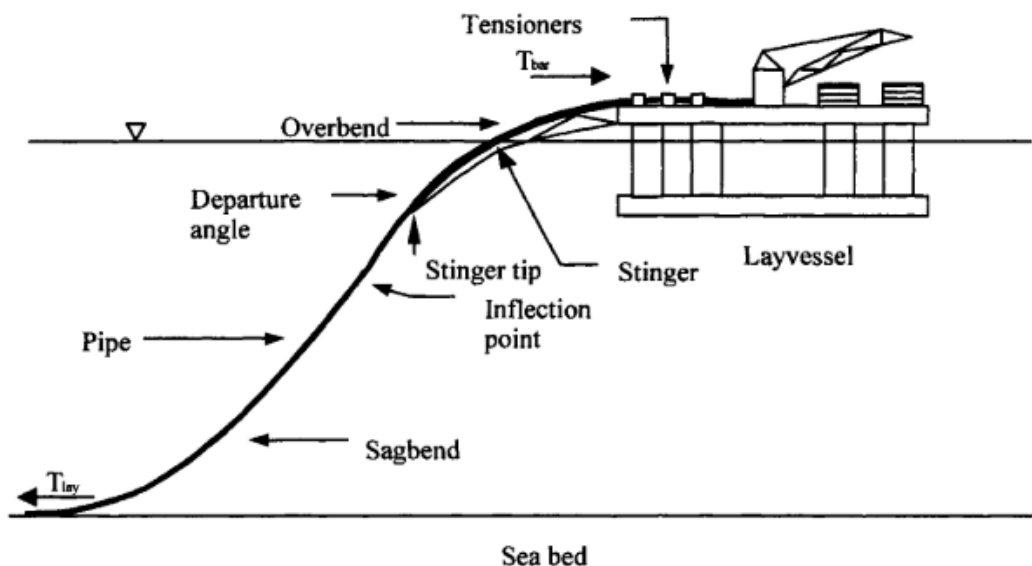


Figure 5-3: S-lay configuration [16]

During the installation, pipelines experience a combination of loads such as tension, bending, pressure and contact forces normal to the pipe at the roller supports and seabed. Typically, pipes are installed in empty conditions to increase the laying rate. S-lay has no limitation in pipe diameter or length. It is also quicker than other methods and suitable for shallow and intermediate water. Major modification of stinger is required in deepwater installations [16]. Figure 5-4 shows an S-lay operation by "Seven Borealis" owned by Subsea 7, Norway [37].



Figure 5-4: Seven Borealis, Subsea 7 [37]

5.3.2 J-Lay Method

The pipe configuration during the installation resembles the letter "J"; hence it is called the J-lay method. J-lay vessels have better dynamic motion characteristics compared to S-lay vessels. Since pipes are welded in a vertical tower, productivity is limited. Hence the lay rate is comparatively low compared to S-lay. J-Lay is not suitable for shallow water applications [16].

J-lay does not have an overbend section since the pipes leave the vessel almost vertical. The angle can vary from 0 to 15 degrees depending on the water depth. Due to this, the bending stresses in the pipes are also low. A stinger is also not required for this operation. The vessels are equipped with collars to hold the pipes, and they act as buckle arresters during the installation. Some vessels like "Seven Borealis" can install pipelines in both S-lay and J-lay

methods [16]. Figure 5-5 shows a schematic of the J-lay operation [38]. Figure 5-6 shows the J-lay vessel Saipem 7000 [39].

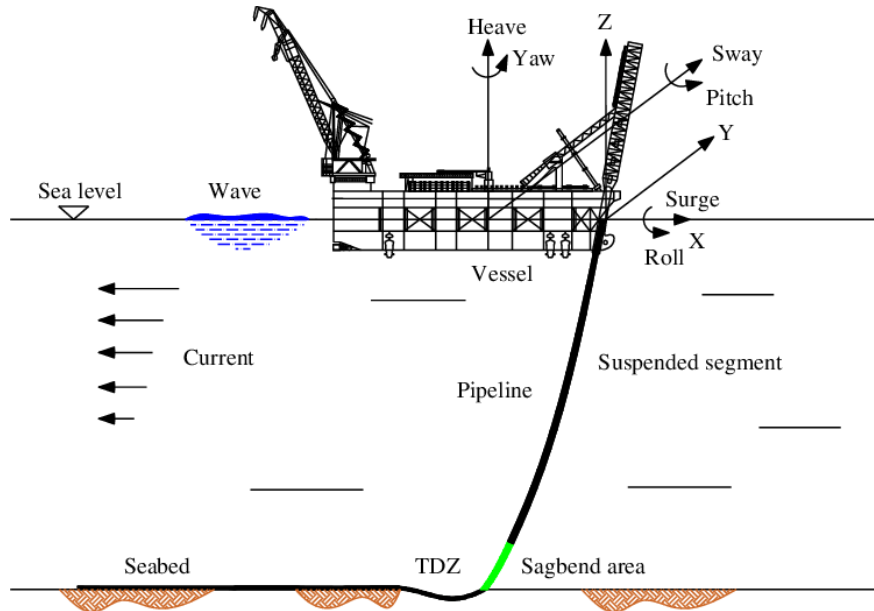


Figure 5-5: A schematic of J-lay operation [38]



Figure 5-6: Saipem 7000 [39]

5.3.3 Reel-Lay Method

Pipes are reeled into large circular reels in the vessel and laid directly from the reels on the seabed. This method uses special vessels designed for this task. Reel-lay is one of the most effective pipe laying methods for infield subsea flowlines and risers up to a 16-inch diameter. The main advantage of reel lay is that the welding and inspection can be done onshore in a controlled environment such as a spool base. A spool base is where fabrication happens and has a long path (about 1km) to lay the prefabricated pipelines until they are spooled into the reels [40].

The spooling is a unique operation where all the stalks are reeled into a spool stationed in the vessel by bending them plastically. The analysis and design for this operation are well researched and optimized constantly. Girth weld is the preferred welding method for joining pipes. Full-scale strain age testing is carried out to replicate the strains that the pipelines will experience during the whole operation [40].

Reel-lay is considered a cost-effective method to install SCRs and SLWRs where the installation site is not far from the spool base. A few such projects are Roncador in Brazil, Blind Faith in GoM, Guara and Lula in Brazil and BC-10 by Shell. "Seven Oceans" by Subsea 7 is one of the pioneering reeling vessels and has a successful track record of installing deep and ultra-deepwater [3]. Figure 5-7 shows a schematic of a reel-lay operation [41], and Figure 5-8 shows Seven Oceans in a pipe laying operation [40].

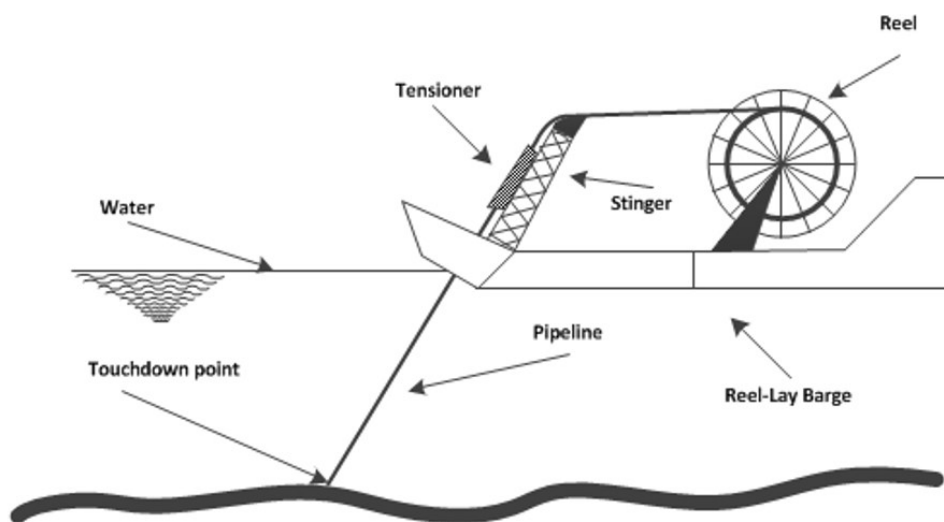


Figure 5-7: A schematic of Reel-lay operation [41]



Figure 5-8: Seven Oceans owned by Subsea 7 [40]

6 Design Basis and Input Data

6.1 Introduction

During this chapter, design methodology and relevant design input data are discussed. An SLWR operated from a spread moored FPSO in 2000m deepwater conditions in the Santos basin in Offshore Brazil is the selected concept for the extreme response analysis. A parametric study on fatigue life at TDP focuses on four other water depths: 1500m, 2000m, 2500m and 3000m. The riser will be designed and optimized to satisfy the strength and fatigue requirements. The input data is the basis for modelling the structure. Some design inputs are referred to the met-ocean and soil reports from the Santos basin. Hence, they are not fully disclosed due to confidentiality. The analysis is carried out using OrcaFlex 11.2 [42]. This is a proven software used in the industry to perform hydrodynamic analysis of offshore structures.

Reference standards and guidelines used in this work are as follows.

- DNV-OS-F101: Submarine Pipeline Systems [30]
- DNV-OS-F201: Dynamic Risers [29]
- DNV-RP-C203: Fatigue Design of Offshore Steel Structures [32]
- DNV-RP-C205: Environmental Conditions and Environmental Loads [43]
- DNVGL-OS-E301: Position Mooring [44]
- NORSOK N-003: Actions and Actions Effects [45]
- API Specification 5L: Specification for a Line Pipe [20]
- API RP 2SK: Design and Analysis of Station Keeping Systems [46]
- Met-ocean report for the Santos basin

6.2 Analysis Method

6.2.1 Global Analysis

Global analysis is based on static and dynamic analysis principles such as model discretization, the strength of materials, environmental loads, and soil mechanics to determine the combined

load effects on the riser system. This can be performed using analytical calculations, numerical simulations, or physical testing. The global riser model includes the complete riser system, including the stiffness, mass, damping and hydrodynamic effects on members and top and bottom boundary conditions [29]. The global analysis approach is shown in Figure 6-1.

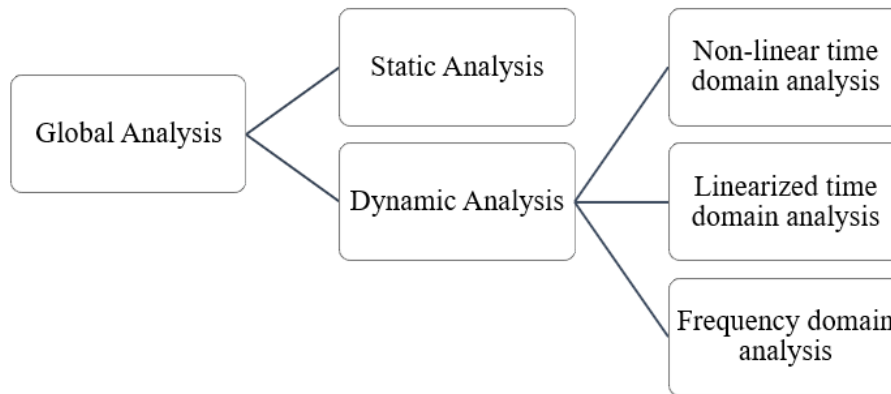


Figure 6-1: Global analysis approach [29]

The static analysis is performed to establish the initial equilibrium configuration of the riser due to the functional loads such as self-weight of the riser, buoyancy effect, hydrostatic effect, and top tension [29]. Static equilibrium configuration is the initial configuration used in the dynamic analysis. OrcaFlex 11.2 [42] calculates the static equilibrium based on the input data. In most situations, the static analysis is fast and reliable. For complex systems, convergence may take a long time. OrcaFlex uses a full nonlinear approach to solve the static equilibrium as suggested by DNV-OS-F201.

The dynamic analysis considers the external forces due to currents, direct wave, low frequency (LF) floater motion and wave frequency (WF) floater motion. These external loadings represent the real loads from Offshore Brazil. WF floater motion is calculated using RAOs (Response Amplitude Operator), and LF floater motion is calculated using vessel offsets from the mean position described in the following sections [29].

As shown above, dynamic analysis can be performed in three different methods. During this study, nonlinear time-domain analysis is used for the analysis. Riser systems are highly nonlinear structures due to nonlinearities introduced by hydrodynamic loading, geometric

stiffness, large rotations in 3-D space and possible material nonlinearities and seafloor contact. This method uses the Newton-Raphson method for stepwise numerical integration of the dynamic equilibrium equation. The nonlinear approach is good in representing possible non-Gaussian responses. Hence, this method estimates extreme responses with adequate numerical confidence [29].

6.2.2 Analysis Software – OrcaFlex 11.2

OrcaFlex [42] is a programme developed by Orcina Ltd. for static and dynamic analysis of offshore systems, including risers, mooring systems, installation and towed systems. This is a fully 3D nonlinear time-domain finite element analysis (FEA) programme. Lumped mass elements formulate the model, simplifying the mathematical formulation and faster response time. Each segment is connected with two straight segments with mass, weight, drag, and stiffness properties. Forces and moments are applied to nodes. Each segment is represented by two co-axial telescoping rods connected by axial and torsional springs and dampers. Formulation of the discretized model of an actual pipe for FEA is shown in Figure 6-2 [42].

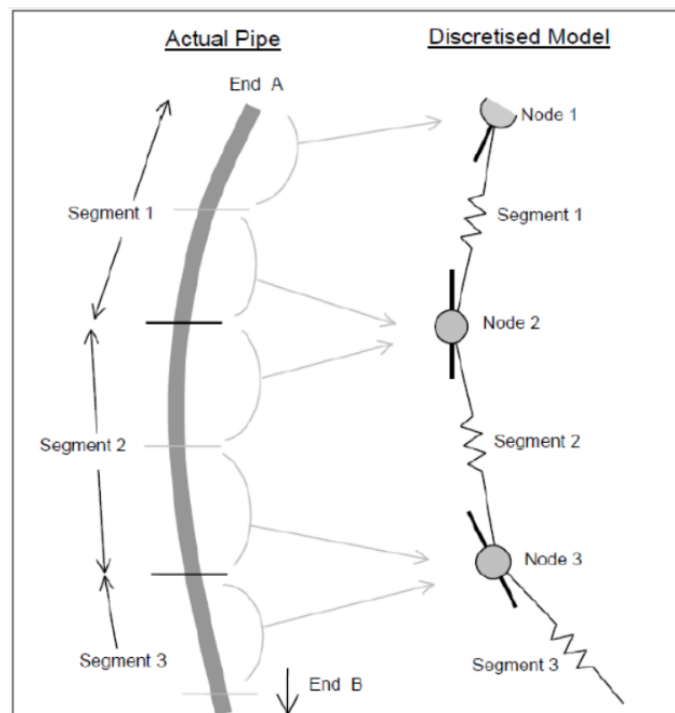


Figure 6-2: FEA model formulation in OrcaFlex [42]

6.3 Environmental Data

6.3.1 Location

The Southeast coast of Brazil is made of the states of Espírito Santo, Rio de Janeiro, São Paulo, Paraná, Santa Catarina and Rio Grande do Sul. This is where the main offshore oil fields and pre-salt reserves of Espírito Santo, Campos, Santos and Pelotas are located as shown in Figure 6-3. Santos Sedimentary basin (central pre-salt cluster) is the location for this study which covers 352,000km² and is located between 23°S and 28°S in the South Atlantic Ocean. It exhibits bathymetries that reach 3000m of depth and a sedimentary thickness of more than 10000m. This is one of the largest sedimentary basins in Brazil [47]. The field in consideration is located approximately 300km away from the shore.

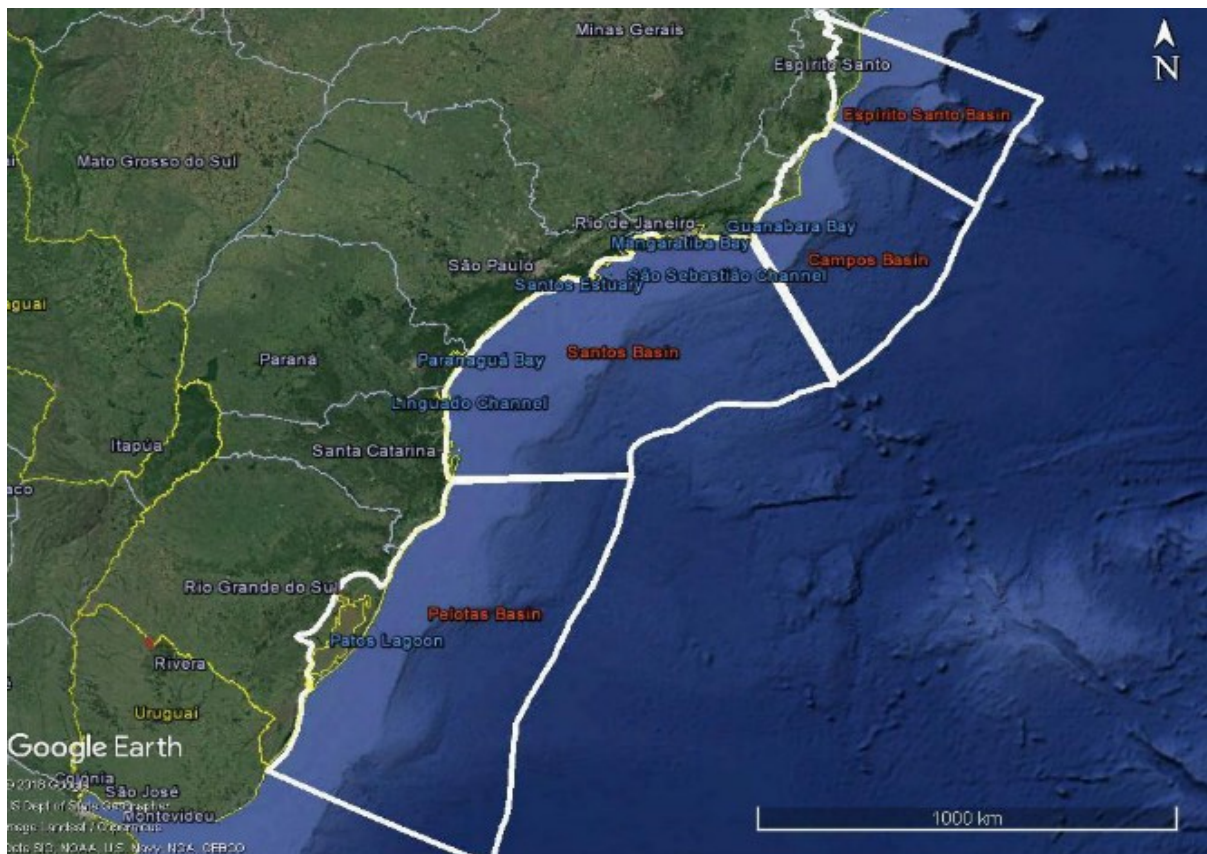


Figure 6-3: Basins of the Brazilian South and Southeast coasts [47]

6.3.2 Water Depth

A 2000m water depth with a constant seawater density of 1025kg/m³ and temperature of 10°C is selected for initial static, dynamic and fatigue analysis. Four water depths (1500m, 2000m, 2500m and 3000m) will be considered in the parametric studies on the fatigue life at the TDP.

6.3.3 Waves

The ULS/ALS extreme analysis is driven by extreme sea states represented by a combination of a 100-year wave and a 10-year current. Bjarte K. et al. [48] and Adejuwon A. et al. [49] have also shown that the above wave and current combination provides the worst response for SLWRs in the Santos basin. Wave induced fatigue is calculated using different H_s and T_p combinations according to the wave scatter diagram. All these data are referred to the met-ocean report from the Santos basin.

JONSWAP (Joint North Sea Wave Project) spectrum is used to model irregular waves, which is a modification of the Pierson-Moskowitz (PM) spectrum. PM spectrum was initially developed for a fully developed sea, while the JONSWAP spectrum extends the PM spectrum to include the fetch limited seas. The following equation describes the JONSWAP spectrum as described in DNV-RP-C205 [43].

$$S_J(\omega) = A_\gamma \cdot S_{PM}(\omega) \cdot \gamma^{\exp\left(-0.5 \cdot \left(\frac{\omega - \omega_p}{\sigma \cdot \omega_p}\right)^2\right)} \quad 30$$

where:

γ – Non-dimensional peak shape factor

A_γ – A normalizing factor [1-0.287 ln (γ)]

σ – Spectral width parameter

$\omega_p = 2\pi / T_p$ (T_p is the peak period in seconds)

$S_{PM}(\omega)$ – PM spectrum, which is given by,

$$S_{PM}(\omega) = \frac{5}{16} \cdot H_s^2 \cdot \omega_p^4 \cdot \omega^{-5} \cdot \exp\left(-\frac{5}{4} \left(\frac{\omega}{\omega_p}\right)^{-4}\right) \quad 31$$

where:

H_s – Significant wave height in meters

Average values for JONSWAP experiment data can be found in DNV-RP-C205 [43]. For $\gamma=1$, the JONSWAP spectrum reduces to the PM spectrum [43]. During this work, γ is calculated using the method proposed by Torsethaugen K. et al. [50] (Equinor Norway also adopts this) as described in the below equation. Extreme wave data for the 100-year return period in the Santos basin are shown in Table 6-1. Wave direction of 120° from the North is considered for all the extreme analyses (OrcaFlex uses a different convention for directions). In contrast, different wave directions from the met-ocean report are used for the fatigue analysis.

$$\gamma = \max \left(1.0, 42.2 \cdot \left(\frac{2\pi \cdot H_s}{gT_p^2} \right)^{\frac{6}{7}} \right) \quad 32$$

Table 6-1: 100-year H_s and T_p values

Significant wave height H_s	9.0 m
Peak period T_p	16.4 s
Shape factor γ	1.5660

6.3.4 Currents

The current profile shows the current velocities over water depth in which the maximum occurs at the sea surface and the minimum at the sea bottom. For extreme response analysis, the current profile of the 10-year return period is used as shown in Table 6-2. These values are based on the met-ocean reports in the Santos basin. Two current directions (120° from North and -60° from North) will be considered in the analysis.

Table 6-2: 10-year current profile

Water depth (m)	Current Velocity (cm/s)
0	132
25	128
50	128
100	126
150	121
200	109

300	78
400	59
700	49
800	52
900	50
1000	46
1200	39
1600	30
1800	34
2000	30

6.3.5 Hydrodynamic Coefficients and Marine Growth

Morison equation is used to calculate hydrodynamic loading on the SLWR. Morison equation is a function of relative fluid velocity and acceleration. Drag coefficient (C_D) and added mass coefficient (C_A) vary with Reynolds number, Keuligan-Carpenter number, and surface roughness of the structure [16]. It is also important to consider marine growth on the surface of the riser since it changes the outside diameter (modelling of marine growth is out of scope in this research). This increases the riser's mass, top tension, and hydrodynamic loading [51].

DNV-OS-F201 [29] provides conservative values to be used as C_D or inertia coefficient C_M ($C_M = C_A + 1$) based on experimental data. The possibility of having marine growth in the riser is taken care of by selecting conservative values for C_D and C_M [25]. C_D values should be carefully selected since low C_D values can result in high fatigue damage due to low hydrodynamic damping, and high C_D values can result in the opposite [25]. The following conservative hydrodynamic coefficients are selected for this study, as shown in Table 6-3.

Table 6-3: Hydrodynamic coefficients of riser sections

Description	Drag Coefficient		Added Mass Coefficient	
	Normal	Axial	Normal	Axial
Bare riser	0.9	0	1.0	0
Riser with strakes	1.4	0.015	2.0	0

6.3.6 Riser-Soil Interaction

One of the major design considerations for SLWR is the fatigue at the touch down zone (TDZ). This is influenced by the soil friction and stiffness values in the TDZ. Hence it is important to use accurate values in the analysis [3]. Soil-riser interaction is thus modelled as linear soil springs (from soil investigation report) and relevant friction coefficients, as shown in Table 6-4. Figure 6-4 shows the orientation of the soil springs [52].

Table 6-4: Soil parameters

Parameter	Value
Lateral (normal) friction coefficient	0.5
Axial friction coefficient	0.2
Normal (vertical) soil stiffness	1150 kN/m/m ²
Lateral and axial (shear) soil stiffness	200 kN/m/m ²

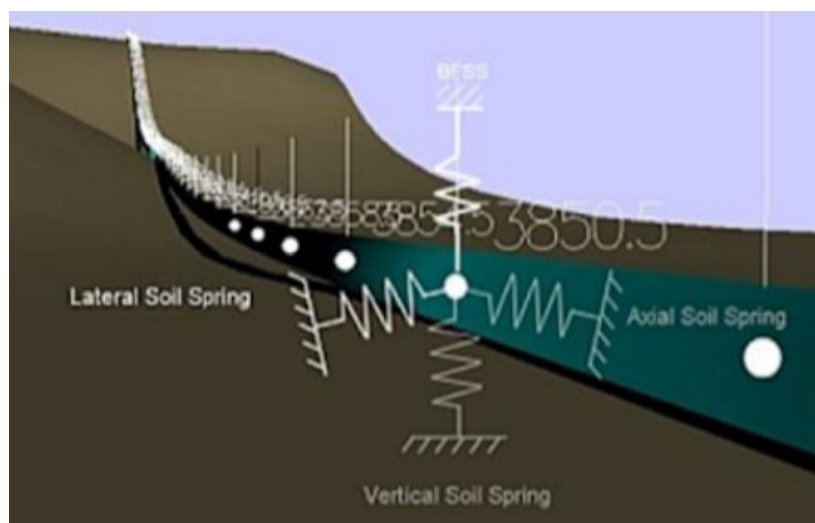


Figure 6-4: Orientation of soil springs [52]

6.4 Vessel Data

6.4.1 FPSO Dimensions, RAOs and Orientation

A spread moored FPSO is the selected vessel for this study. The vessel heading is 30⁰ from North. Its dimensions are shown in Table 6-5. Vessel orientation with respect to North is shown in Figure 6-5. Here, the local coordinates of the vessel are represented by 'x' and 'y', which lie

on the bottom surface of the vessel. 'z' is considered positive upward. The riser hang-off point with respect to the local coordinates of the FPSO is 0.0, 36.0 and -5.6 (x, y, z), respectively. Hang-off angle is maintained at 8° for the static nominal configuration.

Table 6-5: FPSO details

Parameter	Value
Length	300 m
Beam	60 m
Height	30 m
Maximum draught	22 m

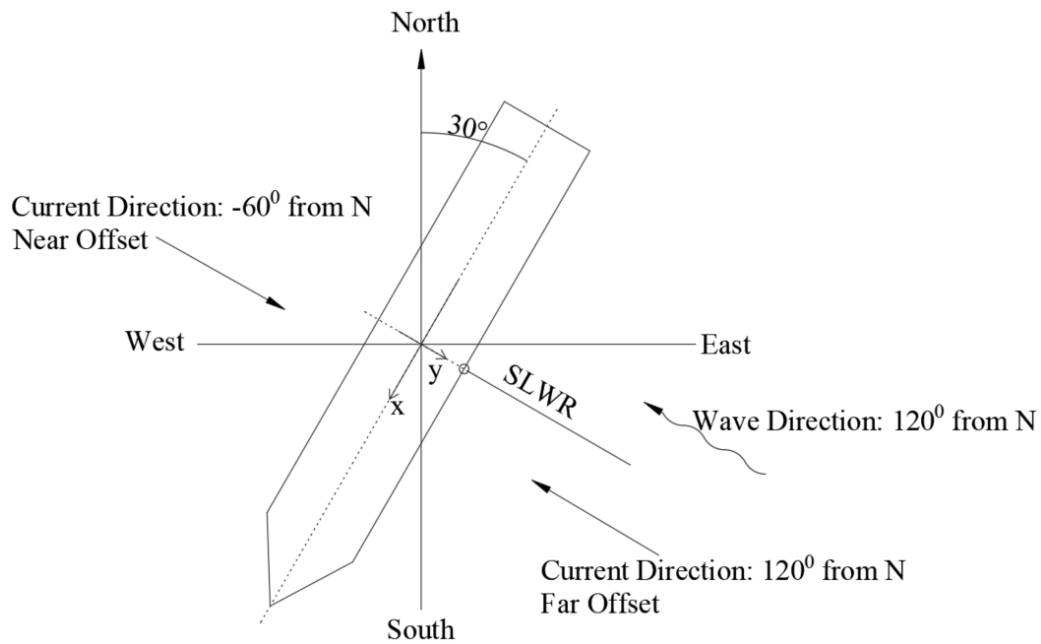


Figure 6-5: Vessel orientation

6.4.2 FPSO Offsets and Motion

Floater offset and motion occur due to static and dynamic loading on the vessel. This is described in three different situations as per DNV-OS-F201.

-
- **Static mean position (nominal position)**
This is due to steady wave drift, wind, and currents. The mean position of the FPSO was used in the static analysis.

 - **Wave frequency floater motion (WF)**
WF floater motion occurs due to the first-order wave forces acting on the floater, which can be described using the vessel's six degrees of freedom motion (6DoF). These motions typically have periods ranging from 3-25 seconds and can be described using Response Amplitude Operators (RAO) of the FPSO [29]. The RAO origin is located at the centre of gravity of the vessel. RAO data are vessel dependent and confidential. These will not be included in the report but will be directly used in the analysis.

 - **Low frequency floater motion (LF)**
LF floater motion is also referred to as slow drift motion. Second-order wave forces and wind gusts induce this. They occur at periods high above the wave periods within a range of 30-300 seconds. This motion can be simply introduced as horizontal floater motion from the mean position known as offsets. There are two types of offsets, namely Far and Near [29]. Vessel offsets below are selected as per API RP 2SK [46]. 7% water depth (140m) is used as ULS condition (intact mooring lines) offset, and 8% of water depth (160m) is used as ALS condition (one mooring line failure or 10000-year return period storm) offset.

The wave and current loading direction are set parallel to the lay direction. This will give the most adverse loading in the Near and Far offsets in the strength calculation [22]. Figure 6-5 shows the riser lay direction and the direction of the environmental loading. A graphical illustration of vessel offsets is shown in Figure 6-6. The summary of vessel offsets is shown in Table 6-6.

Table 6-6: Summary of vessel offsets

Mooring Condition	FPSO Offset (% water depth)	FPSO Offset (m)
ULS (Intact mooring line)	7	140
ALS (Broken mooring line)	8	160

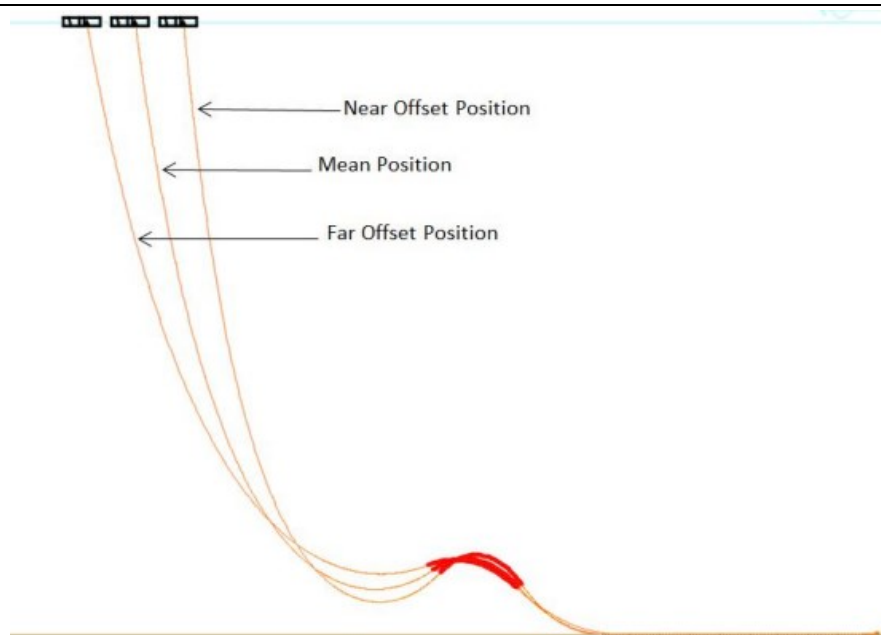


Figure 6-6: Vessel offsets [48]

6.5 Riser Properties

6.5.1 Design Life

The design life for the SLWR is 25 years. A safety factor of 10 is used as per the recommendation of DNV-OS-F201 [29] for production risers. Therefore, the minimum required fatigue life for the SLWR is 250 years for the wave induced fatigue analysis.

6.5.2 Internal Fluid Data

Well fluid density can vary from 800kg/m^3 to 200kg/m^3 . The static configuration of SLWR is checked for three different fluid densities as shown in Table 6-7. Average fluid density is used for dynamic and fatigue analysis. The system pressure test is done using water.

Table 6-7: Summary of fluid properties

Fluid Label	Density kg/m^3	Pressure MPa (Bar)	Reference Level
High	800	65 (650)	20m seabed
Average	500	65 (650)	20m seabed
Low	200	65 (650)	20m seabed
Water	1025	75 (750)	20m seabed

6.5.3 Riser Properties

API 5L X65 steel is selected as the riser material [20]. The required flow rate determines riser diameter, and this calculation is out of the scope of this research. Riser wall thickness is determined for ULS by following DNV-OS-F101 [30]. All pipelines are designed to withstand internal and external pressure to avoid bursting or collapsing. Further consideration is also given to minimum wall thickness to avoid buckling propagation. The thickness required to control buckling propagation is relatively high compared to bursting and collapsing criteria. In practical situations, the design for buckling is not economical but can be mitigated using buckle arresters at critical regions of the riser [25]. Table 6-8 summarises the riser properties used in the analysis. Detailed calculation is attached in Appendix A.

Table 6-8: Summary of riser properties

Parameter	Value
Riser internal diameter	254 mm (10")
Wall thickness	25 mm
Specified minimum yield strength	448 MPa
Tensile strength	531 MPa
Young's modules	207 GPa
Poisson ratio	0.3
Steel density	7850 kg/m ³
Fabrication tolerance	10 %
Ovality	3 %
Safety class	High

6.5.4 Riser Coatings

External coatings are mainly used on flowlines and risers to protect against corrosion, mechanical protection against external loads and clashing, and thermal insulation. The key issue when coatings are used is to control the weight distribution of risers. Further consideration should also be given to long-term hydrostatic creep performance and water absorption [53]. The static and dynamic analysis is based on a coating thickness of 70mm, and the material density is 700kg/m³. These values represent a typical production riser which is relatively light.

In the parametric studies, a 3mm 3LPP coating with a density of 900kg/m^3 will also be considered, which represents a relatively heavy injection riser.

6.5.5 Buoyancy Modules

The buoyancy module is an essential component in the SLWR. External buoyancy modules equipped between the hang-off zone and TDZ of the riser provide upward buoyancy force in water greater than its gravity force. As a general rule of thumb, the modules' buoyancy force is approximately twice the self-weight of the steel pipe with internal fluid [54]. Buoyancy modules are installed at uniform intervals known as pitch. Buoyancy modules readily available in the market are used in the analysis, and their properties are listed below in Table 6-9. A typical buoyancy module attached to a riser is shown in Figure 6-7 [55].

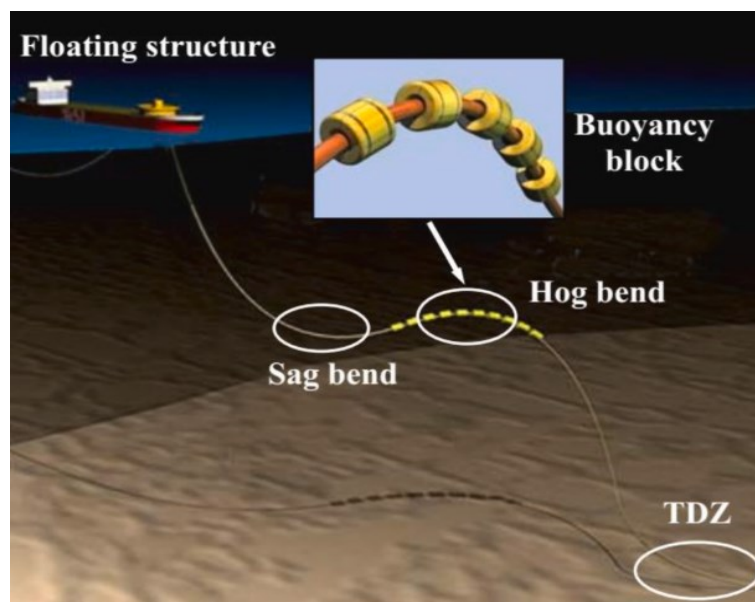


Figure 6-7: A typical buoyancy module [55]

Table 6-9: Buoyancy module properties

Parameter	Value
Length	1.85 m
Outer diameter	1.57 m
Weight	1590 kg
Net buoyancy	1260 kg

In OrcaFlex, buoyancy modules can be modelled as discrete or smeared (spread out evenly) elements. During this study smeared method (equivalent section) is used to define buoyancy modules based on parameters described in Table 6-9. Properties of the discrete floater elements are converted into equivalent floater section, which provides the same upthrust in water. As shown in Figure 6-8, the upthrust provided by the three discrete floater elements (diameter D_f) and the attached pipe (diameter D_p) is equal to the upthrust provided by the equivalent buoyancy section (diameter D_{eq}). Parameters such as drag coefficient and added mass coefficients are also adjusted accordingly [42]. D_{eq} value of 0.955m is used in the static and dynamic analysis. $C_{A,Normal}$ is 1.0 and $C_{A,Axial}$ is 0.255. $C_{D,Normal}$ is 0.864 and $C_{D,Axial}$ is 0.118.

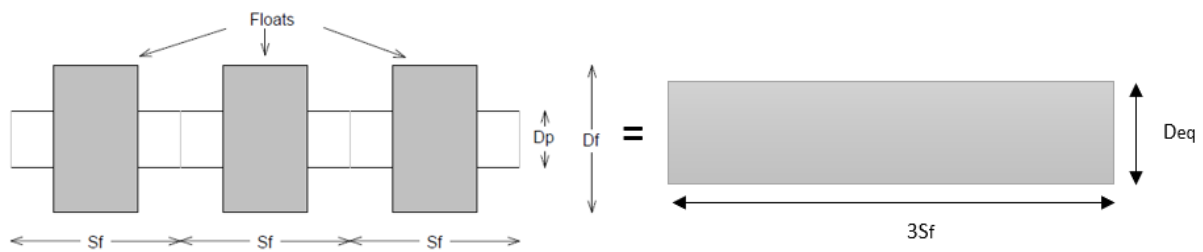


Figure 6-8: Equivalent buoyancy module

6.5.6 Riser End Terminations

The riser's upper termination (flex joint) is modelled as a pin joint near the vessel. A pin joint can only transfer axial forces but not the moments. The stiffness of the flex joint will not influence the response in extreme loading analysis [22]. But in the fatigue analysis, the stiffness of the flex joint will influence the fatigue response. Practically, the fatigue issue near the hang-off point is mitigated by using long tapered sections [22]. The Fatigue life near the upper-end termination is out of the scope of this thesis. Thus, in extreme loading and fatigue analyses, the flex joint is modelled as a pin joint with zero stiffness. An infinite stiffness (fully fixed) at upper-end termination is used to evaluate the influence of the joint stiffness on the fatigue life near TDP. Still, the rest of the analyses consider a pinned upper-end termination. A typical riser flex joint is shown in Figure 6-9 [56].

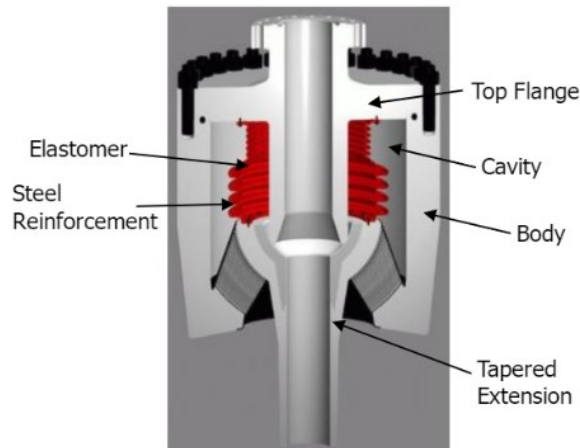


Figure 6-9: A typical riser flex joint [56]

6.6 SLWR Acceptance Criteria

The following minimum criteria should be met as the minimum acceptance criteria per DNV-OS-F201 [29].

- SLWR should fulfil combined loadings criteria.
Bending moment + effective tension + net internal pressure
Bending moment + effective tension + net external pressure
- LRFD utilization factor should be less than or equal to one, as shown in the below equation. If this is not satisfied, the design is unsafe, and a redesign needs to be carried out. Partial safety factors and design factors used in the strength calculations are shown in Table 6-10.

$$g(t) = g(M_d(t), T_{ed}(t), \Delta_p, R_k, \Lambda) \leq 1 \quad 33$$

where:

M_d – Design bending moment

T_{ed} – Design effective tension

Δ_p – Local differential pressure

R_k – Vector of cross-sectional capacities

Λ – Vector of safety factors

-
- Compression should be limited or completely avoided to prevent buckling of the riser
 - The minimum fatigue life of 250 years should be achieved.

Table 6-10: Partial Safety Factors for ULS, ALS and Design

Load and Design Factors	ULS	ALS
Functional γ_F	1.1	1.0
Environmental γ_E	1.3	1.0
Condition γ_C	1.0	1.0
Reduced Functional γ_{RF}	0.91	-
Reduced Environmental γ_{RE}	0.77	-
Safety class γ_{SC}	1.26	1.26
Material resistance γ_M	1.15	1.15
Fabrication factor α_{fab}	0.85	0.85

7 Extreme Response Analysis

7.1 Introduction

In the first phase of the research, extreme response analysis is carried out on the SLWR. This chapter presents the incorporated methodology in the analysis and the relevant outcome and results. The input data used in the analysis is presented in Chapter 6. The main software used in the analysis is OrcaFlex 11.2 [42], and the design standard is DNV-OF-F201 [29]. The procedure followed in the analysis is presented below.

- Establishing the load cases for analysis
- Determine an acceptable SLWR static configuration
- Determination of the worst sea state using random simulation (using seed components)
- SLWR dynamic analysis
- Strength calculation as per LRFD approach in DNV-OS-F201

7.2 Design Load Cases

7.2.1 Environmental Direction

The analysis considers two environmental directions for currents (120° from N and -60° from N) and one direction for waves (120° from N), as shown in Figure 6-5. Two current directions are used in the Near and Far offsets analysis.

7.2.2 Load Case Matrix for SLWR

Static and dynamic analyses are performed for ULS and ALS. Details about limit states and offsets are presented in Chapter 4 and Chapter 6. Static analysis is only due to functional loads. Dynamic analysis is due to the combined load effect of functional loads and environmental loads. The environmental loads refer to a 100-year extreme sea-state and a 10-year current profile. The strength calculation is carried out per the load matrix shown in Figure 7-1. This study does not include the lateral load case since they are not critical in strength calculations [22].

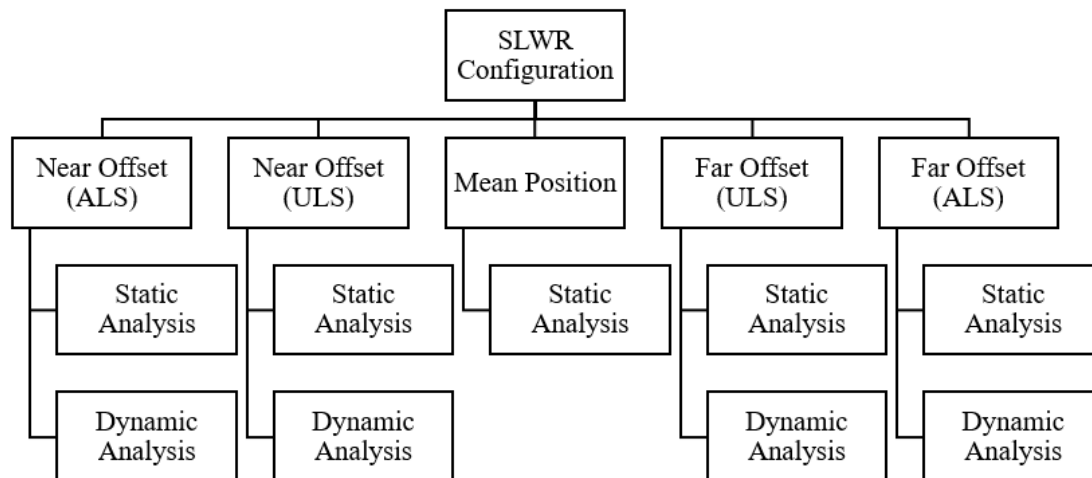


Figure 7-1: SLWR strength calculation load matrix

7.3 SLWR Static Analysis

7.3.1 Optimum SLWR Configuration

SLWR static configuration was achieved by analysing numerous configurations to ensure the “low lazy configuration”. This was achieved by changing the riser length and adjusting the number of buoyancy elements. Table 7-1 summarises different configurations considered in the analysis (notations are referred to in Figure 7-2). Figure 7-2 shows a schematic of the riser from OrcaFlex. The summary is based on an average fluid density of 500 kg/m^3 . Further, different configurations with low and high fluid densities (200 kg/m^3 and 800 kg/m^3) have been considered to finalize static configurations. But these configurations are not included in the report.

Table 7-1: SLWR static configurations (Nominal, ULS, ALS)

Case	θ	$D_B = D_H - D_S$	D_S	X_1
Nominal Position	8.0^0	66.7 m	119.4 m	1471 m
Near Offset (ULS)	8.0^0	115.3 m	78.4 m	1305 m
Far Offset (ULS)	8.8^0	25.2 m	166.0 m	1657 m
Near Offset (ALS)	7.8^0	123.1 m	73.2 m	1280 m
Far Offset (ALS)	9.3^0	18.2 m	174.4 m	1691 m

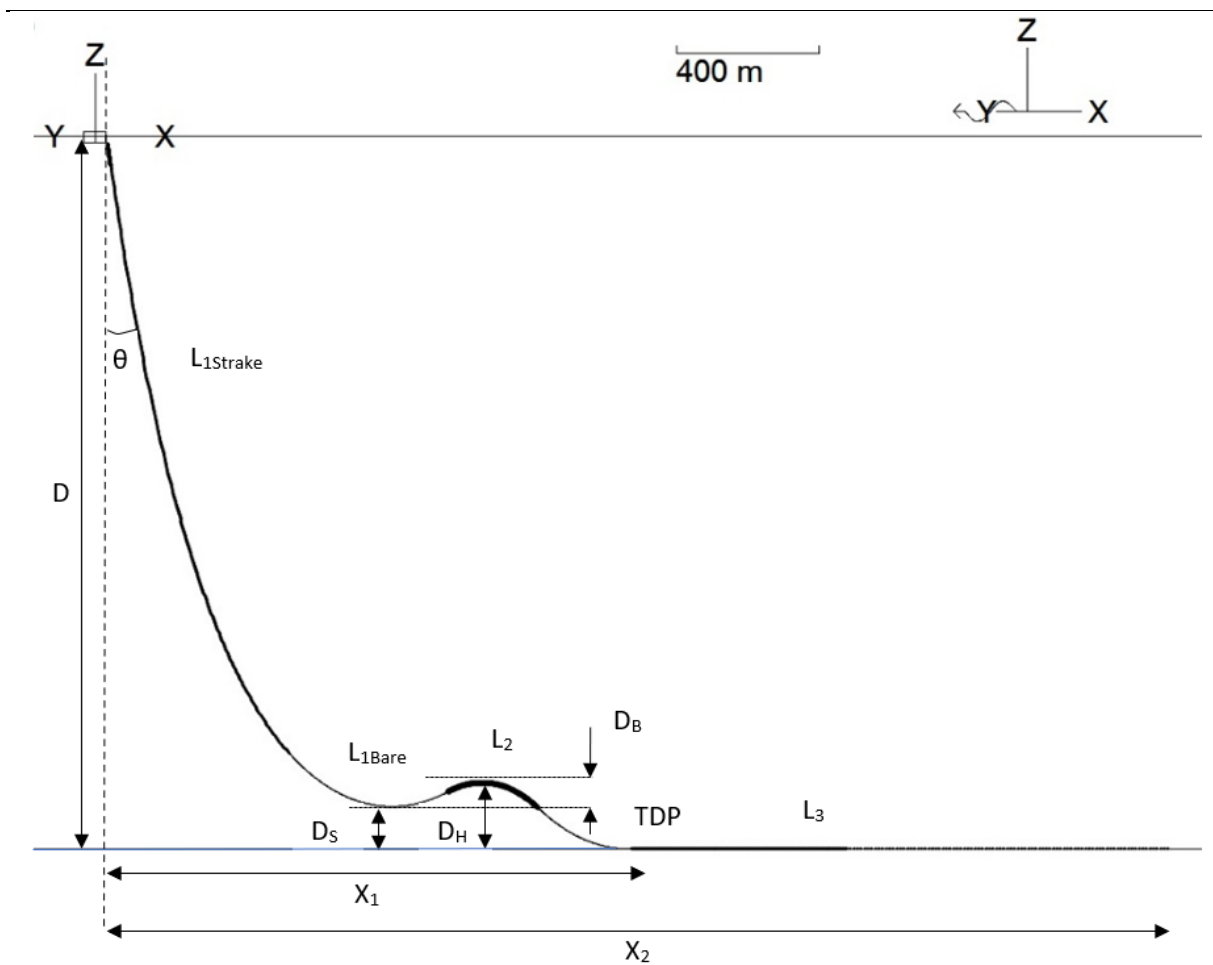


Figure 7-2: SLWR configuration from OrcaFlex

Table 7-2 shows the detailed description of the nominal static configuration for average fluid density. This configuration is also used in the fatigue analysis.

Table 7-2: SLWR nominal static configuration

Parameter	Value
Fluid density	500 kg/m ³
Hang-off angle θ	8°
Upper section length L_1 ($L_{1Strake} + L_{1Bare}$)	1800+500 = 2300 m
Buoyancy section length L_2	275 m
Lower section length L_3	1800 m
Total riser length L ($L_1 + L_2 + L_3$)	4375 m
Net buoyancy of buoyancy modules	70 ton
Horizontal distance to TDP, X_1	1471 m

Horizontal distance to seabed connection, X_2	2975 m
Sag bend height above seabed D_S	119.4 m
Hog bend height above seabed D_H	186.1 m
Height between sag and hog bend $D_B = D_H - D_S$	66.7 m
Water depth D	2000 m

7.3.2 Static Analysis Results

- Effective Tension in Nominal, Far (ULS/ALS) and Near (ULS/ALS) Offsets

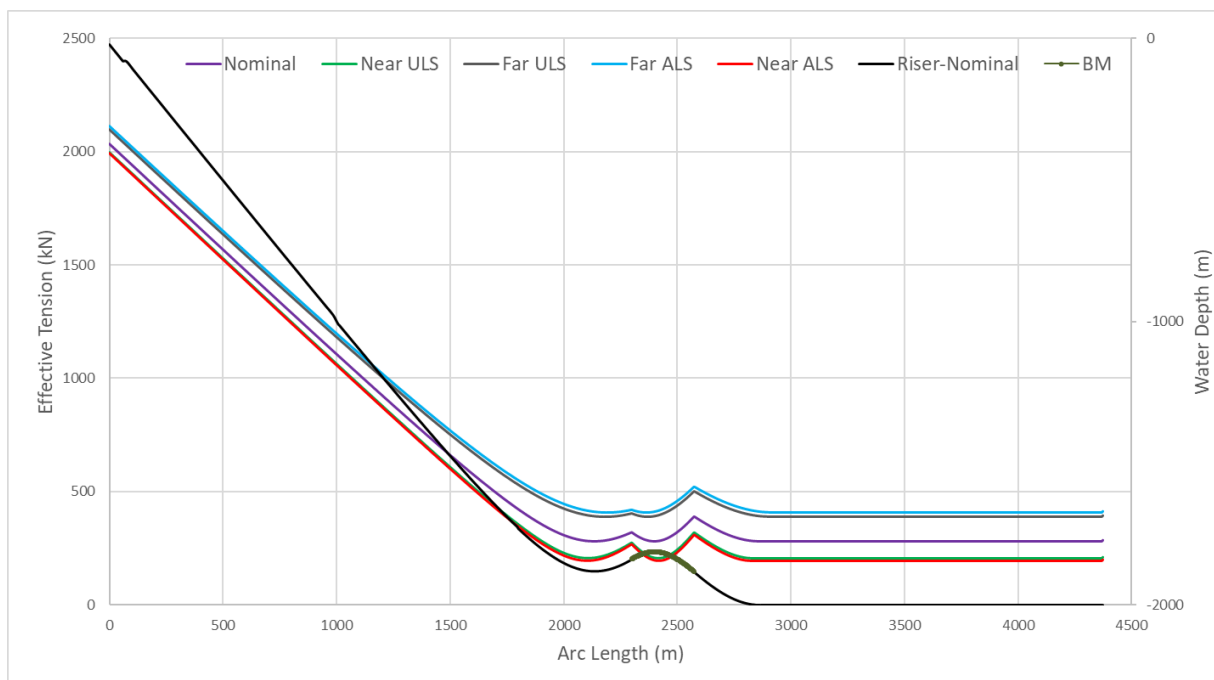


Figure 7-3: Effective Tension variation in static state

- Bending Moment in Nominal, Far (ULS/ALS) and Near (ULS/ALS) Offsets

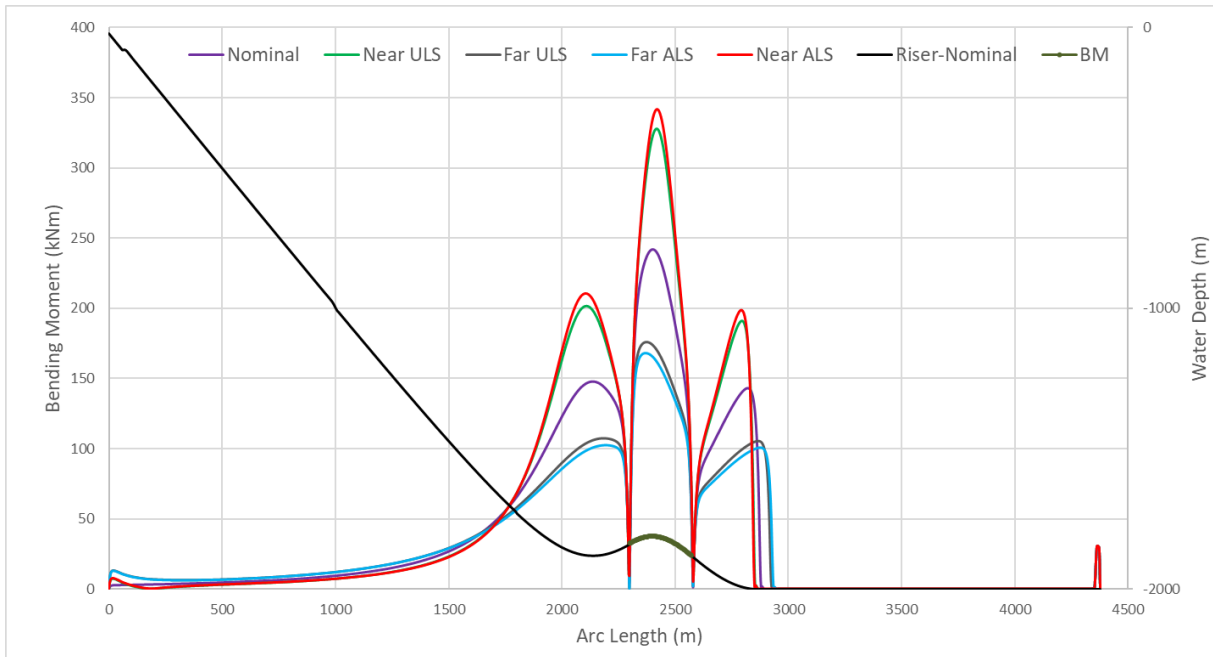


Figure 7-4: Bending Moment variation in static state

- DNV LRFD Utilization Factor in Nominal, Far (ULS/ALS), Near (ULS/ALS) Offsets

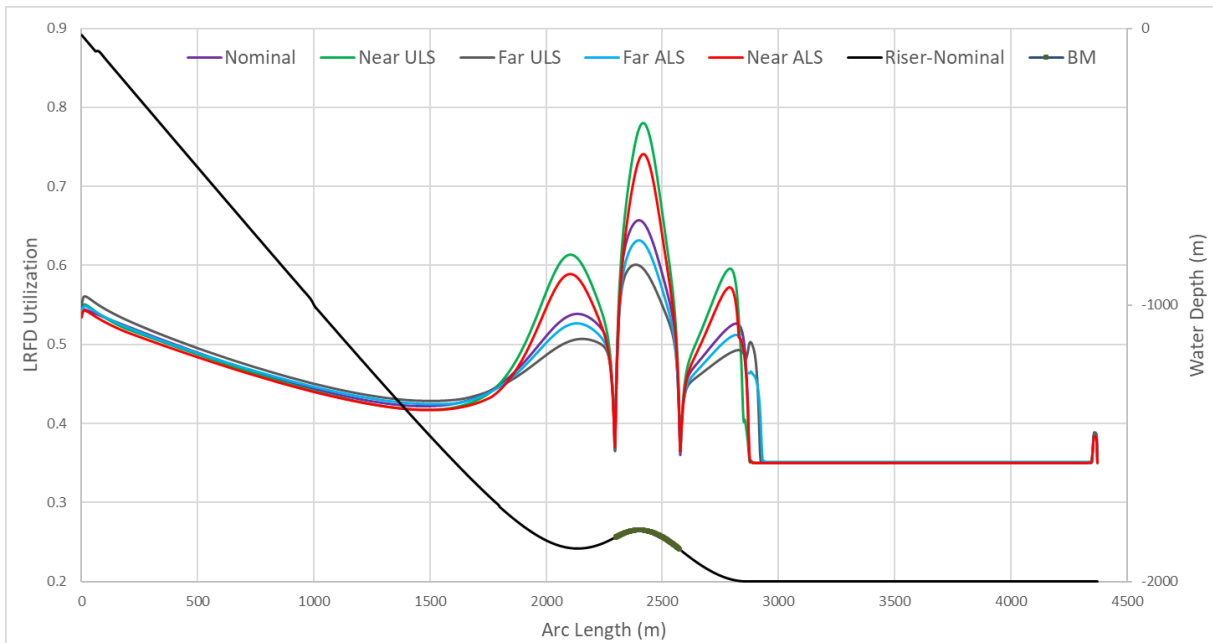


Figure 7-5: DNV LRFD Utilization Factor variation in static state

-
- Summary of Static Analysis

Table 7-3: Summary of static analysis results

Case	Max Effective Tension (kN)	Max Bending Moment (kNm)	Max LRFD Util. Factor
Nominal Position	2034 (Hang-off)	242 (Hog bend)	0.66 (Hog bend)
Near Offset (ULS)	1998 (Hang-off)	328 (Hog bend)	0.78 (Hog bend)
Far Offset (ULS)	2099 (Hang-off)	176 (Hog bend)	0.60 (Hog bend)
Near Offset (ALS)	1994 (Hang-off)	342 (Hog bend)	0.74 (Hog bend)
Far Offset (ALS)	2111 (Hang-off)	168 (Hog bend)	0.63 (Hog bend)

7.3.3 Discussion on Static Analysis

- Far offsets give higher effective tension (ET) due to the additional tension provided by the vessel offset.
- The ET at the sag and hog bends and TDP have similar values. This indicates that the forces acting on those locations are mainly horizontal.
- Near offsets give high bending moment (BM) values due to the smaller curvatures at the sag and hog bends (BM is directly related to the curvature of the sag and hog bends). The BMs at the sag bend and TDP are smaller than the BM at the hog bend.
- BM is the governing factor contributing to a higher LRFD utilization factor (UF) because the contribution from ET is fairly equal in all five cases.
- BM variation and LRFD UF variation follow a similar pattern. Maximum LRFD UF is 0.78 at the hog bend in the Near ULS condition.
- ULS causes a higher LRFD UF than ALS due to the high functional load factors.

7.4 SLWR Dynamic Analysis

7.4.1 Importance of Random Simulation (Seed Number Selection)

The worst sea state for the dynamic analysis of SLWR is defined by a combination of a 100-year profile wave and a 10-year current profile that gives the maximum downward velocity at the riser hang-off point [25]. This method has been further proven accurate for SCRs, and SLWRs by the works carried out by Ramiro A. et al. [57].

Since ocean waves are of random nature (stochastic process), there are different wave realisations for a given H_s and T_p combination [58]. Different wave realizations can be generated by changing the seed number in OrcaFlex. A seed number is a random integer between -2147483648 to +2147483647, generating a random wave realization for a given H_s and T_p [58]. The variation of wave heights for a given H_s and T_p in 2 different seed numbers during a 3-hour wave simulation is shown in Figure 7-6. A similar method is used to evaluate the maximum downward velocity at the hang-off points for the selected H_s and T_p combination.

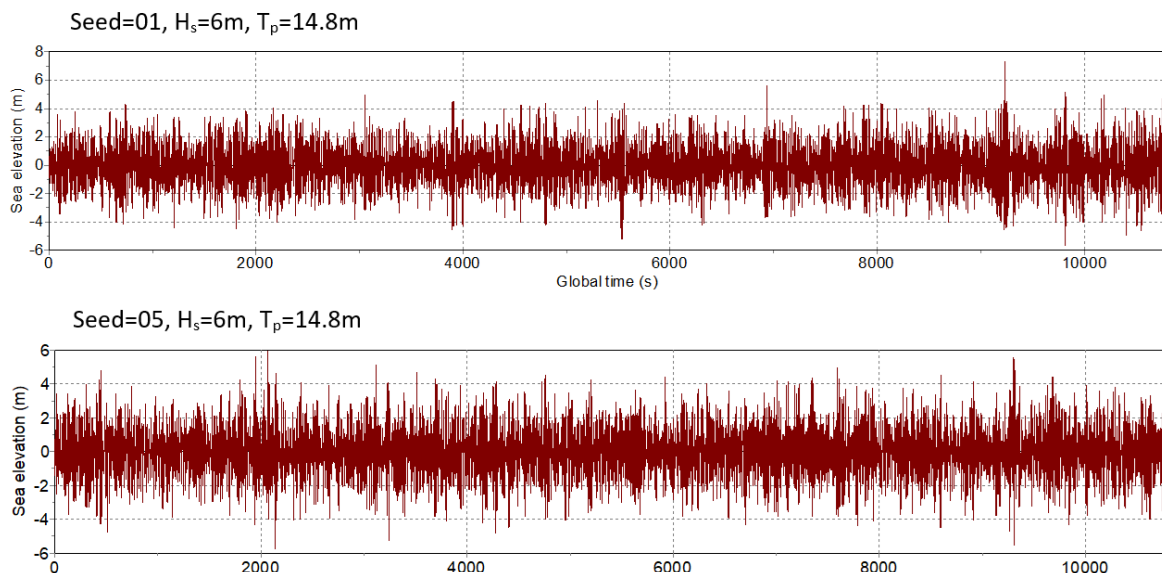


Figure 7-6: Irregular wave realizations for various seed numbers

7.4.2 Analysis Procedure

The calculation procedure adheres to the methods proposed in NORSOK N-003 [59], DNV-OS-F201 [29], DNVGL-OS-E301 [44] and the method proposed by Ramiro A. et al. [57].

- FPSO is modelled with the riser hang-off point.
- 20 random seed components are selected for dynamic simulation to evaluate the worst sea state. The 3-hour maximum downward velocity at the hang-off point is obtained for the 20 random seed components. Table 7-4 shows the selected seed numbers, corresponding downward velocity, and the occurrence time.

Table 7-4: Seed numbers and the maximum downward velocity

#	Seed Number	Dw. Velocity (m/s)	Time (s)
1	1	2.97773	9306.75
2	5	3.78225	9239.25
3	10	2.70546	9791.50
4	15	3.26664	3767.00
5	20	3.18471	5090.00
6	25	2.96618	9897.50
7	30	3.15131	2106.25
8	35	3.19117	3017.50
9	40	3.33410	10730.25
10	45	3.36460	2853.75
11	50	3.44640	112.00
12	55	3.37168	1141.50
13	60	3.13558	3266.00
14	65	3.19193	8768.50
15	70	3.54878	5199.50
16	75	2.93324	2223.75
17	80	2.64659	3267.75
18	85	2.71712	9104.50
19	95	3.09874	10545.25
20	100	3.25959	9938.25

- 90th percentile response for downward velocity is evaluated using extreme value distribution (Gumbel Distribution) [60]. The basic equation of the Gumbel method is shown below. A probability paper is created for downward velocities to estimate the 90th percentile. The seed component corresponding to the 90th percentile is selected for the dynamic analysis [60].

$$F_X(x) = \exp \left\{ - \exp \left\{ - \frac{x - \lambda}{\kappa} \right\} \right\} \quad 34$$

$$\text{Expected value } E[X] = \lambda + 0.57722\kappa \quad 35$$

$$\text{Standard deviation } STD[X] = 1.28255\kappa \quad 36$$

Figure 7-7 shows the results of the analysis. The seed number corresponding to the selected downward velocity is highlighted in a black circle (seed no. 70). This seed number will be used in the dynamic analysis.

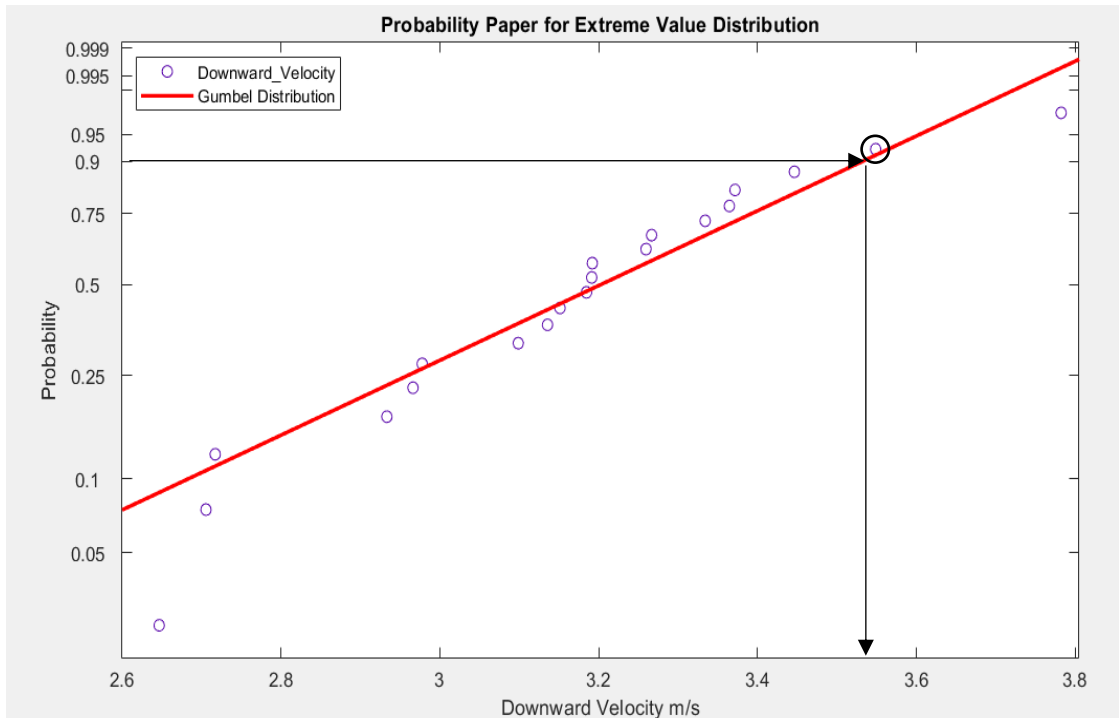


Figure 7-7: Gumbel Distribution for the downward velocity at hang-off point

- Dynamic analysis is carried out for near and far offsets (established in static analysis) using the seed number 70. A simplified method was used in the dynamic analysis instead of running the whole 3-hour simulation. A total simulation time of 120 seconds was used in the analysis. The worst response (downward velocity) occurs during this period. Approximately five-wave periods were set before the identified time, and three-wave periods were set after the identified time. Wave build-up time was set to 15 seconds [42]. This is shown in Figure 7-8. The 3-hour time history of downward velocity (seed no. 70) is shown in Figure 7-9.

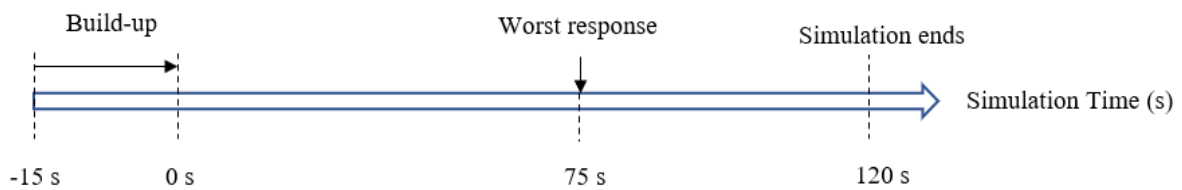


Figure 7-8: Time and simulation stages

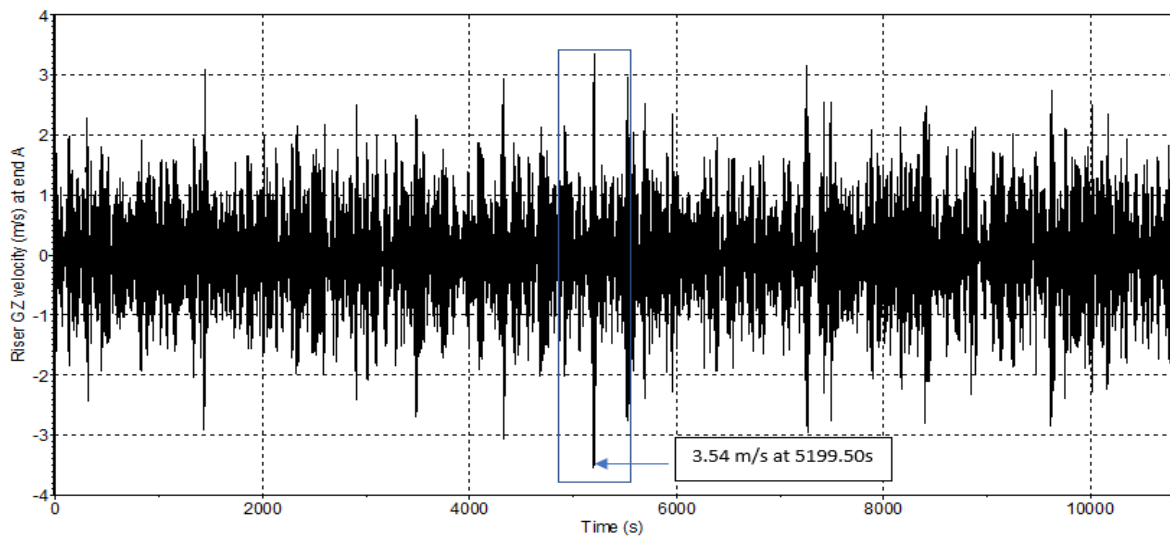


Figure 7-9: 3-hour time history of downward velocity

- Following analysis, results (effective tension, bending moment and LRFD utilization) are presented and discussed for dynamic analysis.

7.4.3 Dynamic Analysis Results

- Effective Tension in Far (ULS/ALS) and Near (ULS/ALS) Offset

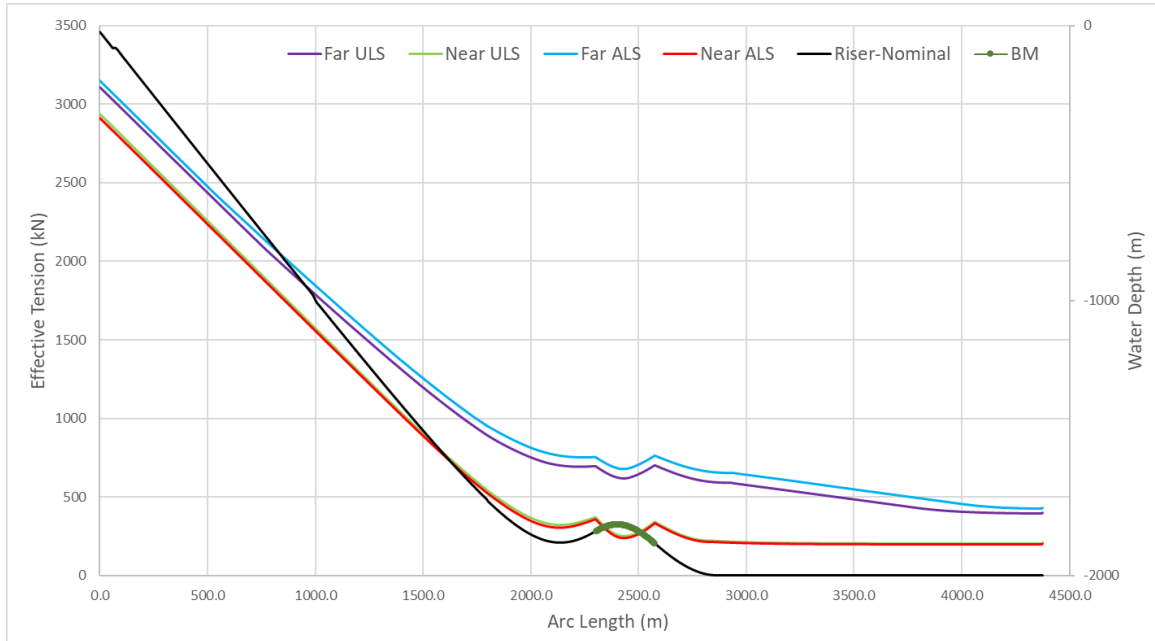


Figure 7-10: Effective Tension variation in dynamic state

- Bending Moment in Far (ULS/ALS) and Near (ULS/ALS) Offset

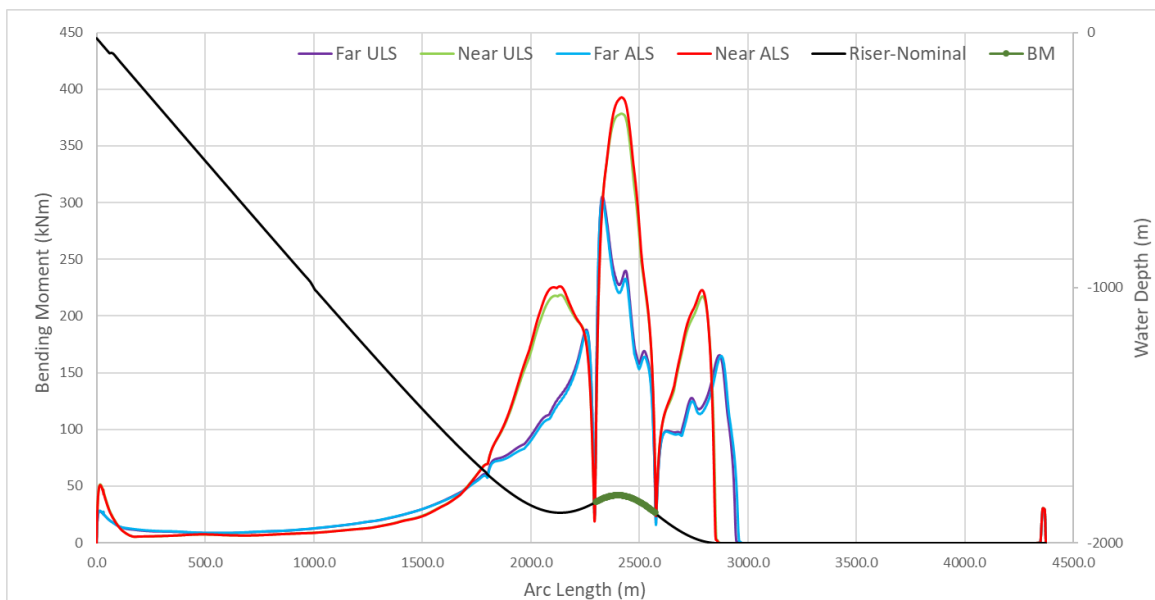


Figure 7-11: Bending Moment variation in dynamic state

- DNV LRFD Utilization Factor in Far (ULS/ALS) and Near (ULS/ALS) Offsets

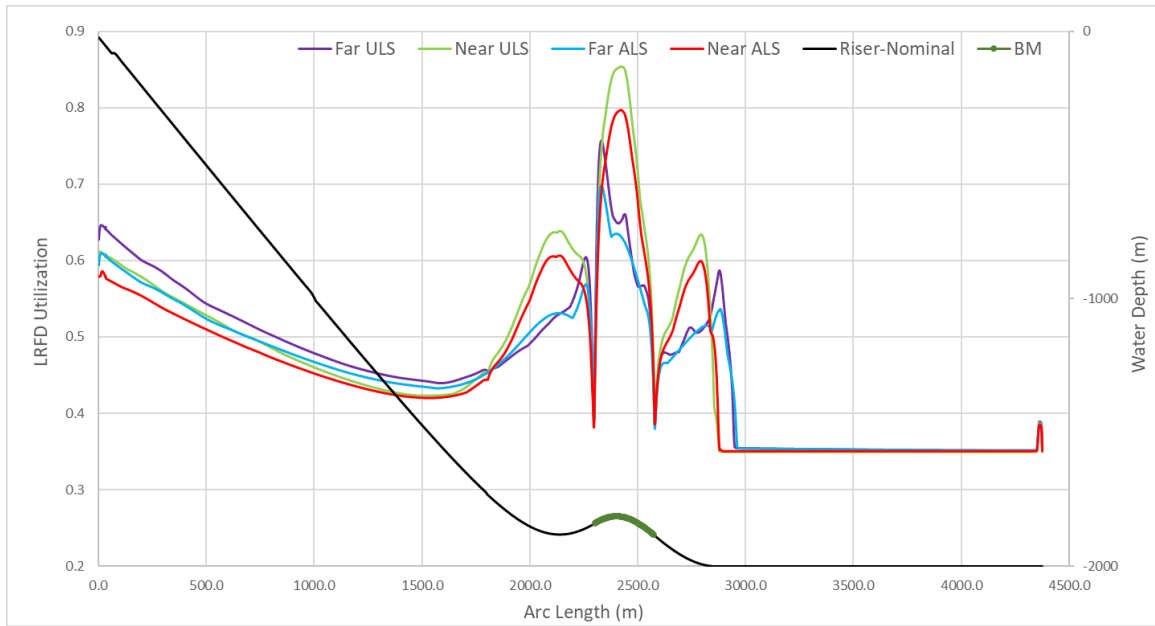


Figure 7-12: DNV LRFD Utilization Factor variation in dynamic state

- Hang-off angle variation in Far (ULS/ALS) and Near (ULS/ALS) Offsets

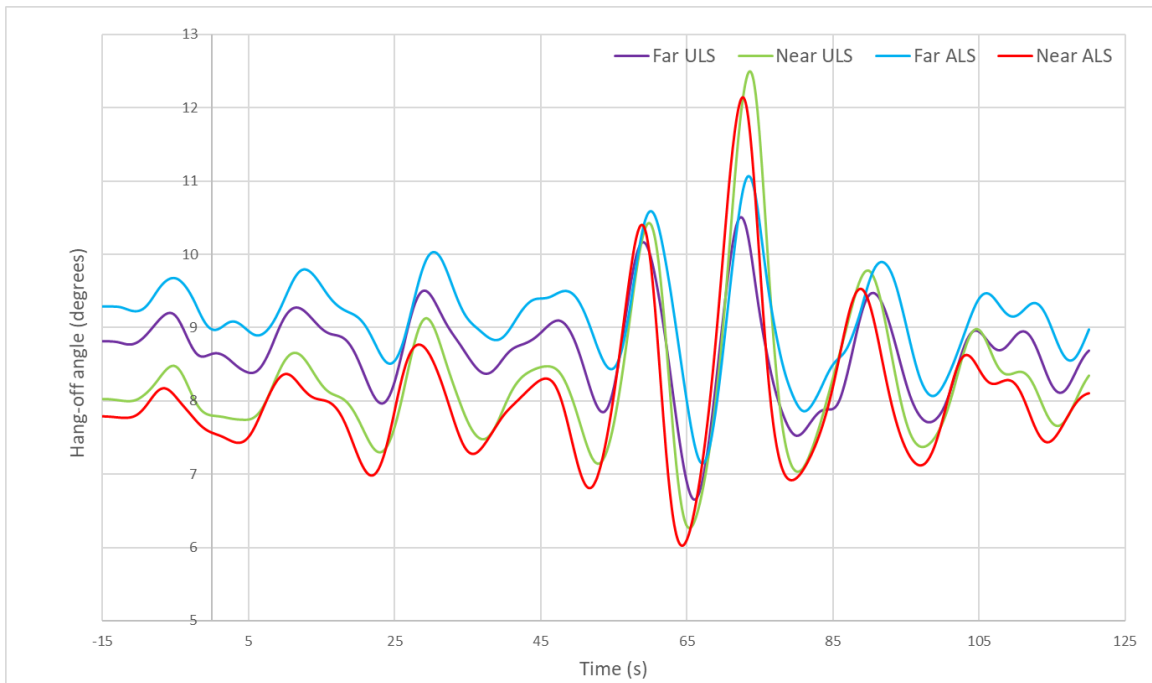


Figure 7-13: Hang-off angle variation in dynamic state

-
- Summary of Dynamic Analysis

Table 7-5: Summary of dynamic analysis

Case	Max Effective Tension (kN)	Max Bending Moment (kNm)	Max LRFD Util. Factor
Near Offset (ULS)	2936 (Hang-off)	378 (Hog bend)	0.85 (Hog bend)
Far Offset (ULS)	3106 (Hang-off)	306 (Hog bend)	0.76 (Hog bend)
Near Offset (ALS)	2908 (Hang-off)	393 (Hog bend)	0.80 (Hog bend)
Far Offset (ALS)	3148 (Hang-off)	303 (Hog bend)	0.70 (Hog bend)

7.4.4 Discussion on Dynamic Analysis

- Compared to the static analysis, the dynamic analysis causes higher ET and BM due to the environmental loads. This causes higher LRFD UF in dynamic analysis.
- The maximum utilization observed is 0.85, which implies a safe design. Further optimization can be carried out to obtain a more economical design.
- A rapid BM fluctuation in the Far offsets can be seen. This is due to the rapid variation of the curvature in Far offsets (low curvature in Far offsets compared to the Near offsets).
- LRFD UF in ULS is higher than in ALS despite the higher offset. This is due to the reduced load effects factors in ALS.
- Hang-off angle variation in all the four configurations is between +3 and -3 from the mean position. These values lie in the acceptable limits for the riser flex joint.
- The maximum hang-off angle occurs when the floater experiences the highest downward velocity.
- Configurations are established to avoid the compressive forces in the riser. Compressive forces can lead to the buckling of the pipelines.

7.5 Summary of Extreme Response Analysis

Table 7-6 summarizes the analysis results from the static and dynamic analysis. Based on the information, the following conclusions can be made.

- The increase of ET in the dynamic analysis compared to static analysis for all the four cases is about 30%.
- The increase of BM in dynamic analysis for Far offsets is much higher than the Near offset values.
- Near ULS has the highest LRFD UF factor, and Far ULS has the lowest value.
- The highest hang-off angle occurs when the FPSO experiences the highest downward velocity.
- Riser can be further optimized to achieve higher LRFD UF while satisfying the fatigue design requirements.

Table 7-6: Summary of static and dynamic analysis

Case	Max Effective Tension (kN)			Max Bending Moment (kNm)			Max LRFD Util. Factor		
	Stat.	Dyna.	% Inc.	Stat.	Dyna.	% Inc.	Stat.	Dyna.	% Inc.
Near (ULS)	1998	2936	31.9	328	378	13.2	0.78	0.85	8.2
Near (ALS)	1994	2908	31.4	342	393	13.0	0.74	0.80	7.5
Far (ULS)	2099	3106	32.4	176	306	42.5	0.60	0.76	21.1
Far (ALS)	2111	3148	32.9	168	303	44.6	0.63	0.70	10.0

8 Fatigue Response Analysis

8.1 Introduction

Fatigue damage is a process of progressive localized plastic deformation occurring in a material subjected to fluctuating or cyclic stresses and strains at high-stress concentration locations that can create cracks or complete fractures after a sufficient number of fluctuations. The stress level at this level is called “fatigue stress” and is much lower than the yield or tensile stress [61]. In the offshore environment, an SLWR experiences oscillatory motion (cyclic loading) due to random waves, currents and vessel motion. These cause the SLWR to move up and down and continuous interaction with the seabed. This is the main cause of fatigue damage at the TDP [62]. Due to the high cycle fatigue (HCF is caused due to small elastic strains under a high number of load cycles typically greater than 10000 before failure [32]) condition imposed on these devices, the fatigue data normally shows statistical fluctuations, as shown in Figure 8-1.

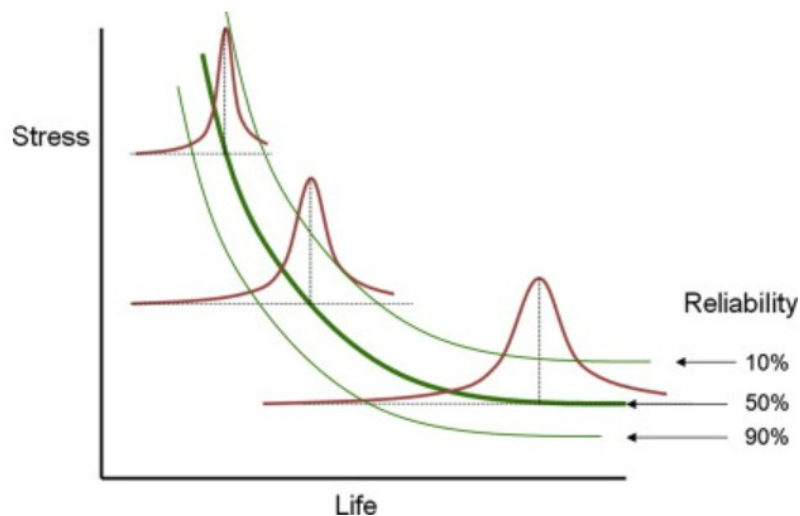


Figure 8-1: Fatigue life statistical behaviour [61]

8.2 Fatigue Analysis Methodology

Fatigue analysis normally involves two main steps. These are analyses of stresses induced by cyclic loading followed by “Rainflow” counting to arrive at the stress cycles and stress range. The “Palmgren-Miner” rule is used to determine these stresses [62].

Fatigue life is the inverse of fatigue damage. Fatigue life prediction is complicated due to the associated uncertainties. These major uncertainties are mentioned below [62].

- The S-N curves are subjected to statistical scatter (the variation in the life of components subject to the same load history).
- Minor's rule is subjected to uncertainty
- Pipe wall thickness is not uniform
- Eccentricities during the fabrication
- Uncertainties associated with the wave scatter diagram
- Uncertainties associated with modelling

The fatigue life at a point of the riser is defined as the time to grow a crack over the wall thickness [22]. Karunakaran et al. [22] state that the critical region for fatigue damage in a riser is the welded joint near the TDZ due to complex riser-soil interaction. This is further illustrated in Figure 8-2 [62]. Therefore, it is important to ensure that the riser satisfies the required fatigue design life of 250 years. During this study, OrcaFlex is used to analyze wave induced fatigue of the riser.

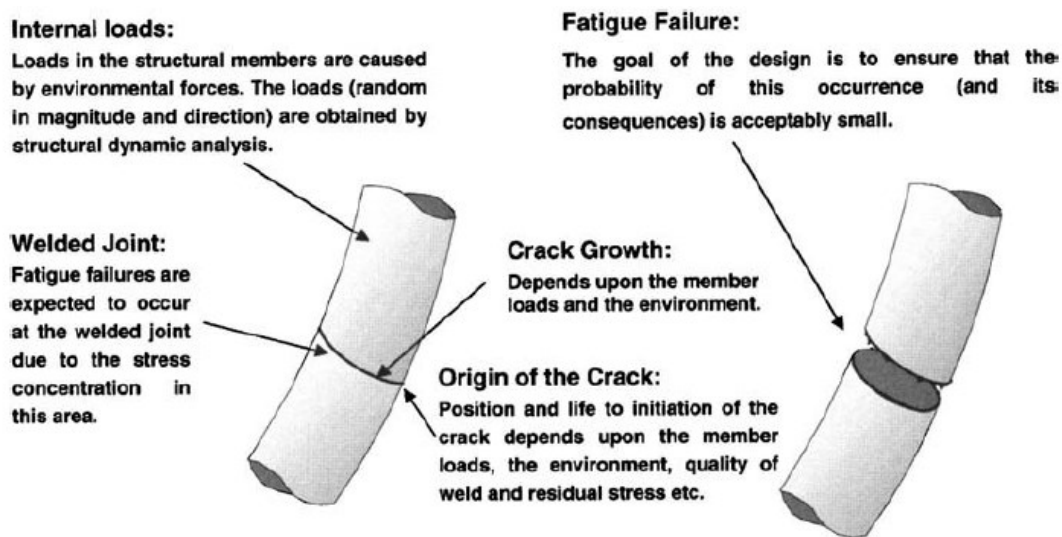


Figure 8-2: Fatigue in welded joints [62]

8.3 Sources of Riser Fatigue

As per Bai et al. [16], there are four main causes of riser fatigue. They are as follows.

- Wave induced fatigue
- Vortex-induced vibrations (VIV) induced fatigue
- Slug induced fatigue
- Fatigue during riser installation

This thesis only focuses on wave induced fatigue damage of the SLWR. The rest of the details are presented for the completeness of the report.

8.3.1 Wave Induced Fatigue

Riser excitation due to the motion of the floater cause wave induced fatigue. This depends on the met-ocean conditions (wave scatter diagram) and the floating facility's response amplitude operators (RAOs) [63]. DNV-OS-F201 [29] specifies two main sources of wave induced fatigue damage, as mentioned below.

- Wave Frequency floater motion (WF)
This is also referred to as the 1st order wave loading and floater motion-induced fatigue. (Discussed in Chapter 6)
- Low Frequency floater motion (LF)
This is also referred to as 2nd order floater motion-induced fatigue. (Discussed in Chapter 6)

8.3.2 VIV Induced Fatigue

VIV induced fatigue is one of the major design issues for steel risers, particularly for locations with high current velocities. High-frequency vibrations of the riser due to vortex shedding result in high-frequency stress cycles, leading to high fatigue damage rates [16]. VIV can occur anytime when a bluff body is exposed to fluid flow that produces vortex shedding at or near the body's natural frequency [63].

Deepwater risers are highly susceptible to VIV for two reasons [16].

- Current velocities are typically high in deepwater areas.
- Increased riser length lowers the riser's natural frequency, thereby lowering the magnitude of the current required to excite VIV.

Helical strakes are commonly used as a method to suppress the cause of vibrations. These strakes are lightweight, and the installation does not cause major problems [63]. A typical VIV suppressing strake is shown in Figure 8-3.



Figure 8-3: VIV suppressing strakes [63]

8.3.3 Slug Induced Fatigue

This is common in production risers, especially SLWRs, due to their wave shape [63]. Under certain flow regimes, a multiphase flow can result in slug flow. The sequence of relatively high-density slugs and low-density bubbles propagate along the riser. The variation of slug and the bubble density at a location of the riser can significantly vary with time. Due to this weight variation, the riser undergoes bending cycles, which causes fatigue [64]. It has been found that the slug induced riser motion can cause larger displacements than those generated by moderate waves in the absence of slugging [65]. Figure 8-4 shows an idealized slug unit followed by a gas pocket [65].

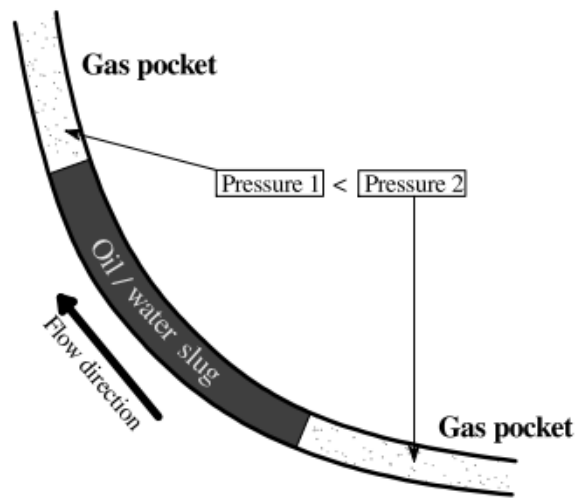


Figure 8-4: A slug unit followed by a gas pocket [65]

8.3.4 Fatigue During Riser Installation

Deepwater riser installation can be carried out using three methods described in Chapter 5. When laying risers or pipelines in deepwater, a pipe joint may take two or three days to travel from the barge to the sea bottom. The lay method and pipe joining method will influence the travel time. During this period, every pipe joint is subjected to dynamic loading caused by floater motion, waves, and currents. The cyclic loading can result in significant fatigue damage to pipes when they reach the sea bottom [66].

8.4 Wave Induced Fatigue

8.4.1 Introduction to DNV Approach

Wave induced fatigue is mainly governed by vessel motion. The nominal vessel position is used in all the analyses. DNV-OS-F201 recommends following DNV-RP-C203 [32] for the fatigue analysis of risers. The method of analysis is based on S-N curves. The S-N curves in DNV-RP-C203 are derived from laboratory fatigue testing of small specimens and are based on the mean-minus-two-standard deviation. S-N curves are associated with a 97.7% probability of survival during design life.

The basic design S-N curve is given as follows.

$$\log N = \log \bar{a} - m \cdot \log (\Delta\sigma) \quad 37$$

where:

N – Predicted number of cycles to failure for stress range $\sigma\Delta$

m – The negative inverse slope of the S-N curve

$\Delta\sigma$ – Stress range with unit MPa

$$\Delta\sigma = \Delta\sigma_0 \cdot SCF \left(\frac{t}{t_{ref}} \right)^k \quad 38$$

where:

$\Delta\sigma_0$ – Nominal stress range

SCF – Stress concentration factor

t_{ref} – Reference wall thickness for welded connection (25mm)

t – Pipe wall thickness ($t = t_{ref}$ for $t < t_{ref}$)

k – Thickness exponent on fatigue strength (0.1 for tubular butt welds made from one side)

$\log \bar{a}$ – Intercept of log N-axis by S-N curve

$$\log \bar{a} = \log a - 2 \cdot s_{\log N} \quad 39$$

where:

$\log a$ – Intercept of mean S-N curve with the $\log N$ axis

$s_{\log N}$ – Standard deviation of $\log N$

Following S-N curves from DNV-RP-C203 [32] are used in the fatigue analysis.

- D- Curve in seawater with cathodic protection (D in SW with CP) for the outer wall
- E- Curve in the air (E in Air) for the inner wall

These curves have been proven suitable for riser fatigue analysis in offshore environments by several researchers [5], [25], [53], [67]. Relevant S-N curves are shown in Figure 8-5 and Figure 8-6.

The SCF is used to account for the uncertainties like stress magnification from geometrical imperfections between adjacent joints. The SCF can be obtained by the finite element method (FEM) or by using the closed-form expression (Eq.40) proposed in DNV-RP-C203 [32]. As per Karunakaran et al. [53] and Orimolade et al. [67], an SCF value of 1.2 can be used to analyse the SLWR.

$$SCF = 1 + \frac{3e}{t} \exp\left(\left(-\frac{D}{t}\right)^{-0.5}\right) \quad 40$$

where:

e – Eccentricity due to imperfections in the geometry

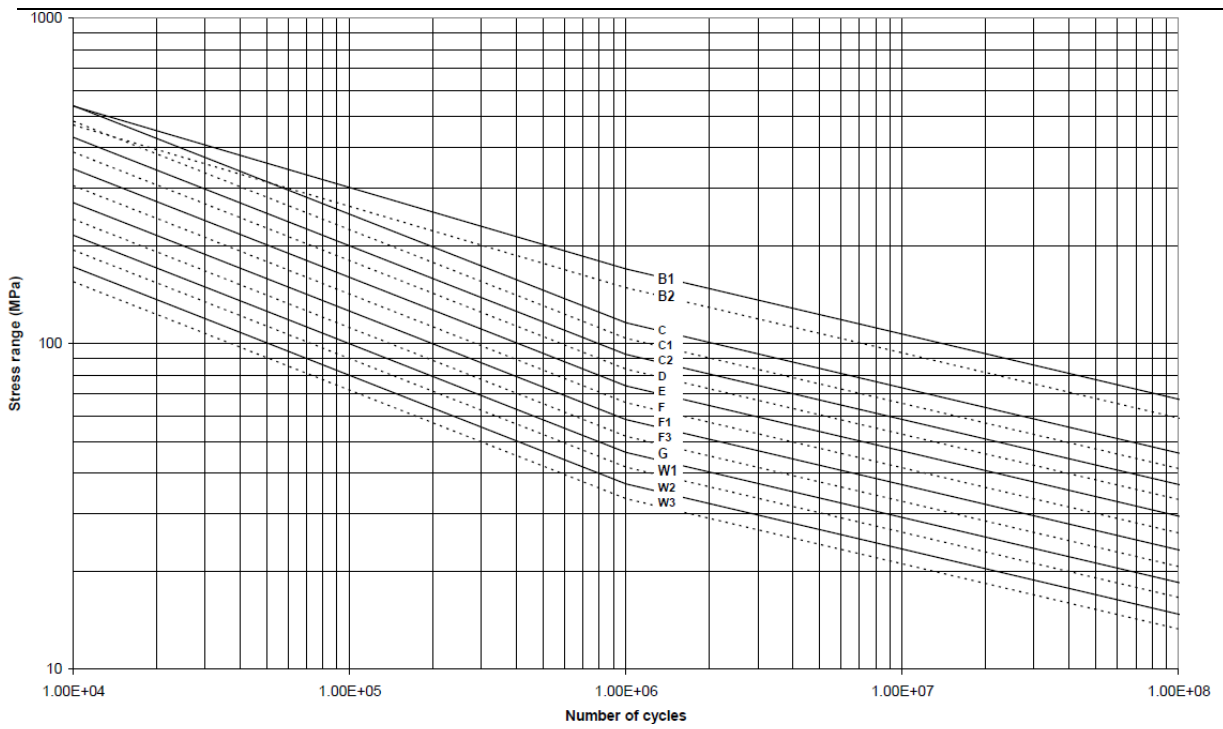


Figure 8-5: S-N curves in seawater with cathodic protection [32]

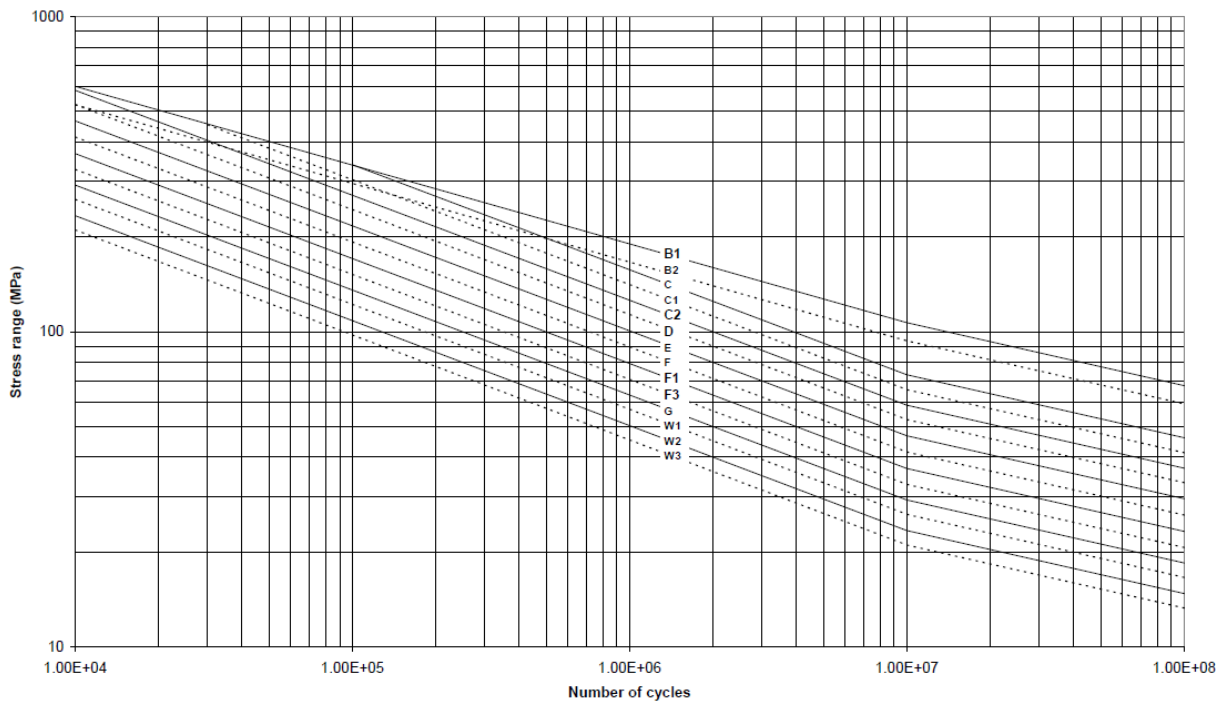


Figure 8-6: S-N curves in the air [32]

The fatigue life of the riser is calculated based on the S-N curves by assuming linear cumulative damage, which is expressed using the Palmgren-Minor rule. As per the Palmgren-Minor rule, accumulated fatigue damage (D_{fat}) can be expressed as below [32].

$$D_{fat} = \sum_{i=1}^k \frac{n_i}{N_i} = \frac{1}{\bar{a}} \sum_{i=1}^k n_i \cdot (\Delta\sigma_i)^m \quad 41$$

where:

\bar{a} – Intercept of the design S-N curve with the log N-axis

m – The negative inverse slope of the S-N curve

k – Number of stress blocks

n_i – Number of stress cycles in stress block i

N_i – Number of cycles to failure at constant stress range $\Delta\sigma_i$

8.4.2 Analysis Procedure

DNV-RP-F204: Riser Fatigue [68] suggests a general WF and LF fatigue damage calculation approach. This method is adopted in the fatigue analysis, and the relevant steps are mentioned below. The data here are referred to the met-ocean report from the Santos basin. The complete data set is not presented here due to confidentiality.

- Directional frequencies of waves are extracted from the met-ocean report. It is shown in Table 8-1. Sectors with a low frequency of occurrence (<1%) are combined with their adjacent sector to reduce the number of load cases. This leads to a reduced simulation time [69].

Table 8-1: Directional frequency of waves

Direction	Original Sector frequency %	Modified sector frequency %
0°	0.01	-
30°	0.09	-
60°	18.84	18.94
90°	20.27	20.27

120°	18.01	18.01
150°	19.4	19.40
180°	18.57	18.57
210°	4.44	4.81
240°	0.29	-
270°	0.05	-
300°	0.02	-
330°	0.01	-
Total	100.0	100.0

- The wave scatter diagram is subdivided into several representative blocks (sea state lumping). This will reduce the number of H_s and T_p combinations used in the analysis, significantly reducing the simulation time while providing results with sufficient accuracy [70]. Sea state lumping method has been proven to give accurate results for rigid risers by the previous works carried out by several researchers [3], [5], [25], [67]. Wave lumping is a trial-and-error procedure. The fatigue damage of each block in consideration should not exceed 5% of the total damage. If it is more than 5%, blocks need to be rearranged until the target value is achieved. Directional wave scatter diagrams for the dominant directions as per Table 8-1 are selected for the blocking. A sample block diagram for sector 60° is presented for reference in Figure 8-7. Rest of the sea state diagrams are not included in the report due to confidentiality.

Hs [m]		Tp [s]														
		4	5	6	7	8	9	10	11	12	13	14	15	16	17	
0.5	1.0	Block 1			Block 2			Block 3			Block 4			Block 5		
1.0	1.5	Block 6			Block 7			Block 8			Block 9			Block 10		
1.5	2.0	Block 6			Block 7			Block 8			Block 9			Block 10		
2.0	2.5	Block 6			Block 7			Block 8			Block 9			Block 10		
2.5	3.0	Block 11			Block 12			Block 13			Block 14					
3.0	3.5	Block 11			Block 12			Block 13			Block 14					
3.5	4.0	Block 15			Block 16											
4.0	4.5	Block 15			Block 16											
4.5	5.0	Block 17														
5.0	5.5	Block 17														

Figure 8-7: Subdivision of sea states in sector 60°

Representative H_s and T_p combinations for each block are obtained using the weighted average method for each block. Representative H_s for Block-1 can be calculated as per the below equation. T_p is also calculated using the same method. Based on Figure 8-7, 17 different H_s and T_p combinations were generated for sector 60°.

$$H_{s,Block1} = \frac{(\sum_{H_s=0.5}^{H_s=1.0} n_i) * H_{s=1.0} + (\sum_{H_s=1.0}^{H_s=1.5} n_i) * H_{s=1.5}}{(\sum_{H_s=0.5}^{H_s=1.5} n_i)} \quad 42$$

where:

n_i – Number of each H_s occurrence in the block

Representative sea states and their lumped frequency of occurrence (calculated as per Eq.43) are shown in Table 8-2. Exposure hours per year are calculated as shown in Eq.44. Wave lumping is carried out for all the scatter diagrams in different sectors. Only sectors highlighted in the Table 8-1 will be considered in the analysis. The total number of load cases (for all the sectors) used in the analysis is 113.

$$Lumped\ Frequency = \frac{(\sum Wave\ occurrences\ in\ considered\ block)}{(\sum Wave\ occurrences\ in\ the\ sector)} \quad 43$$

$$\frac{Exposure}{Year} = Lumped\ Frequency * Sector\ Probability * 365 * 24 \quad 44$$

Table 8-2: Representative sea states and their lumped probabilities

Block #	H_s (m)	T_p (m)	γ	Lumped Frequency	Exposure/Year (hrs)
1	1.47	6.29	1.709	0.0359	59.6
2	1.48	7.71	1.215	0.1031	171.1
3	1.50	9.57	1.000	0.0014	2.3
4	1.44	12.30	1.000	0.0010	1.6
5	1.50	15.50	1.000	0.0001	0.1
6	2.16	6.44	2.285	0.1608	266.9

7	2.25	7.86	1.680	0.4775	792.2
8	2.27	9.64	1.197	0.0205	34.1
9	2.22	12.57	1.000	0.0025	4.1
10	2.07	16.63	1.000	0.0003	0.5
11	3.06	7.45	2.398	0.0786	130.5
12	3.17	8.65	1.917	0.1074	178.2
13	3.07	11.72	1.107	0.0004	0.7
14	3.00	17.50	1.000	0.0001	0.1
15	4.05	8.74	2.323	0.0098	16.2
16	4.29	10.50	1.780	0.0001	0.2
17	5.00	9.60	2.369	0.0005	0.9
			Total	1.000	1659.1

- OrcaFlex is used to calculate the short-term fatigue damage in each sea state. The simulation time for each load case is 45 minutes. OrcaFlex uses a deterministic random wave analysis method to calculate fatigue damage with the Rainflow counting technique [42]. The Rainflow counting method analyses fatigue data to reduce a spectrum of varying stresses (strains) into a set of stress reversals. This allows the application of the Palmgren-Minor rule to assess the fatigue life of a structure with complex loading [42]. Damage is calculated at eight equally spaced points for both the inner and outer circumference of the pipe. The worst damage from the eight values is selected as the damage at the particular location.
- The weighed fatigue damage accumulation from all sea-states is then calculated using the below equation.

$$D_L = \sum_{i=1}^{N_s} D_i P_i$$

45

where:

D_L – Long-term fatigue damage

N_s – Number of discrete sea states in the wave scatter diagram (17 for sector 60°)

P_i – Sea-state probability (as per Table 8-2)

D_i – Short-term fatigue damage

- This is repeated for all the wave directions as per Table 8-1, and total long-term fatigue damage is calculated by summing up all the fatigue damages from all the sectors.

8.4.3 Fatigue Analysis Results

- Fatigue Life for Inner Wall (E in Air) and Outer Wall (D in SW with CP)

An exaggerated graph of fatigue life near the TDP is shown in Figure 8-9.

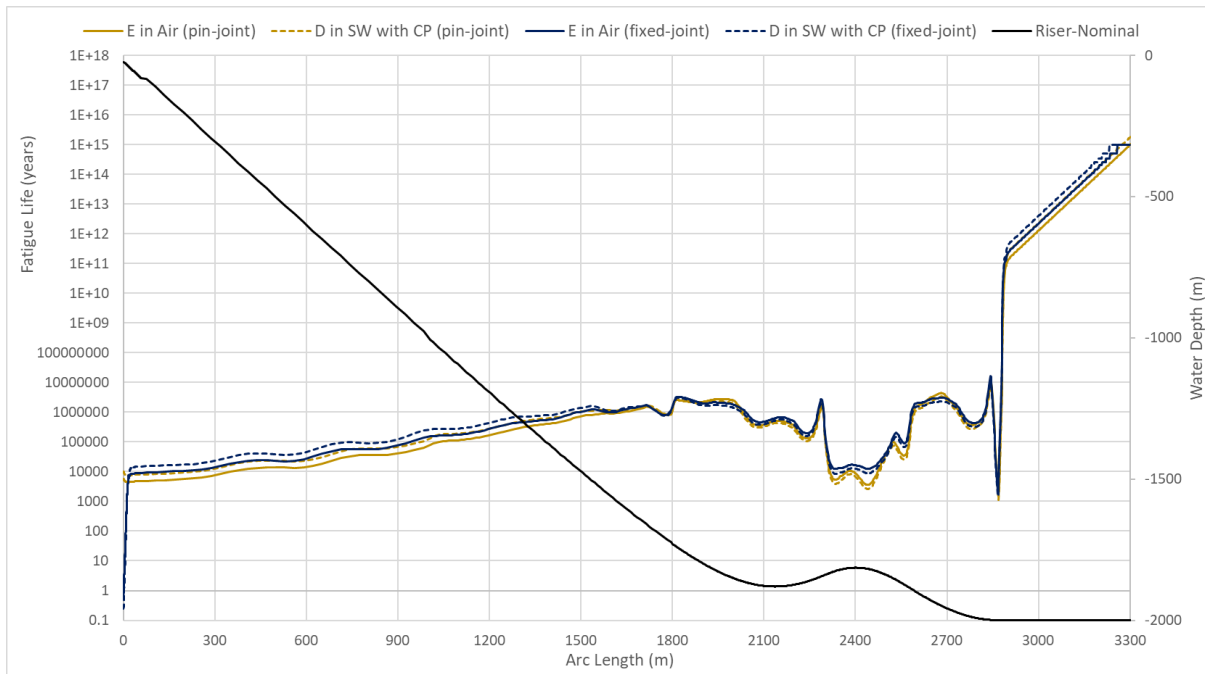


Figure 8-8: Fatigue life of SLWR against arc length

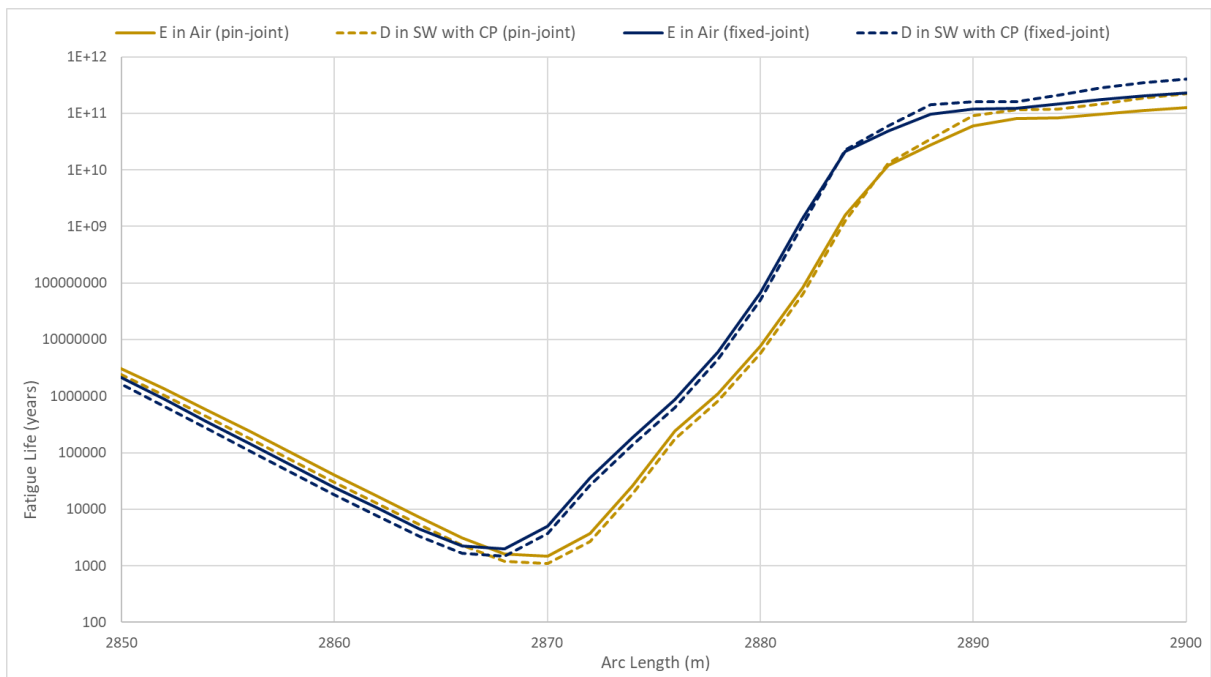


Figure 8-9: Fatigue life near the TDP

- Summary of Fatigue Life (and Fatigue Damage) near the TDP

Table 8-3: Fatigue damage near the TDP

S-N Curve	Fatigue damage	Fatigue life (years)
Inner wall (pin-joint)	0.00067	1491
Outer wall (pin-joint)	0.00091	1095
Inner wall (fixed-joint)	0.00051	1991
Outer wall (fixed-joint)	0.00069	1458

8.5 Discussion on Fatigue Analysis

- Fatigue life at TDP increases when the flex joint's stiffness is considered. Increased hang-off point stiffness helps dampen the cycle stresses in the sag bend, hog bend and TDP. For a conservative approach, analysis is carried out using a pin joint at the riser hang-off point since it predicts high fatigue damage at TDP (low fatigue life).

-
- Fatigue life at the hang-off point is very low for the fixed joint condition. However, this is mitigated by using tapered flex joints near the riser hang-off point in real life (Fatigue damage near the hang-off point is out of the scope of this thesis work).
 - The inner wall (E in Air) and outer wall (D in SW with CP) follow a similar trend in fatigue life variation along the whole arc length. The outer wall has lower fatigue life than the Inner wall. This difference is about 35%.
 - TDP has the lowest fatigue life along the whole riser length when the riser hang-off point is considered as a pin joint.
 - The fatigue life required for a safe design is 250 years; hence the configuration is acceptable.

9 Parametric Study on Fatigue Life near TDP

9.1 Introduction

The parametric study focuses on the fatigue life at the TDP for different SLWR configurations in different water depths with different coatings. The SLWR studied in the previous chapters is used as the base case for the analysis. The following factors are considered in the analysis.

- Only the nominal vessel position is considered.
- The riser hang-off point is considered a pin joint
- Only the fatigue life at TDP is considered.
- Fatigue analysis load cases and simulation times are same as in Chapter 8.
- Density of 70mm coating is 700kg/m^3 (production riser) while 900kg/m^3 for 3mm 3LPP coating (injection riser).
- An average fluid density of 500kg/m^3 is considered in all the analyses.
- Only the results for the outer wall (D in SW with CP Curve) are shown in this chapter. The results for the inner wall (E in Air) are shown in Appendix C. This is because the fatigue life variations for both walls follow a similar trend, as shown in Chapter 8.
- All the notations used during these analyses are referred Figure 9-1.

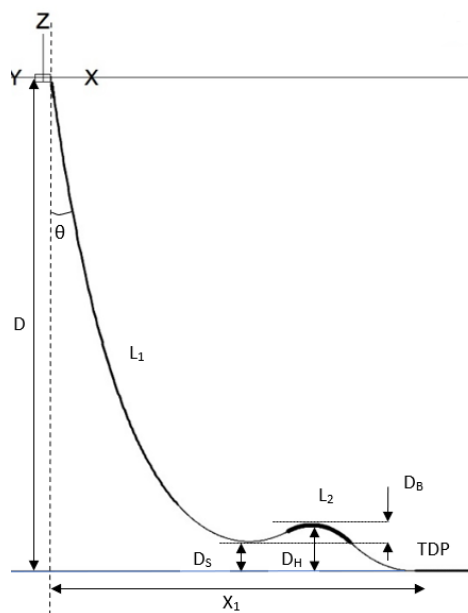


Figure 9-1: SLWR notations for fatigue analysis

This analysis considers eight different scenarios, as shown in Figure 9-2. Hereafter, different scenarios will be identified with their SET number.

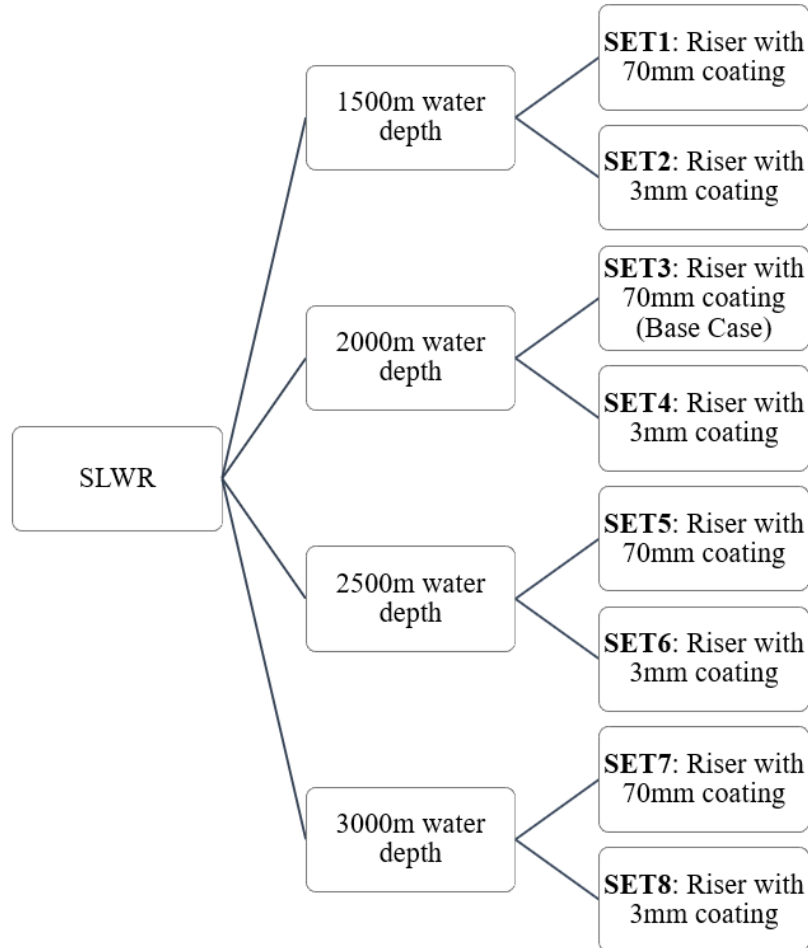


Figure 9-2: Different SLWR analysis scenarios

9.2 Selection of Different SLWR Configurations

A set of 25 different SLWR configurations for each SET was achieved for the study. All these configurations are designed per LRFD guidelines for static and dynamic states. In total, there are 200 (25*8) different SLWR configurations. These configurations were achieved by changing the following parameters of the SLWR.

- The net buoyancy of the floaters
- The length of the buoyancy section (L_2)
- The length from the riser hang-off point to the buoyancy section (L_1)

The SLWR configuration matrix for SET1 (1500m water depth with 70mm coating) is shown in Figure 9-3. Same D_S and D_B values as shown in Figure 9-3 are used to generate configurations in SET1 to SET8. Five different SLWR configurations of S1-A1 to S1-A5 (D_B is 67m and D_S is varying) are shown in Figure 9-4 for clarity (the rest of the 20 configurations in SET1 is not shown here). A detailed description of the 25 different configurations of each SET is attached in Appendix B.

		D_S (m)				
		120	162	208	254	300
D_B (m)	67	S1-A1	S1-A2	S1-A3	S1-A4	S1-A5
	100	S1-B1	S1-B2	S1-B3	S1-B4	S1-B5
	140	S1-C1	S1-C2	S1-C3	S1-C4	S1-C5
	180	S1-D1	S1-D2	S1-D3	S1-D4	S1-D5
	220	S1-E1	S1-E2	S1-E3	S1-E4	S1-E5

Figure 9-3: SLWR configuration matrix for fatigue analysis [SET1]

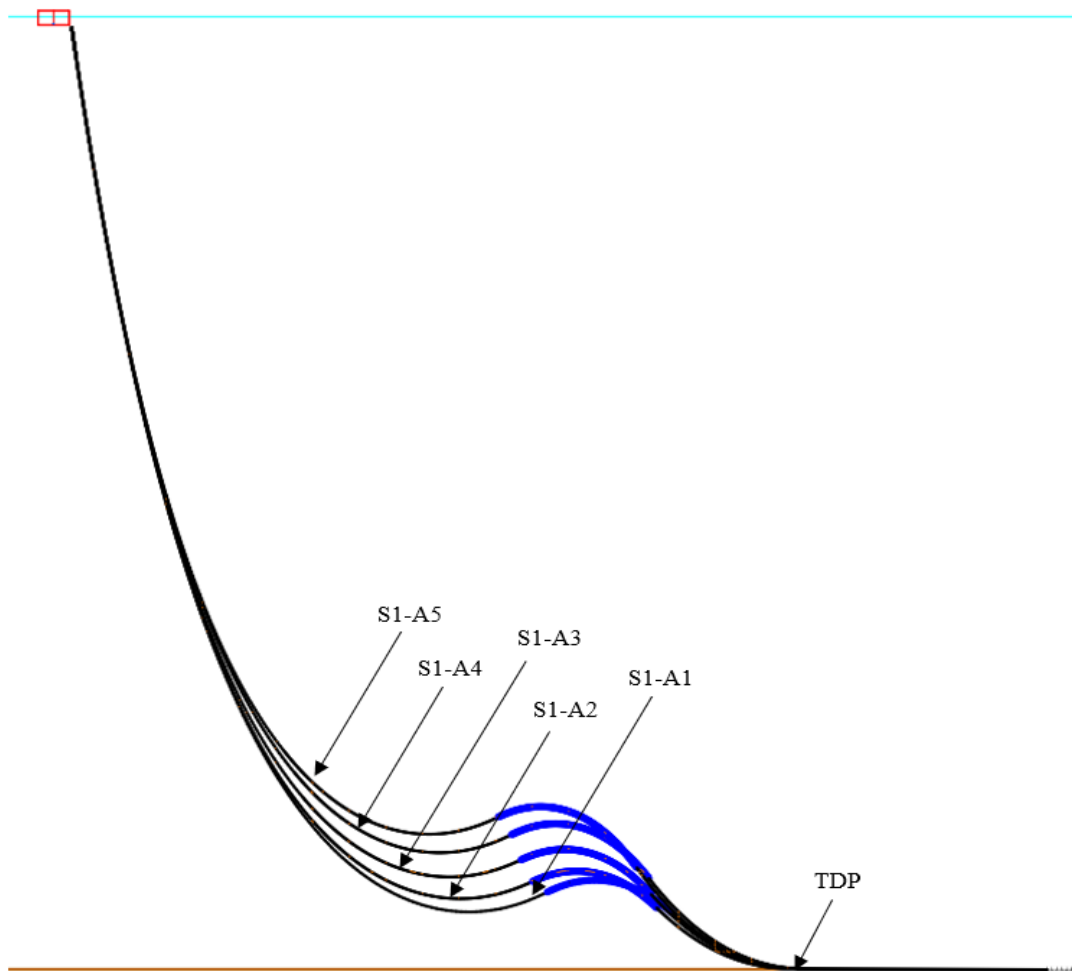


Figure 9-4: Different SLWR configurations for S1-A1 to S1-A5 [SET1]

9.3 Analysis Results

9.3.1 Analysis for 1500m Water Depth with 70mm Coating [SET1]

- Variation of Fatigue Life at TDP against D_B

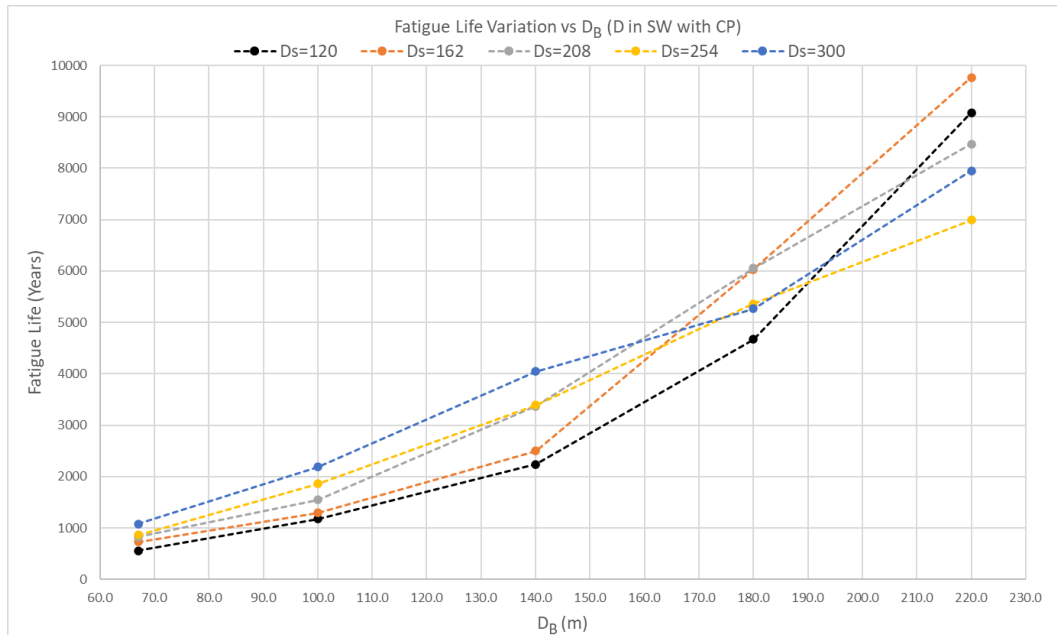


Figure 9-5: Fatigue life variation against D_B (outer wall) [SET1]

- Variation of Fatigue Life at TDP against D_S

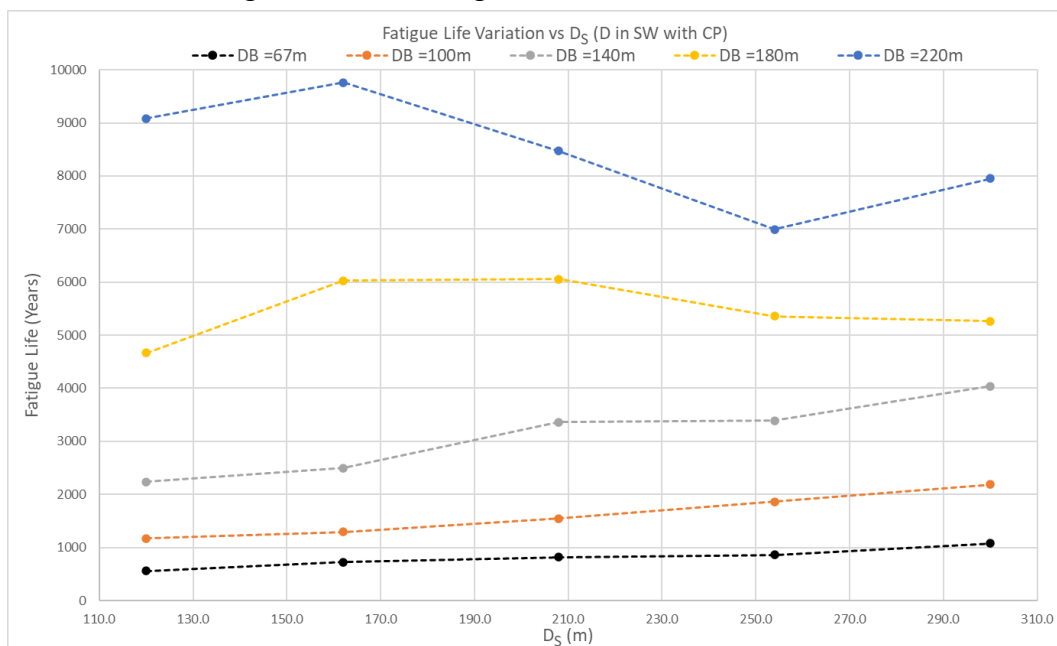


Figure 9-6: Fatigue life variation against D_S (outer wall) [SET1]

-
- Summary of fatigue life at TDP

Table 9-1: Summary of fatigue life (outer wall) [SET1]

	Fatigue Life at TDP (Years)				
D_B (m)	D_S=120m	D_S =162m	D_S =208m	D_S =254m	D_S =300m
67.0	557	725	822	860	1076
100.0	1171	1291	1548	1860	2188
140.0	2237	2501	3366	3394	4043
180.0	4668	6029	6056	5359	5263
220.0	9083	9763	8468	6994	7949

Remarks

- The outer wall (D in SW with CP) predicts low fatigue life than the inner wall (E in Air) at the TDP. Fatigue life difference for these two curves varies between 30-40% for all the cases. This is true for all the eight different SETs in consideration.
- Variation in both curves follows a similar trend. This is true for all the other eight SETs in consideration.
- Fatigue life always increases with the increase of D_B irrespective of the D_S value. This statement is also true for all the other SETs.
- Curves diverge from each with the increase of D_B. The rate of divergence is significant after the D_B =100m.
- For low D_B values, fatigue life variation against D_S is marginal, but they show an uptrend. For high D_B values, fatigue life variation against D_S is unpredictable.

9.3.2 Analysis for 1500m Water Depth with 3mm Coating [SET2]

- Variation of Fatigue Life at TDP against D_B

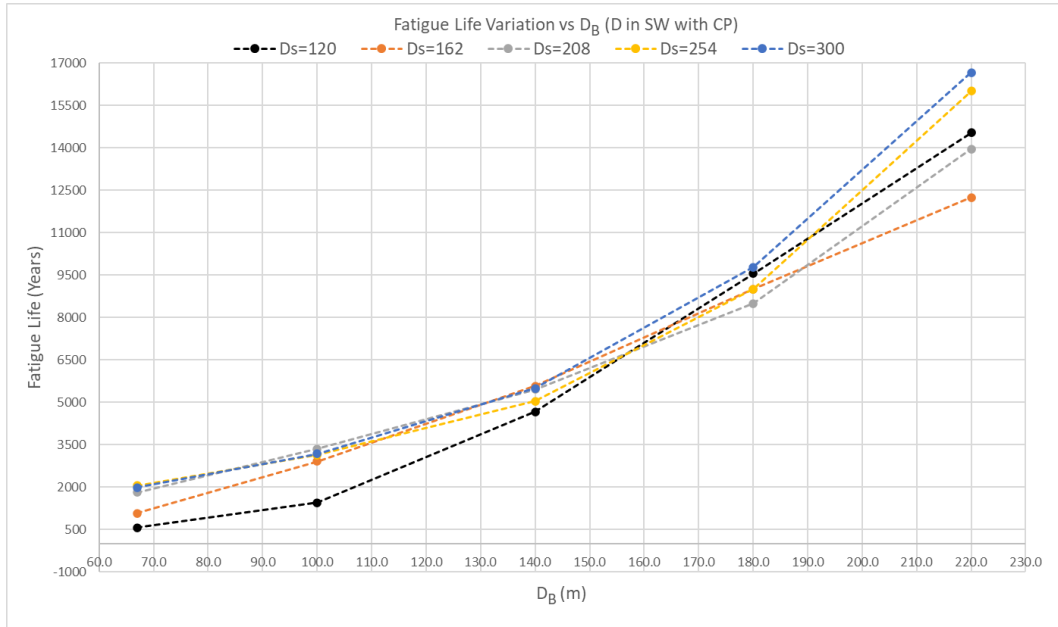


Figure 9-7: Fatigue life variation against D_B (outer wall) [SET2]

- Variation of Fatigue Life at TDP against D_S

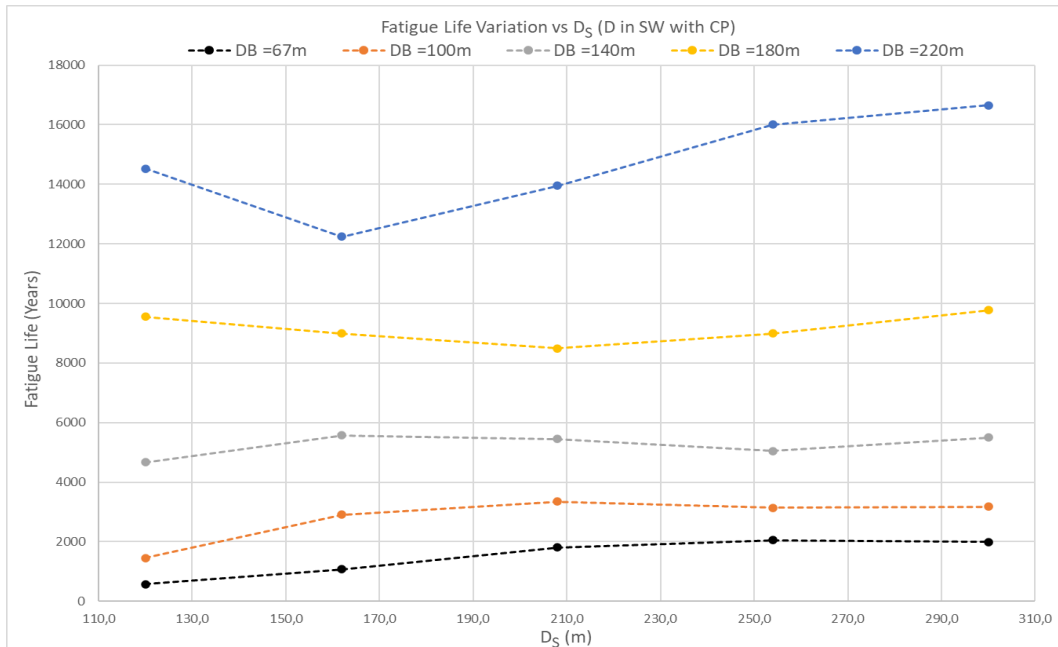


Figure 9-8: Fatigue life variation against D_S (outer wall) [SET2]

-
- Summary of fatigue life at TDP

Table 9-2: Summary of fatigue life (outer wall) [SET2]

	Fatigue Life at TDP (Years)				
D_B (m)	D_S=120m	D_S =162m	D_S =208m	D_S =254m	D_S =300m
67.0	569	1078	1811	2055	1987
100.0	1451	2905	3348	3138	3176
140.0	4662	5571	5452	5040	5498
180.0	9549	8997	8497	8995	9771
220.0	14529	12245	13948	16009	16654

Remarks

- Curves converge to each other until D_B=160m and then diverge again. All the curves follow the same trend.
- The fatigue life variation against D_S is mostly flat for curves except for D_B=220m.

9.3.3 Analysis for 2000m Water Depth with 70mm Coating [SET3]

- Variation of Fatigue Life at TDP against D_B

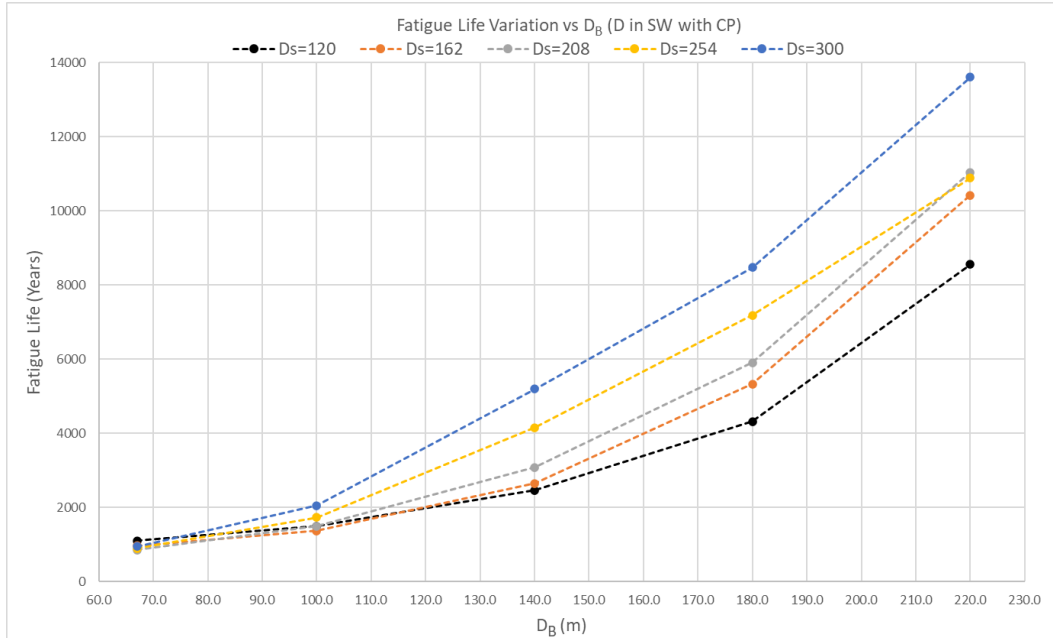


Figure 9-9: Fatigue life variation against D_B (outer wall) [SET3]

- Variation of Fatigue Life at TDP against D_s

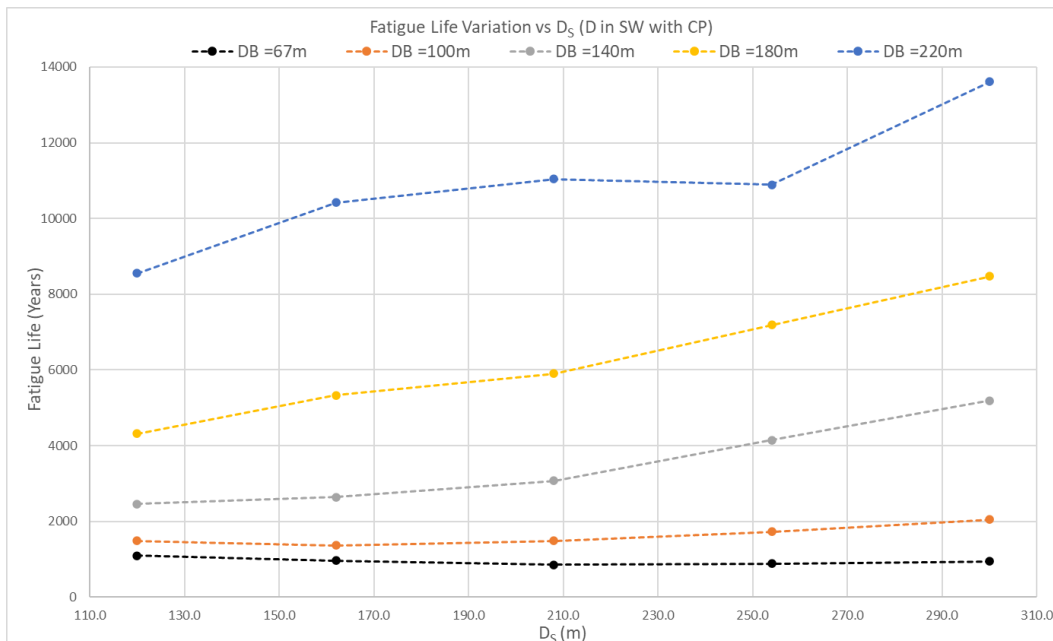


Figure 9-10: Fatigue life variation against D_s (outer wall) [SET3]

-
- Summary of fatigue life at TDP

Table 9-3: Summary of fatigue life (outer wall) [SET3]

D_B (m)	Fatigue Life at TDP (Years)				
	D_S=120m	D_S =162m	D_S =208m	D_S =254m	D_S =300m
67.0	1095	969	853	888	949
100.0	1489	1364	1489	1726	2046
140.0	2461	2645	3077	4151	5194
180.0	4314	5332	5901	7187	8472
220.0	8554	10424	11040	10893	13610

Remarks

- For D_B=67m, fatigue life is almost similar in all the cases. After D_B=100m, the rate of divergence is significant.
- Fatigue life is always increasing for high D_B values with the increase of D_S. For low D_B values, this variation is mostly marginal.

9.3.4 Analysis for 2000m Water Depth with 3mm Coating [SET4]

- Variation of Fatigue Life at TDP against D_B

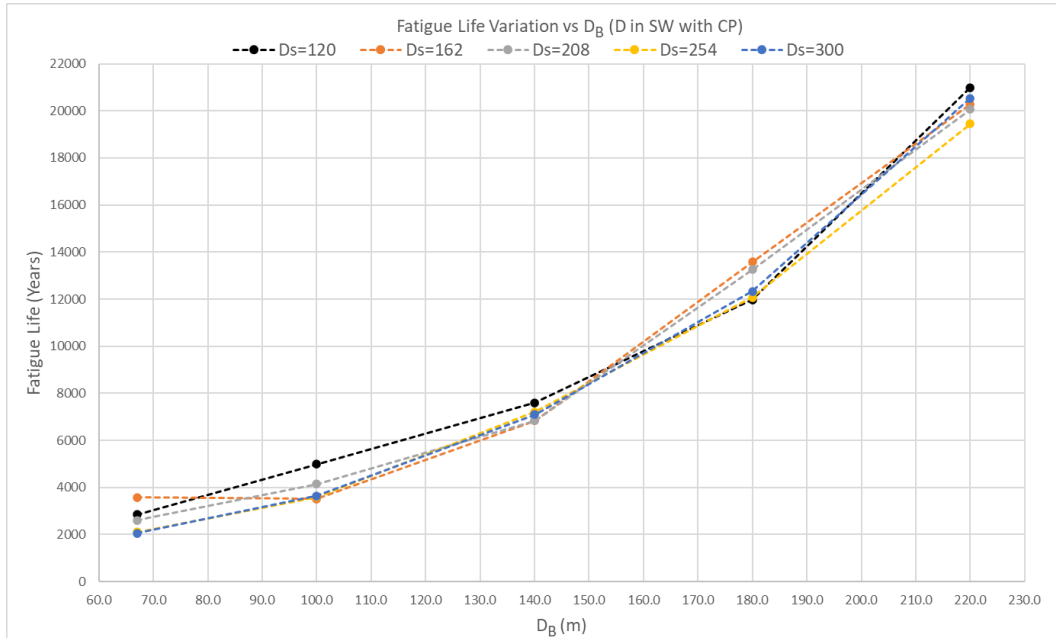


Figure 9-11: Fatigue life variation against D_B (outer wall) [SET4]

- Variation of Fatigue Life at TDP against D_S

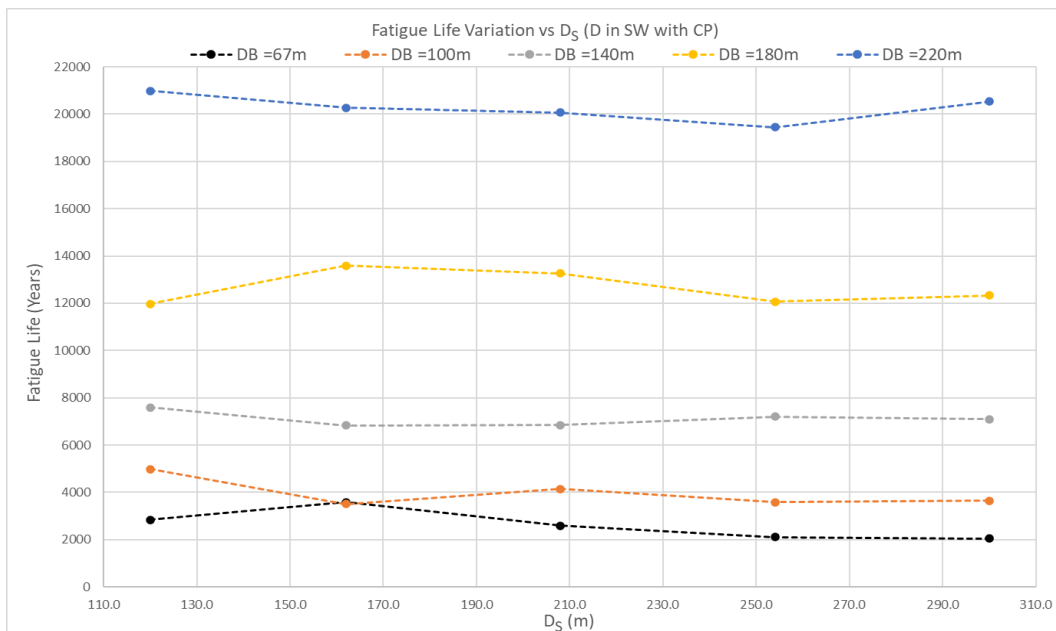


Figure 9-12: Fatigue life variation against D_S (outer wall) [SET4]

-
- Summary of fatigue life at TDP

Table 9-4: Summary of fatigue life (outer wall) [SET4]

	Fatigue Life at TDP (Years)				
D_B (m)	D_S=120m	D_S =162m	D_S =208m	D_S =254m	D_S =300m
67.0	2845	3579	2596	2101	2044
100.0	4982	3510	4138	3589	3646
140.0	7594	6834	6841	7202	7092
180.0	11981	13583	13258	12068	12324
220.0	20994	20269	20065	19441	20536

Remarks

- Curves are converged for all the values of D_B. They do not diverge even for higher D_B values.
- All the curves show almost flat behaviour regardless of the D_B value.

9.3.5 Analysis for 2500m Water Depth with 70mm Coating [SET5]

- Variation of Fatigue Life at TDP against D_B

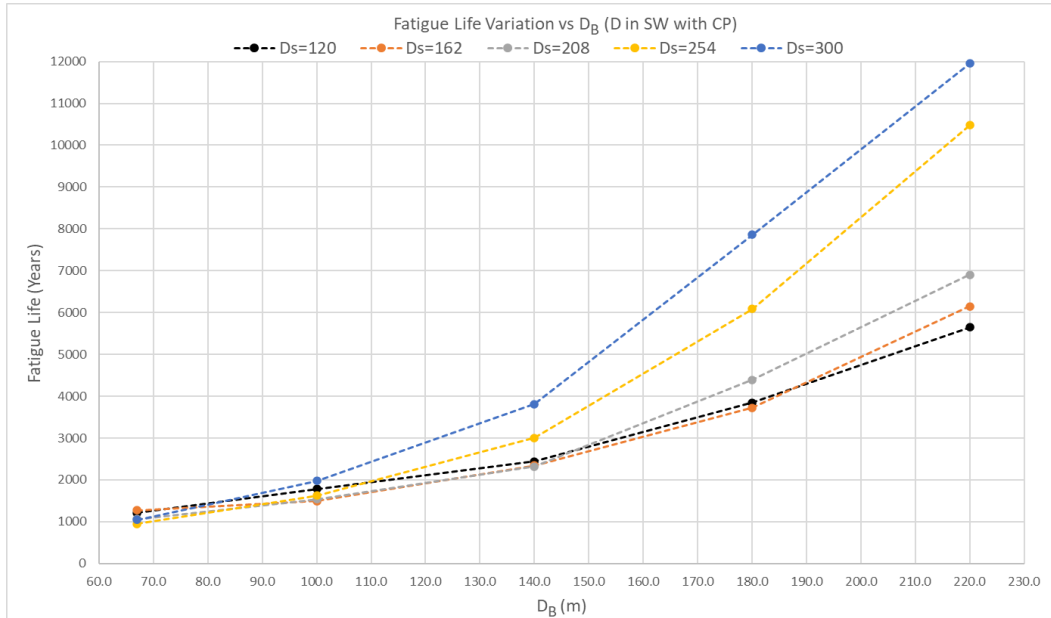


Figure 9-13: Fatigue life variation against D_B (outer wall) [SET5]

- Variation of Fatigue Life at TDP against D_S

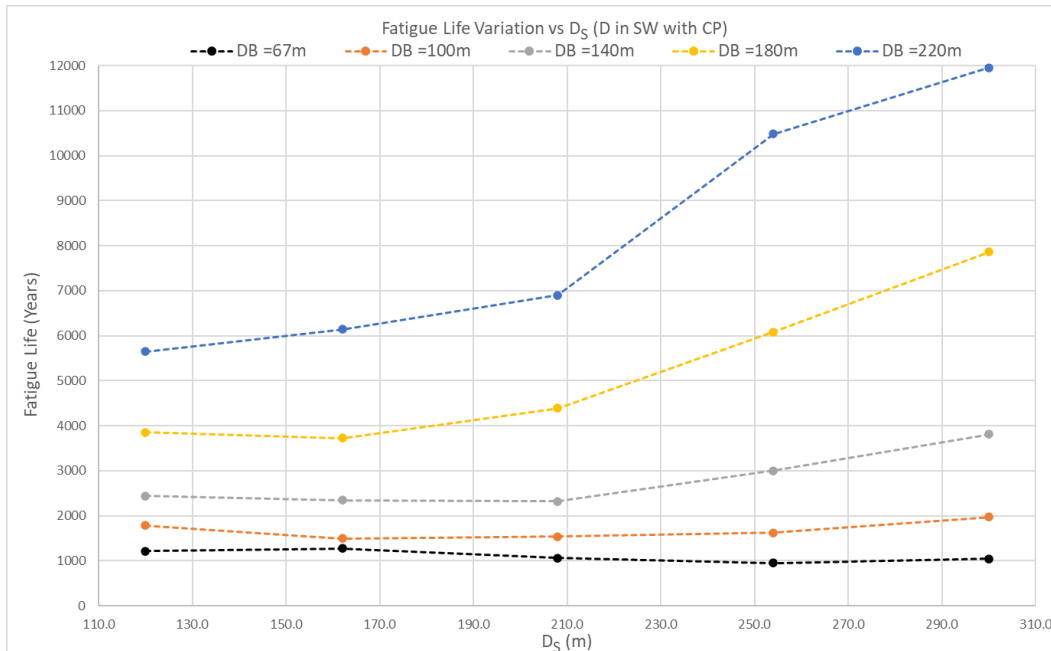


Figure 9-14: Fatigue life variation against D_S (outer wall) [SET5]

-
- Summary of fatigue life at TDP

Table 9-5: Summary of fatigue life (outer wall) [SET5]

	Fatigue Life at TDP (Years)				
D_B (m)	D_S=120m	D_S =162m	D_S =208m	D_S =254m	D_S =300m
67.0	1214	1274	1063	948	1048
100.0	1787	1496	1537	1627	1976
140.0	2443	2347	2323	3000	3811
180.0	3851	3725	4393	6086	7861
220.0	5651	6145	6903	10479	11954

Remarks

- For D_B=67m, fatigue life is almost similar in all the cases. After D_B=100m, the rate of divergence is significant.
- Fatigue life is always increasing for high D_B values with the increase of D_S.
- For low D_B values, fatigue life variation against D_S is marginal. Their variation is mostly flat.

9.3.6 Analysis for 2500m Water Depth with 3mm Coating [SET6]

- Variation of Fatigue Life at TDP against D_B

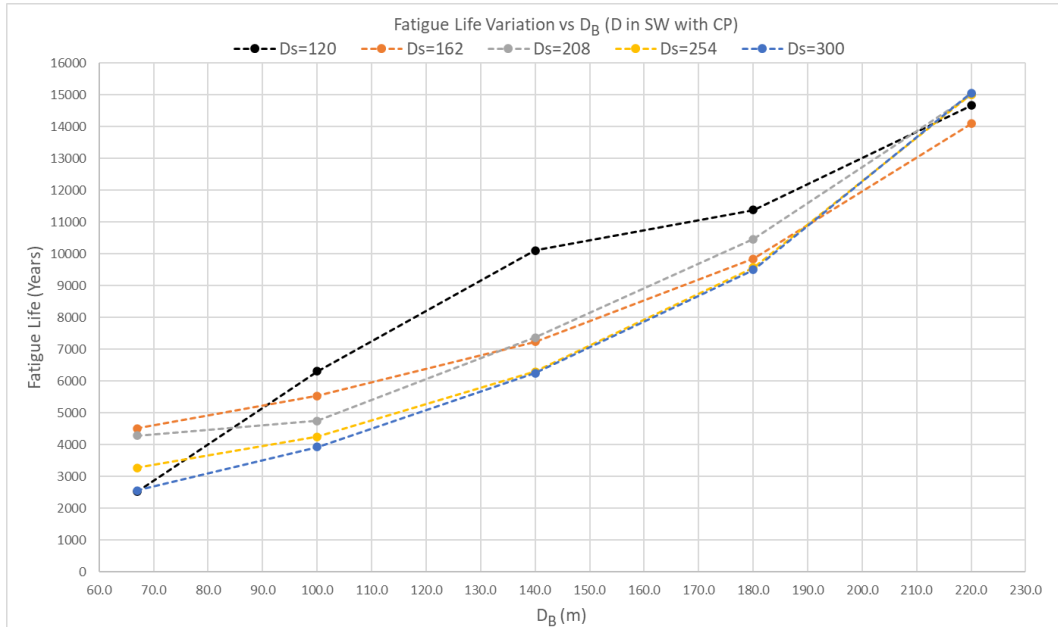


Figure 9-15: Fatigue life variation against D_B (outer wall) [SET6]

- Variation of Fatigue Life at TDP against D_s

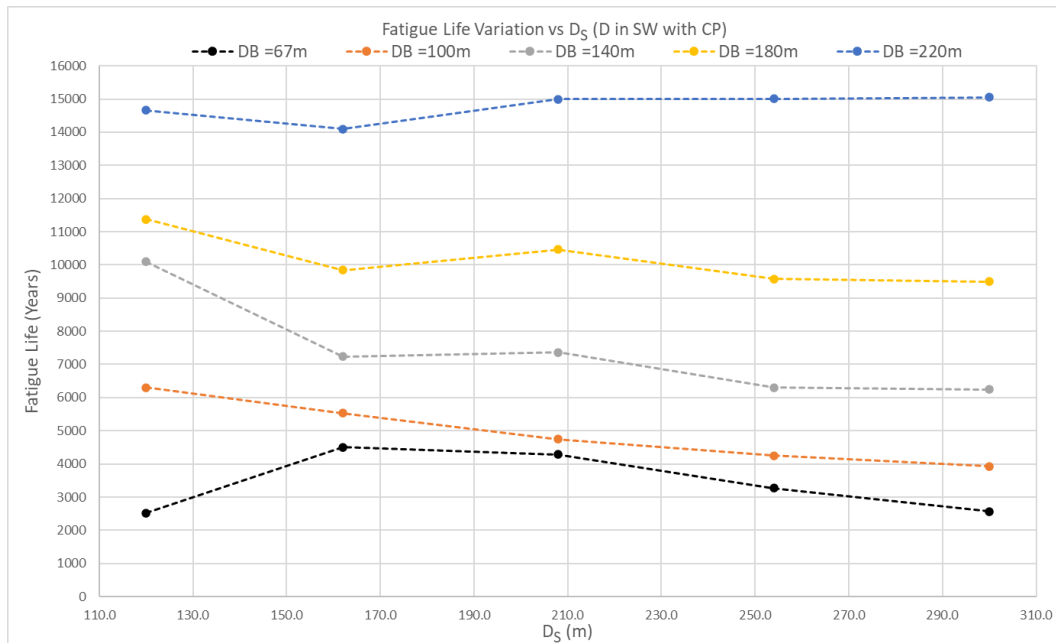


Figure 9-16: Fatigue life variation against D_s (outer wall) [SET6]

-
- Summary of fatigue life at TDP

Table 9-6: Summary of fatigue life (outer wall) [SET6]

	Fatigue Life at TDP (Years)				
D_B (m)	D_S=120m	D_S =162m	D_S =208m	D_S =254m	D_S =300m
67.0	2519	4505	4287	3271	2563
100.0	6307	5534	4745	4246	3923
140.0	10099	7235	7362	6299	6249
180.0	11371	9838	10459	9572	9498
220.0	14661	14095	14998	15005	15051

Remarks

- Fatigue life values converge when $D_B=220m$.
- Fatigue life variation against D_S shows a downward trend for the cases.

9.3.7 Analysis for 3000m Water Depth with 70mm Coating [SET7]

- Variation of Fatigue Life at TDP against D_B

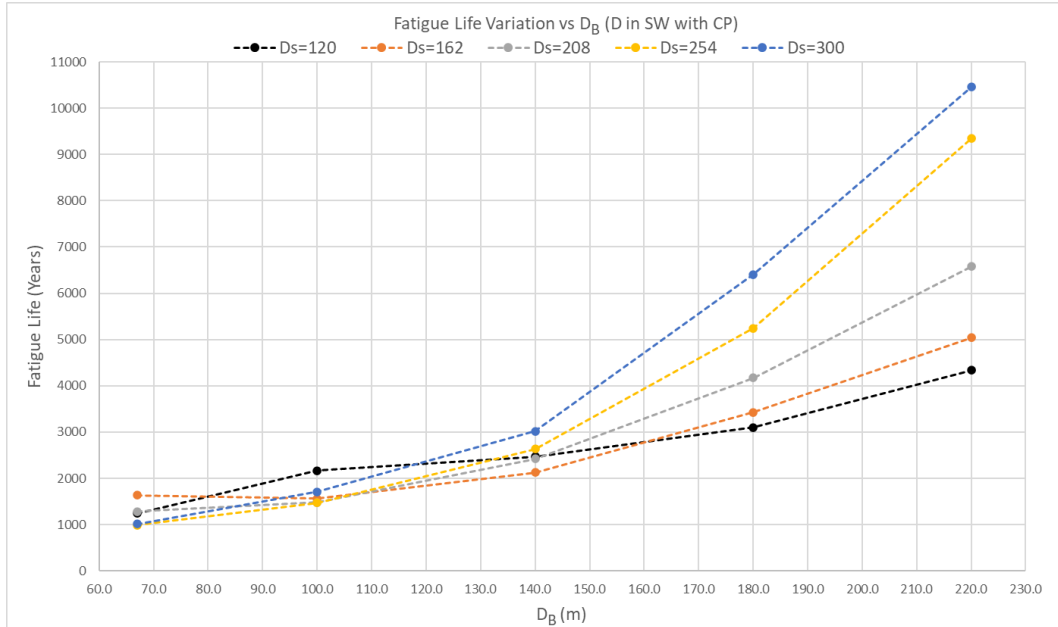


Figure 9-17: Fatigue life variation against D_B (outer wall) [SET7]

- Variation of Fatigue Life at TDP against D_S

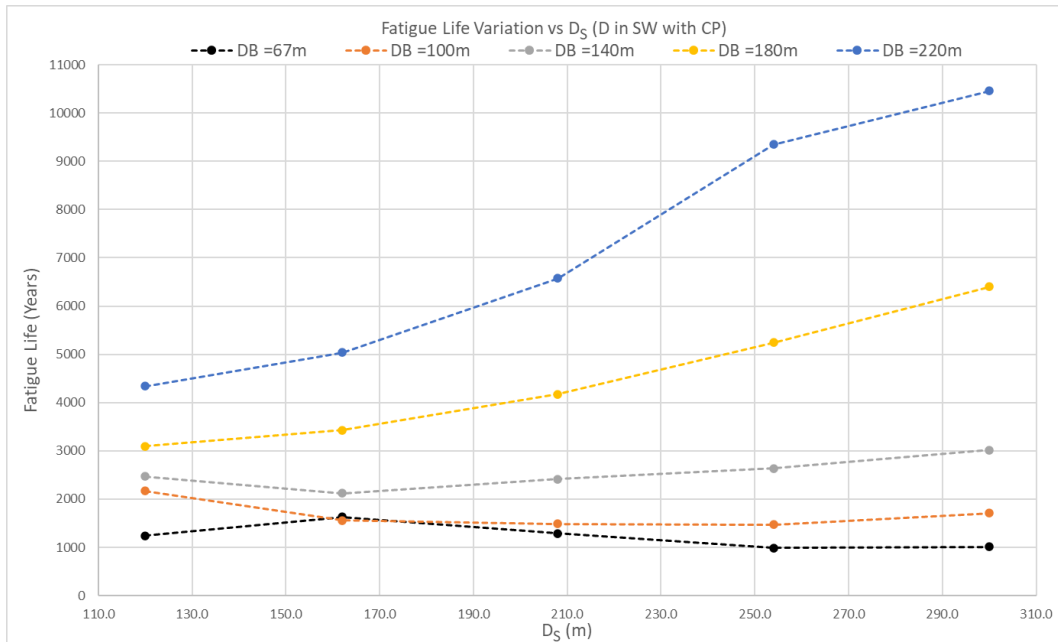


Figure 9-18: Fatigue life variation against D_S (outer wall) [SET7]

-
- Summary of fatigue life at TDP

Table 9-7: Summary of fatigue life (outer wall) [SET7]

	Fatigue Life at TDP (Years)				
D_B (m)	D_S=120m	D_S =162m	D_S =208m	D_S =254m	D_S =300m
67.0	1243	1632	1287	990	1011
100.0	2171	1559	1484	1472	1712
140.0	2468	2124	2417	2635	3015
180.0	3098	3429	4173	5248	6403
220.0	4338	5040	6579	9347	10457

Remarks

- Curves converge when D_B=100m and start diverging, and the divergence rate is high.
- Fatigue life variation for low D_B values is not significant. They show a flat variation.
- For high D_B values, fatigue life variation against D_S shows an uptrend.

9.3.8 Analysis for 3000m Water Depth with 3mm Coating [SET8]

- Variation of Fatigue Life at TDP against D_B

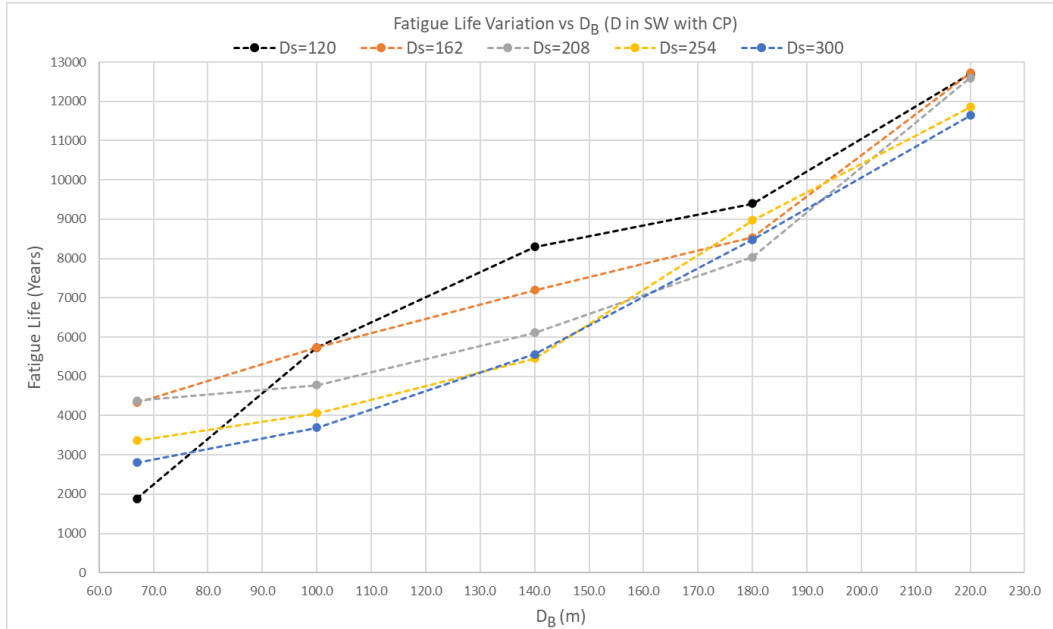


Figure 9-19: Fatigue life variation against D_B (outer wall) [SET8]

- Variation of Fatigue Life at TDP against D_s

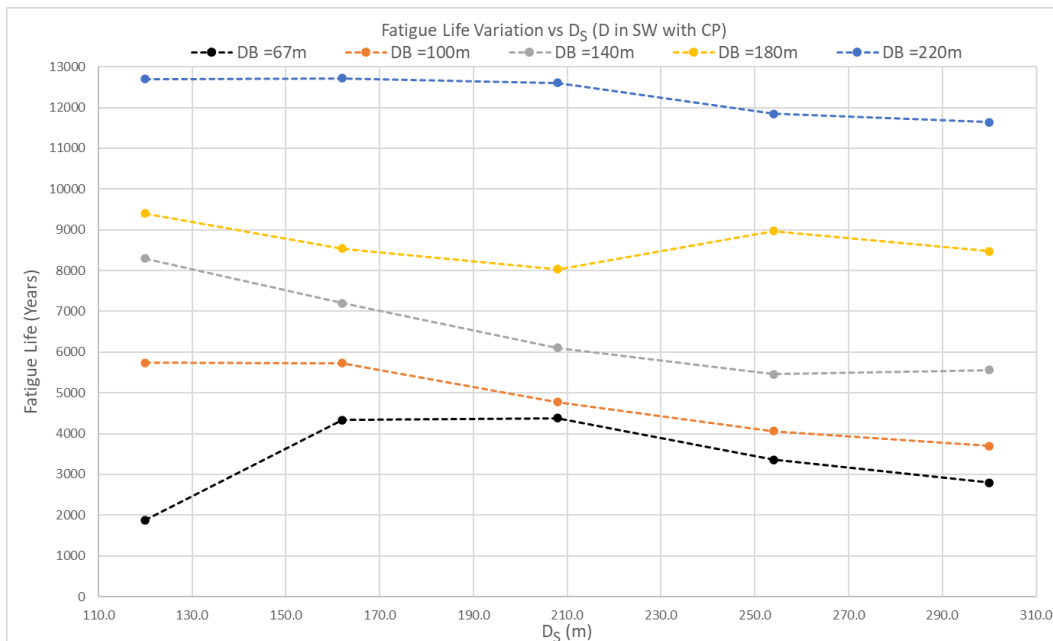


Figure 9-20: Fatigue life variation against D_s (outer wall) [SET8]

-
- Summary of fatigue life at TDP

Table 9-8: Summary of fatigue life (outer wall) [SET8]

	Fatigue Life at TDP (Years)				
D_B (m)	D_S=120m	D_S =162m	D_S =208m	D_S =254m	D_S =300m
67.0	1881	4334	4383	3363	2800
100.0	5734	5730	4772	4063	3697
140.0	8291	7198	6107	5455	5558
180.0	9402	8536	8032	8969	8478
220.0	12698	12721	12601	11850	11643

Remarks

- Curves start in a more diverged pattern, and they converge when D_B=180m.
- Fatigue life variation against D_S shows a downtrend for the D_B values.

9.4 Summary of Fatigue Life Variation near TDP (Outer Wall)

The summary is presented only for the outer wall. The summary for the inner wall is presented in Appendix D.

9.4.1 Summary of Fatigue Life Variation Against D_B for 70mm Coating

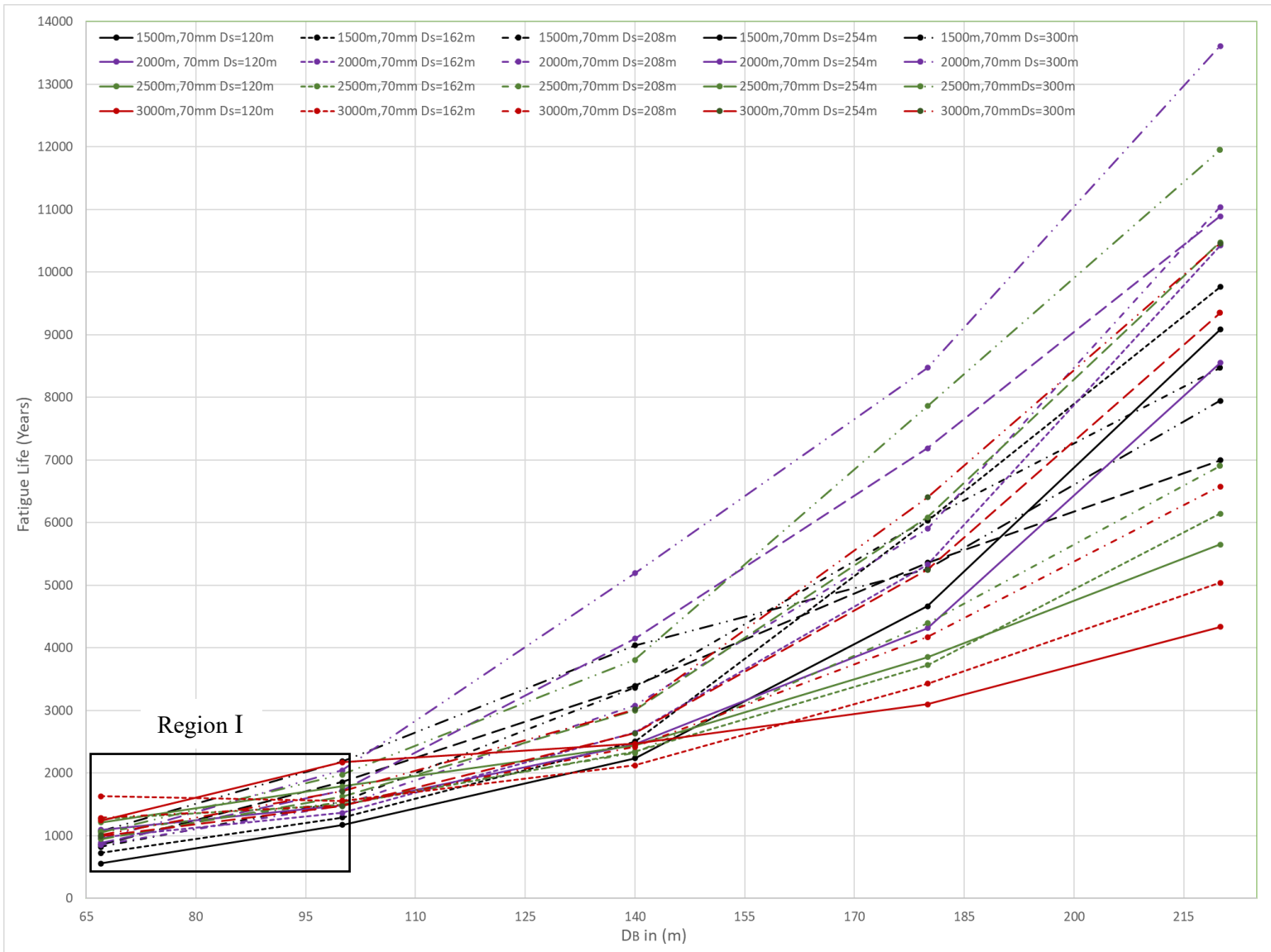


Figure 9-21: Summary of fatigue life variation against D_B for 70mm coating (outer wall)

- Despite the water depth and D_s value, fatigue life has an uptrend in all the cases considered in the analysis with the change of D_B .

- The rate of increase in Region I is marginal. When going beyond Region I, the rate of increase becomes significant (similar to an exponential behaviour).
- The high-low curves for 2000m, 2500m, and 3000m show similar behaviour, while curves for 1500m behave differently.
- High D_S values lead to high fatigue life, while low D_S values generally lead to low fatigue life with the change in D_B .

9.4.2 Summary of Fatigue Life Variation Against D_B for 3mm Coating

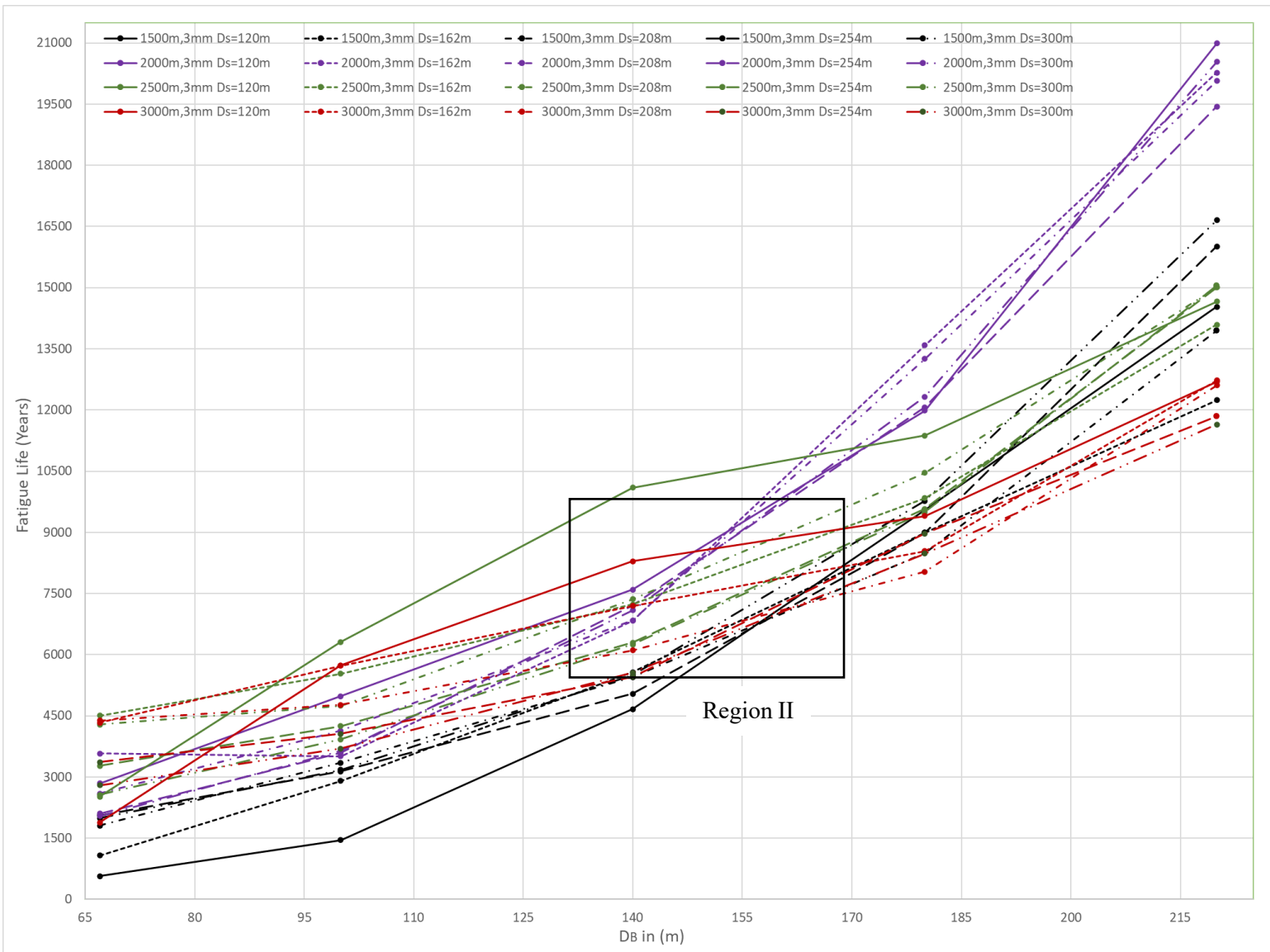


Figure 9-22: Summary of fatigue life variation against D_B for 3mm coating (outer wall)

- This behaviour is completely different from the behaviour of curves for 70mm coating thickness. Overall, curves for 3mm coating show high fatigue life.
- For low D_B values, curves start from a more scattered position and converge when D_B is around 150m (Region II). Then they start to diverge again.
- Curves for different D_S values in all the SETs flock together. This behaviour is unique for 3mm coating.

9.4.3 Summary of Fatigue Life Variation Against D_S for 70mm Coating

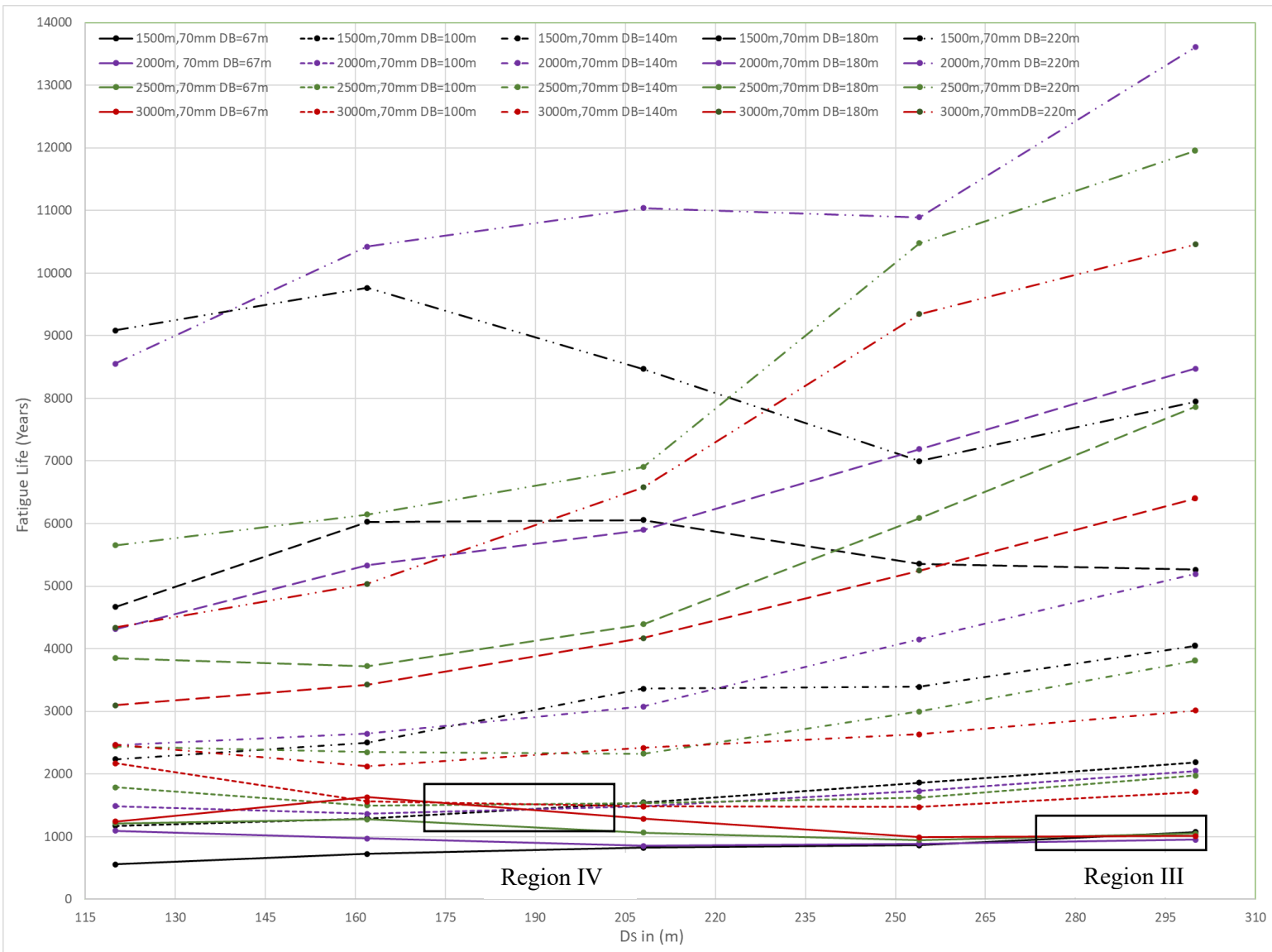


Figure 9-23: Summary of fatigue life variation against D_S for 70mm coating (outer wall)

- For low D_B values, fatigue life variation against D_S is mostly flat.
- All curves of $D_B=67\text{m}$ converge together with the increase of D_S (Region III).
- All the curves of $D_B=100\text{m}$ converge together in Region IV and start diverging again.
- For high D_B values, fatigue life variation against D_S has an uptrend except for 1500m water depth.

9.4.4 Summary of Fatigue Life Variation Against D_S for 3mm Coating

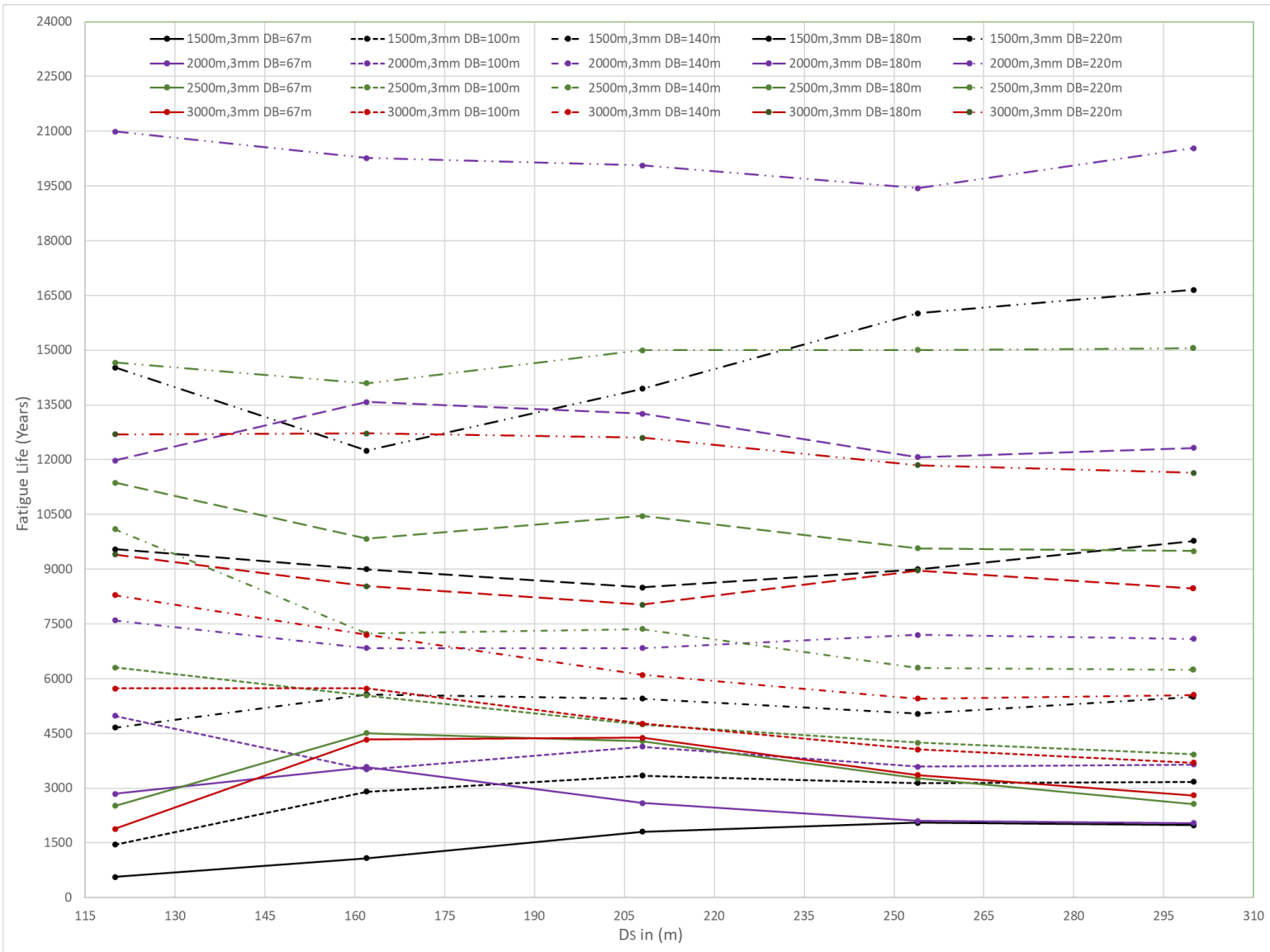


Figure 9-24: Summary of fatigue life variation against D_S for 3mm coating (outer wall)

-
- Fatigue life for 3mm coating is comparatively high than 70mm coating.
 - Most of the curves show a downtrend or flat behaviour when D_S increases.
 - For low D_S values, fatigue life is high. This behaviour is completely different from the behaviour for 70mm coating.

9.5 Discussion on Fatigue Life Variation near TDP

- The inner wall always predicts high fatigue life than the Outer wall. Fatigue life difference for these two curves varies between 30-40% for all the cases. This is not affected by the water depth.
- Fatigue life variation in both walls follows a similar trend near TDP. This applies to all the other eight SETs in consideration.
- Fatigue life always increases with the increase of D_B irrespective of the D_S value. This is not affected by water depth or coating thickness.
- Increasing the D_S value does not always yield to high fatigue life. The rate of fatigue life change is marginal compared to variation against D_B .
- Fatigue life for 70mm coating is predictable, while it is not true for 3mm coating.
- In general, Low D_S and D_B values should be avoided to have a better fatigue life.

10 Conclusions and Recommendations for Future Work

10.1 Conclusions

Static and dynamic analyses of an SLWR concept suitable for deployment in 2000m water depth in the Santos basin in Offshore Brazil are presented in the first part of the report. The second part presents the parametric study of fatigue life analysis at the TDP of the SLWR for different water depths (1500m, 2000m, 2500m, 3000m) with two different coatings (70mm, 3mm). The riser has a 254mm internal diameter with a 25mm wall thickness and is made of API 5L X65 Carbon steel. A spread moored FPSO is selected as the floater. The riser hang-off point is modelled as a pin joint.

All the analyses are carried out using OrcaFlex software. Vessel response is carried out for a 100-year wave to determine the worst response (downward velocity at the riser hang-off point). The worst response leads to the highest loads in the riser; hence it is incorporated in the dynamic analysis. The dynamic analysis uses a combined environmental load condition of 100-year wave and 10-year current, while fatigue analysis considers the wave scatter diagram. Several analyses have been carried out to verify the integrity of the riser, which are explained below. Code checks are based on DNV-OF-F201: Dynamic Risers.

10.1.1 Extreme Response Analysis

In the static analysis, it was observed that Far offsets give the highest effective tension while Near offsets produce high bending moments. Bending moment is the main factor which leads to a higher LRFD utilization factor because the effective tension variation in all the five different scenarios (Nominal, Near ULS, Far ULS, Near ALS, Far ALS) is marginal.

In the dynamic analysis, the increase of effective tension for all the cases is about 30% compared to static analysis. Near offsets have higher bending moment values. But Far offsets show a significant 42% increase in bending moment compared to their static state values, while Near offsets only show an increase of 13%. LRFD utilization factors in ULS are higher than in ALS despite the higher offsets. This is due to the reduced load effect factors in ALS.

Furthermore, the highest hang-off angle occurs when the FPSO experiences the highest downward velocity.

10.1.2 Fatigue Analysis

Fatigue analysis is based on the data from the scatter diagram in the Santos basin. Wave lumping is carried out to reduce the load cases in the analysis. 113 load cases are considered in the analysis, and the simulation time for one load case is 45 minutes. Two different S-N curves were considered in the analysis “E in Air” for “Inner Wall” and “D in Sea Water with Cathodic Protection” for “Outer Wall”. Fatigue life at the touch down point is the main consideration of this analysis.

Fatigue life at the TDP is increased with the stiffness of the hang-off point. Increased stiffness of the hang-off point helps to dampen the cycle stresses in the sag bend, hog bend and TDP. But for a conservative approach, the hang-off point is modelled as a pin-joint which gives high fatigue damage (low fatigue life). In real life, fatigue damage at the riser hang-off is mitigated by using tapered flex joints. Both inner and outer walls show a similar fatigue life variation along the arc length. The inner wall shows a 35% higher fatigue life near the TDP than the outer wall. Hence, outer wall fatigue is decisive in the design. The required fatigue life for a safe design is 250 years. The minimum fatigue life observed is 1095 years near the TDP; hence the fatigue design is acceptable.

10.1.3 Parametric Study on Fatigue Life near TDP

The parametric study focuses on the fatigue life at TDP for four different water depths (1500m, 2000m, 2500m, 3000m) with two different coatings (70mm coating with density 700kg/m^3 : production riser and 3mm 3LPP coating with density 900kg/m^3 : injection riser). The analysis follows a similar procedure as in the previous fatigue analysis. Eight different scenarios with 200 different SLWR configurations were considered in the analysis.

Inner wall fatigue life is always higher than outer wall fatigue life. Fatigue life difference for these two walls varies between 30-40% for all the cases. This is not affected by the water depth or the coating thickness. Further, fatigue life always increases with the increase of D_B

irrespective of the D_s value, water depth and coating thickness. Figure 10-1 further illustrates this (the upper bound refers to the maximum value out of all fatigue lives, and the lower bound refers to the minimum value).

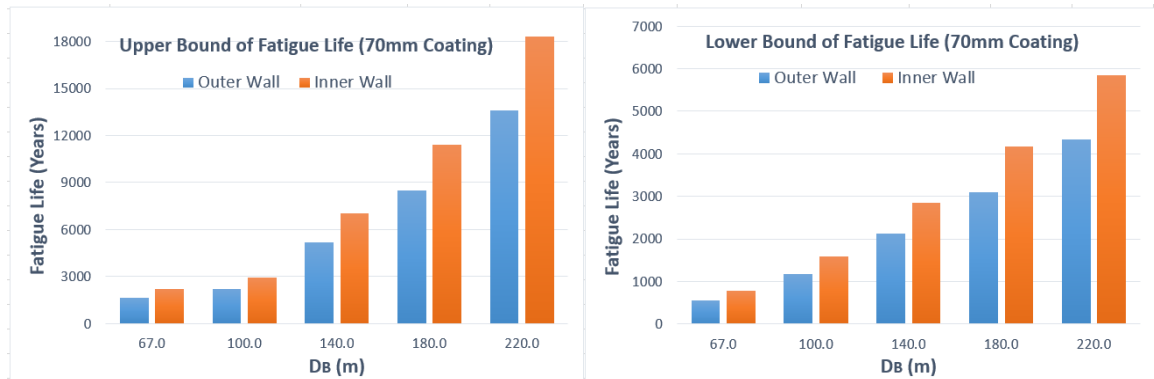


Figure 10-1: Upper and lower bound fatigue life variation against D_B (70mm coating)

In contrast, increasing the D_s value does not always yield to high fatigue life. Fatigue life behaviour can vary depending on water depth, coating thickness and D_B value. The rate of fatigue life change is also marginal compared to the variation against D_B . Figure 10-2 further illustrates this.

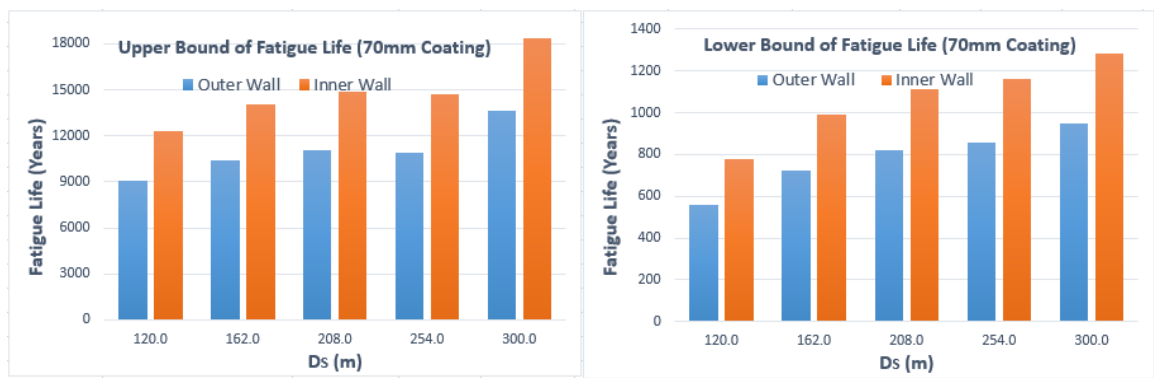


Figure 10-2: Upper and lower bound fatigue life variation against D_s (70mm coating)

10.2 Recommendations for Future Work

- Fatigue analysis data may be further studied to develop a parametric relationship with fatigue life, D_S and D_B (Regression analysis).
- VIV-induced fatigue analysis may be carried out to see if the behaviour seen in the wave induced fatigue correlates with the findings from VIV fatigue.

Bibliography

- [1] G. Zhang *et al.*, “Giant discoveries of oil and gas fields in global deepwaters in the past 40 years and the prospect of exploration,” *Journal of Natural Gas Geoscience*, vol. 4, no. 1, pp. 1–28, 2019, doi: 10.1016/j.jnggs.2019.03.002.
- [2] W. Han, S. Yu, H. Zhao, Y. Zhao, and L. Chen, “Strategies of Efficient Exploration and Development of Deepwater Oil and Gas Overseas,” *Frontiers of Engineering Management*, vol. 3, no. 4, p. 314, 2016, doi: 10.15302/j-fem-2016050.
- [3] D. Karunakaran, S. Subramanian, and R. Baarholm, “Steel lazy wave riser configuration for turret moored FPSO with Disconnectable turret in deepwater,” *Proceedings of the International Conference on Offshore Mechanics and Arctic Engineering - OMAE*, vol. 5B, no. 2010, 2015, doi: 10.1115/OMAE2015-41800.
- [4] J. Cheng and P. Cao, “Design of steel lazy wave riser for disconnectable FPSO in the Gulf of Mexico,” *Proceedings of the International Conference on Offshore Mechanics and Arctic Engineering - OMAE*, vol. 4 B, pp. 1–14, 2013, doi: 10.1115/OMAE2013-10921.
- [5] A. Felisita, O. T. Gudmestad, D. Karunakaran, and L. O. Martinsen, “Review of steel lazy wave riser concepts for the North Sea,” *Journal of Offshore Mechanics and Arctic Engineering*, vol. 139, no. 1, 2017, doi: 10.1115/OMAE2015-41182.
- [6] E. H. Phifer, F. Kopp, R. C. Swanson, D. W. Allen, and C. G. Langner, “Design and installation of Auger steel catenary risers,” *Proceedings of the Annual Offshore Technology Conference*, vol. 1994-May, pp. 399–408, 1994, doi: 10.4043/7620-ms.
- [7] D. Karunakaran, N. T. Nordsve, and A. Olufsen, “An Efficient metal riser configuration for ship and semi based production systems,” *Proceedings of the International Offshore and Polar Engineering Conference*, vol. 2, pp. 156–162, 1996.
- [8] J. Xia and R. D’Souza, “Floating production platform selection for developing deepwater gas fields off North West Australia,” *Society of Petroleum Engineers - SPE Asia Pacific Oil and Gas Conference and Exhibition 2012, APOGCE 2012*, vol. 2, pp. 813–828, 2012, doi: 10.2118/158717-ms.
- [9] A. Olufsen, L. G., G. P., and W. A., “Evaluation ranks deepwater, harsh-environment floater, riser concepts,” *Oil and Gas Journal 101(3):39-46*, 2003, Accessed: Feb. 18, 2022. [Online]. Available: https://www.researchgate.net/publication/291909483_Evaluation_ranks_deepwater_harsh-environment_floater_riser_concepts

-
- [10] M. Maddahi and S. J. Mortazavi, "A review on offshore concepts and feasibility study considerations," *Society of Petroleum Engineers - SPE Asia Pacific Oil and Gas Conference and Exhibition 2011*, vol. 2, no. September, pp. 1579–1599, 2011, doi: 10.2118/147875-ms.
- [11] E. London T, D. Arun S, and Q. L Allen, "A Comparison Between Turret and Spread Moored F(P)SOs for Deepwater Field Developments," *Deep Offshore Technology 2001*, pp. 1–23, 2001.
- [12] E. Q. de Andrade, L. L. de Aguiar, S. F. Senra, E. F. N. Siqueira, A. L. F. L. Torres, and M. M. Mourelle, "Optimization procedure of steel lazy wave riser configuration for spread moored FPSOs in deepwater offshore Brazil," *Proceedings of the Annual Offshore Technology Conference*, vol. 3, pp. 2057–2067, 2010, doi: 10.4043/20777-ms.
- [13] M. M. Padua *et al.*, "A journey of floating production systems in Brazil," *Proceedings of the Annual Offshore Technology Conference*, vol. 2020-May, pp. 1–8, 2020, doi: 10.4043/30554-ms.
- [14] C. A. Miller, "Risiers Introduction," *Encyclopedia of Maritime and Offshore Engineering*, pp. 1–11, 2017, doi: 10.1002/9781118476406.emoe485.
- [15] DNV GL, *DNVGL-SE-0476 Offshore riser systems*, no. August. 2017.
- [16] Y. Bai and Q. Bai, *Subsea Pipelines and Risers (Ocean Engineering)*. 2005. [Online]. Available: <https://www.sciencedirect.com/book/9780080445663/subsea-pipelines-and-risers>
- [17] NORSOK, *Norsok Standard Materials Selection M-001*, vol. 6, no. August. 2002.
- [18] S. Berge *et al.*, *Handbook on Design and Operation of Flexible Pipes*. 2017.
- [19] X. Li, X. Jiang, and H. Hopman, "A review on predicting critical collapse pressure of flexible risers for ultra-deep oil and gas production," *Applied Ocean Research*, vol. 80, no. June, pp. 1–10, 2018, doi: 10.1016/j.apor.2018.08.013.
- [20] American Petroleum Institute, "API Specification 5L - Forty-Sixth Edition," 2018. <https://www.api.org/products-and-services/standards/important-standards-announcements/standard-5l> (accessed Mar. 02, 2022).
- [21] B. Yue, M. Campbell, D. Walters, H. Thompson, and K. Raghavan, "Improved SCR Design for Dynamic Vessel Applications," *Proceedings of the ASME 2010 29th International Conference on Ocean, Offshore and Arctic Engineering OMAE2010 June 6-11, 2010, Shanghai, China*, no. July, pp. 1–23, 2016.

-
- [22] D. Karunakaran, T. S. Meling, S. Kristoffersen, and K. M. Lund, "Weight Optimized SCRs for Deepwater Harsh Environments," *2005 Offshore Technology Conference held in different density coatings. In this paper, the availability of Houston, TX, U.S.A., 2–5 May 2005*, pp. 1–9, 2005.
- [23] J.-L. Legras, D. N. Karunakaran, and R. L. Jones, "Fatigue Enhancement of SCRs: Design Applying Weight Distribution and Optimized Fabrication," 2013, doi: 10.4043/23945-ms.
- [24] M. Lal, F. Wang, X. Lu, and A. Sebastian, "Strength and fatigue performance of steel lazy wave risers with change in configuration parameters," *Proceedings of the International Conference on Offshore Mechanics and Arctic Engineering - OMAE*, vol. 5B-2019, pp. 1–8, 2019, doi: 10.1115/OMAE2019-95135.
- [25] G. M. Gemilang and D. Karunakaran, "Feasibility Study of Selected Riser Concepts in Deep Water and Harsh Environment," *Proceedings of the ASME 2017 36th International Conference on Ocean, Offshore and Arctic Engineering OMAE2017*, pp. 1–10, 2017.
- [26] B. K. Marsh, *Standards, specifications and codes of practice*. Woodhead Publishing Limited, 2003. doi: 10.1016/B978-075065686-3/50274-3.
- [27] J. Brekke, S. Chakrabarti, and J. Halkyard, *Drilling and Production Risers*, no. 2001. Elsevier Ltd, 2005. doi: 10.1016/b978-0-08-044381-2.50016-3.
- [28] American Petroleum Institute, *API RP 2RD (R2006): Design of Risers for Floating Production Systems (FPSs) and Tension-Leg Platforms (TLPs)*. 1996. Accessed: Feb. 04, 2022. [Online]. Available: https://www.techstreet.com/standards/api-rp-2rd-r2006?product_id=47839
- [29] Det Norske Veritas (DNV), *DNV-OS-F201 Dynamic Risers*, no. October. 2010. [Online]. Available: <http://rules.dnvgl.com/docs/pdf/DNV/codes/docs/2010-10/Os-F201.pdf>
- [30] Det Norske Veritas (DNV), *DNV-OS-F101: Submarine pipeline systems*, no. Outubro. 2013. [Online]. Available: <http://rules.dnvgl.com/docs/pdf/DNV/codes/docs/2013-10/OS-F101.pdf>
- [31] L. V. S. Sagrilo, E. C. P. de Lima, F. J. M. de Sousa, C. M. S. Dantas, M. Q. de Siqueira, and A. L. F. L. Torres, "Steel Lazy Wave Riser Design: API-RP-2RD and DNV-OS-F201 Criteria," *Proceedings of the International Conference on Offshore Mechanics and Arctic Engineering - OMAE*, vol. 1 A, pp. 107–113, Nov. 2008, doi: 10.1115/OMAE2005-67040.

-
- [32] Det Norske Veritas (DNV), *DNV-RP-C203 : Recommended Practice—Fatigue Design of Offshore Steel Structures*, vol. 4, no. October. 2006.
- [33] N. Singh and S. Nair, “Pipeline design philosophy and standards - a comparative study and recommendations,” *Offshore Technology Conference Asia 2016, OTCA 2016*, pp. 3356–3367, 2016, doi: 10.4043/26666-ms.
- [34] Det Norske Veritas, “TA&R No. 677 - Comparison of API, ISO, and Norsok offshore structural standards,” no. 677, 2006.
- [35] R. Maneschy, B. Romanelli, C. Butterworth, J. Pedrosa, C. Escudero, and T. Vargas, “Steel Catenary Risers (SCRs): From Design to Installation of the First Reel CRA Lined Pipes. Part II: Fabrication and Installation,” *OTC Brasil 2015: The Atlantic: From East to West - An Ocean of Innovation*, pp. 2350–2365, 2015, doi: 10.4043/26332-ms.
- [36] NORSOK, *Common Requirements Welding and Inspection Of Piping*, no. December. 2010.
- [37] Subsea 7, “Fact Sheet - Seven Borealis.”
- [38] T. Zhang, S. Gong, X. Wang, and C. Liu, “Influences of Pipelay Parameters on Dynamic Behavior of Deepwater J-Lay System,” *Journal of Pipeline Systems Engineering and Practice*, vol. 12, no. 1, p. 04020061, 2021, doi: 10.1061/(asce)ps.1949-1204.0000513.
- [39] Saipem, “Saipem 7000 | Saipem,” www.saipem.com.
<https://www.saipem.com/en/identity-and-vision/assets/saipem-7000> (accessed Feb. 11, 2022).
- [40] S. N. Smith and A. J. Clough, “Deepwater pipeline and riser installation by the reel-lay method,” *Proceedings of the Annual Offshore Technology Conference*, vol. 1, no. 1, pp. 751–762, 2010.
- [41] X. Hu, M. Duan, and P. Liu, “Risk and Reliability Analysis of Deepwater Reel-Lay Installation: A Scenario Study of Pipeline during the Process of Tensioning,” *Natural Resources*, vol. 03, no. 03, pp. 156–163, 2012, doi: 10.4236/nr.2012.33020.
- [42] D. Ulverston, C. La, a J. U. K. Telephone, W. Site, and OrcaFlex, “OrcaFlex Manual 9.8a,” *Interface*, vol. 44, no. 0, pp. 1–429, [Online]. Available: <http://www.orcina.com/SoftwareProducts/OrcaFlex/Documentation/OrcaFlex.pdf>
- [43] Det Norske Veritas, *DNV-RP-C205: Environmental conditions and environmental loads*, no. October. 2010.

-
- [44] Det Norske Veritas, “Position mooring DNVGL-OS-E301,” *October*, no. October, 2010.
- [45] Standards Norway, *Actions and action effects N-003*, no. September. 2007.
- [46] API, *API Recommended Practice 2SK, Design and Analysis of Stationkeeping Systems for Floating Structures*, no. October 2005. 2008.
- [47] D. C. Zacharias and A. Fornaro, “Brazilian offshore oil exploration areas: an overview of hydrocarbon pollution,” *Ambiente e Agua - An Interdisciplinary Journal of Applied Science*, vol. 15, no. 5, p. 1, Sep. 2020, doi: 10.4136/ambi-agua.2569.
- [48] B. Knapstad and D. Karunakaran, “Optimisation of Steel Lazy Wave Risers,” 2017.
- [49] A. O. Adejuwon and D. Karunakaran, “Ultra-Deep water High Pressure Riser Concept Offshore Brazil,” 2018.
- [50] K. Torsethaugen and S. Haver, “Simplified double peak spectral model for ocean waves,” *Proceedings of the International Offshore and Polar Engineering Conference*, pp. 76–84, 2004.
- [51] Y. Li, “Sensitivity study of SCR fatigue at touch down point: Effect of marine growth,” *Proceedings of the International Offshore and Polar Engineering Conference*, vol. 4, pp. 281–286, 2012.
- [52] <https://thenavalarch.com/>, “Horizontal Pipe Soil Resistance – Vertical Spring Generator.” <https://thenavalarch.com/software/oil-gas/subsea-engineering/horizontal-pipe-soil-resistance-vertical-spring-generator/>
- [53] J.-L. Legras, D. N. Karunakaran, and R. L. Jones, “Fatigue Enhancement of SCRs: Design Applying Weight Distribution and Optimized Fabrication,” *Offshore Technology Conference held in Houston, Texas, USA, 6–9 May 2013*, 2013, doi: 10.4043/23945-ms.
- [54] S. Li and C. Nguyen, “Dynamic Response of Deepwater Lazy- Wave Catenary Riser,” *Deep Offshore Technology International, Amsterdam*, pp. 1–20, 2010.
- [55] W. Ruan, J. Shi, B. Sun, and K. Qi, “Study on fatigue damage optimization mechanism of deepwater lazy wave risers based on multiple waveform serial arrangement,” *Ocean Engineering*, vol. 228, no. March, p. 108926, 2021, doi: 10.1016/j.oceaneng.2021.108926.
- [56] G. Hu, C. Huang, F. Yin, M. Cerkovnik, and G. Yang, “Effect of flexible joint modelling method on deepwater catenary riser hang-off fatigue response,”

- [57] A. R. Amorim, D. N. Karunakaran, D. A. S. Lima, G. Rombado, and B. Tveraaen, “An efficient method to estimate extreme response of risers from floaters in multidirectional sea states,” *Proceedings of the International Offshore and Polar Engineering Conference*, pp. 1199–1203, 2021.
- [58] G. Suwarno and C. H. Lee, “Wave seed selection on irregular wave analyses and the max extreme time windows from 3 hours simulations,” *Offshore Technology Conference Asia 2016, OTCA 2016*, pp. 4585–4597, 2016, doi: 10.4043/26564-ms.
- [59] T. Norsok, T. N. Oil, T. Federation, and N. Industry, “N-003 Actions and action effects,” no. November, pp. 1–244, 2013.
- [60] S. Haver, *Met-Ocean Modelling and Prediction of Extremes*, no. May. 2018.
- [61] Q. Xin, *Durability and reliability in diesel engine system design*. 2013. doi: 10.1533/9780857090836.1.113.
- [62] T. K. Sen, “Probability of Fatigue Failure in Steel Catenary Risers in Deep Water,” *Journal of Engineering Mechanics*, vol. 132, no. 9, pp. 1001–1006, 2006, doi: 10.1061/(asce)0733-9399(2006)132:9(1001).
- [63] M. Abelanet, D. Karunakaran, R. Jones, S. Eyssautier, and P. White, “Deepwater steel catenary risers require attention to fatigue factors,” <https://www.offshore-mag.com/>, 2013. <https://www.offshore-mag.com/subsea/article/16761371/deepwater-steel-catenary-risers-require-attention-to-fatigue-factors>
- [64] B. Campbell *et al.*, “Slugging Fatigue Assessment for Steel Lazy Wave Risers,” Aug. 2021, doi: 10.4043/30922-MS.
- [65] P. Gundersen, K. Doynov, T. Andersen, and R. Haakonsen, “Methodology for determining remnant fatigue life of flexible risers subjected to slugging and irregular waves,” *Proceedings of the International Conference on Offshore Mechanics and Arctic Engineering - OMAE*, vol. 3, no. February 2016, pp. 321–330, 2012, doi: 10.1115/OMAE2012-83412.
- [66] D. R. Stephens and J. Mandke, “Probabilistic Fatigue Analysis Of Offshore Pipelines During The Laying Operation,” *Proceedings of the Annual Offshore Technology Conference*, vol. 1981-May, pp. 341–344, May 1981, doi: 10.4043/4104-MS.
- [67] A. P. Orimolade, D. Karunakaran, and T. S. Meling, “Steel Lazy Wave Risers from Turret Moored FPSO for Deepwater Harsh Environment,” *ASME 2015 34th*

International Conference on Ocean, Offshore and Arctic Engineering OMAE2015, no. 2010, pp. 1–9, 2015.

- [68] D. N. Veritas, *DNV-RP-F204: Riser Fatigue*. 2010.
- [69] A. Chang, J. Du, S. Wang, and H. Li, “Wave-scatter lumping strategies for fatigue damage assessment,” *Proceedings of the 11th (2014) Pacific/Asia Offshore Mechanics Symposium, PACOMS 2014*, no. October, pp. 83–89, 2014.
- [70] T. Y. Lin, Y. Q. Zhao, and H. H. Huang, “Representative environmental condition for fatigue analysis of offshore jacket substructure,” *Energies (Basel)*, vol. 13, no. 20, 2020, doi: 10.3390/en13205494.

Appendix A: Riser Wall Thickness Calculations

This calculation is based on DNV-OS-F101. The selected wall thickness is 25mm, and the inner diameter of the pipe is 254mm in API 5L X65 grade steel.

DNV-OS-F101 version
 DNV-OS-F101 2007 Code check are done according to the 2007 version of DNV-OS-F101.

Kilometer Post
 Start: 0,000 End: 100,000
 Pipe section 1

Material Input
 SMYS [MPa]: 448,2
 SMTS [MPa] X65: 530,9
 f_y temp [MPa]: 0
 f_u temp [MPa]: 0
 Young's modulus [GPa]: 207
 Poisson's ratio [-]: 0,3
 Anisotropy factor [-]:
 Hardening factor [-]: 0,92
 Fabrication factor [-]: 0,85
 Suppl. req. U fulfilled: Yes

Load Input

	Pressure [barg]	@ level [m]	Content mass density [kg/m ³]
Design	650	-2000	500
System test	750	-2000	1025

 Incidental to design pressure ratio [-]: 1,1
 Water depth [m]: 2000 and mass density [kg/m³]: 1025

	Functional	Environmental
Moment [kNm]	0	0
Axial force [kN]	0	0
Strain [%]	3	3

 Load condition factor [-]: 1

Geometry Input
 Steel diameter [mm] ID: 254
 Steel thickness [mm] D/t = 12,2: 25
 Fabrication tolerance [%]: 10
 Corrosion allowance [mm]: 1
 Ovality [%]: 3
 Girth weld factor [-]: 1

Design Input					Results		
Failure mode	Condition	Safety class	Corr.	Der.	Calc. t _{req.} [mm]	Utilisation [-]	Utilisation [-]
Burst	Operation	High	<input checked="" type="checkbox"/>	<input type="checkbox"/>	24,52	0,981	<div style="width: 98.1%;"></div>
Burst	System test	System test	<input checked="" type="checkbox"/>	<input type="checkbox"/>	20,81	0,838	<div style="width: 83.8%;"></div>
Collapse	Empty	High	<input checked="" type="checkbox"/>	<input type="checkbox"/>	19,62	0,716	<div style="width: 71.6%;"></div>
Propagating buckling	Empty	High	<input checked="" type="checkbox"/>	<input type="checkbox"/>	27,69	1,248	Buckle arrestors recommended
Load comb., LCC, lc = a					-	-1,000	
Load comb., LCC, lc = b					-	-1,000	
Load comb., DCC, lc = a	System test	High	<input type="checkbox"/>	<input type="checkbox"/>	7,81	0,669	<div style="width: 66.9%;"></div>
Load comb., DCC, lc = b					-	0,845	<div style="width: 84.5%;"></div>



Pipeline Engineering Tool (PET)

Pressure Containment (bursting) report

Project: X65Pipe_10Inch

Section: Pipe section 1

KP Start: 0,000

KP End: 100,000

Date: 02.05.2022

RELEVANT INPUT PARAMETERS:	Operation	System test
Nominal inner steel diameter [mm]:	254,00	
Nominal steel wall thickness [mm]:	25,00	
Fabrication tolerance [%]:	10,00	
Corrosion allowance [mm]:	1,00	
Specified minimum yield stress [MPa]:	448,2	
Specified minimum tensile strength [MPa]:	530,9	
Derating in yield stress due to temperature [MPa]:	0,0	
Derating in tensile strength due to temperature [MPa]:	0,0	
Depth [m]:	2000,0	
Density of external fluid [kg/m ³]:	1025,0	
Material strength factor [-]:	1,00	1,00
Internal pressure at reference level [bar]:	650,0	750,0
Reference level for internal pressure [m]:	-2000,0	-2000,0
Density of internal fluid [kg/m ³]:	500,0	1025,0
Incidental to design pressure ratio [-]:	1,10	1,00
Safety Class :	HIGH	SYSTEM TEST
Corroded wall thickness :	YES	YES
Derated material properties :	NO	NO
INTERMEDIATE RESULTS:	Operation	System test
Characteristic yield stress [MPa]:	448,2	448,2
Characteristic ultimate strength [MPa]:	530,9	530,9
Steel wall thickness used in code check [mm]:	21,50	21,50
Pressure containment resistance, yielding limit state [bar]:	787,8	787,8
Pressure containment resistance, ultimate [bar]:	811,4	811,4
Pressure containment resistance, minimum [bar]:	787,8	787,8
Local design pressure [bar]:	650,0	750,0
Local incidental pressure [bar]:	715,0	750,0
External pressure [bar]:	201,1	201,1
Pressure difference [bar]:	513,9	548,9
Material resistance factor [-]:	1,15	1,15
Safety class resistance factor [-]:	1,308	1,046
FINAL RESULTS:	Operation	System test
Code check, utility with given wall thickness [-]:	0,98	0,84
Required nominal wall thicness [mm]:	24,52	20,81

Appendix B: Riser Configurations for Fatigue Analysis

Appendix B1: Riser Configurations for Fatigue Analysis [SET1]

#	Angle	Net Buoyancy (tons)	Floater Length (m)	Top Length (m)	Total Length (m)	$D_B = D_H - D_S$ (m)	D_S (m)	Diff. (m)	TDP (m)	ID
		Variable	Variable	Variable		Constant				
1	8	65.0	310	1693	3803	66.6	119.6	0.0	1202	S1-A1
2	8	68.5	310	1645	3755	66.8	162.7	43.1	1199	S1-A2
3	8	73.0	330	1590	3720	66.9	208.8	46.1	1200	S1-A3
4	8	77.4	355	1534	3689	66.4	254.6	45.8	1200	S1-A4
5	8	81.0	365	1481	3646	66.5	299.9	45.3	1190	S1-A5
6	8	73.0	316	1733	3849	100.9	119.6	0.0	1257	S1-B1
7	8	77.5	340	1681	3821	101.0	162.1	42.5	1264	S1-B2
8	8	81.0	345	1627	3772	100.5	208.3	46.2	1252	S1-B3
9	8	85.5	370	1571	3741	101.1	254.3	46.0	1252	S1-B4
10	8	89.0	385	1516	3701	100.1	299.2	44.9	1240	S1-B5
11	8	81.6	320	1777	3897	140.9	119.3	0.0	1309	S1-C1
12	8	86.0	345	1723	3868	140.9	162.3	43.0	1311	S1-C2
13	8	89.5	353	1668	3821	140.2	208.2	45.9	1300	S1-C3
14	8	93.8	377	1612	3789	140.9	253.5	45.3	1295	S1-C4
15	8	97.5	392	1555	3747	140.7	300.2	46.7	1282	S1-C5
16	8	89.5	316	1820	3936	180.6	119.2	0.0	1347	S1-D1
17	8	93.8	344	1765	3909	180.4	161.5	42.3	1350	S1-D2
18	8	97.5	352	1710	3862	180.9	207.9	46.4	1336	S1-D3
19	8	102.0	387	1650	3837	180.7	253.3	45.4	1334	S1-D4
20	8	105.6	402	1593	3795	180.5	299.5	46.2	1318	S1-D5
21	8	99.0	350	1853	4003	220.8	119.8	0.0	1404	S1-E1
22	8	102.5	366	1799	3965	219.8	162.3	42.5	1396	S1-E2
23	8	106.0	374	1744	3918	219.9	208.1	45.8	1379	S1-E3
24	8	110.5	410	1682	3892	219.9	254.5	46.4	1375	S1-E4
25	8	114.0	427	1626	3853	219.7	299.1	44.6	1375	S1-E5

		D_S (m)				
		120	162	208	254	300
D_B (m)	67	S1-A1	S1-A2	S1-A3	S1-A4	S1-A5
	100	S1-B1	S1-B2	S1-B3	S1-B4	S1-B5
	140	S1-C1	S1-C2	S1-C3	S1-C4	S1-C5
	180	S1-D1	S1-D2	S1-D3	S1-D4	S1-D5
	220	S1-E1	S1-E2	S1-E3	S1-E4	S1-E5

Appendix B2: Riser Configurations for Fatigue Analysis [SET2]

#	Angle	Net Buoyancy (tons)	Floater Length (m)	Top Length (m)	Total Length (m)	$D_B=D_H-D_S$ (m)	D_S (m)	Diff. (m)	TDP (m)	ID
		Variable	Variable	Variable		Constant				
1	8	82.8	310	1693	3803	66.6	119.6	0.0	1200	S2-A1
2	8	87.1	310	1645	3755	66.7	162.0	42.4	1195	S2-A2
3	8	92.8	330	1590	3720	66.7	208.1	46.1	1198	S2-A3
4	8	98.5	355	1534	3689	66.4	254.1	46.0	1198	S2-A4
5	8	103.0	365	1481	3646	66.3	299.2	45.1	1186	S2-A5
6	8	92.9	316	1733	3849	100.9	119.6	0.0	1255	S2-B1
7	8	98.7	340	1681	3821	101.2	161.9	42.3	1261	S2-B2
8	8	103.0	345	1627	3772	100.2	207.6	45.7	1251	S2-B3
9	8	108.8	370	1571	3741	101.0	253.8	46.2	1248	S2-B4
10	8	385.0	385	1516	3701	100.8	299.4	45.6	1239	S2-B5
11	8	103.9	320	1777	3897	141.0	119.0	0.0	1307	S2-C1
12	8	109.4	345	1723	3868	140.7	161.7	42.7	1309	S2-C2
13	8	114.0	353	1668	3821	140.4	208.0	46.3	1298	S2-C3
14	8	119.5	377	1612	3789	141.1	253.4	45.4	1292	S2-C4
15	8	124.0	392	1555	3747	140.3	299.5	46.1	1278	S2-C5
16	8	114.0	316	1820	3936	180.6	119.2	0.0	1345	S2-D1
17	8	119.5	344	1765	3909	180.7	161.4	42.2	1348	S2-D2
18	8	124.2	352	1710	3862	181.1	207.7	46.3	1334	S2-D3
19	8	130.0	387	1650	3837	181.1	253.3	45.6	1332	S2-D4
20	8	134.5	402	1593	3795	180.7	299.3	46.0	1316	S2-D5
21	8	126.0	350	1853	4003	220.7	119.4	0.0	1400	S2-E1
22	8	130.5	366	1799	3965	219.8	162.0	42.6	1392	S2-E2
23	8	135.0	374	1744	3918	220.1	207.8	45.8	1377	S2-E3
24	8	140.8	410	1682	3892	220.2	254.4	46.6	1373	S2-E4
25	8	145.5	427	1626	3853	220.8	299.6	45.2	1357	S2-E5

		D_S (m)				
		120	162	208	254	300
D_B (m)	67	S2-A1	S2-A2	S2-A3	S2-A4	S2-A5
	100	S2-B1	S2-B2	S2-B3	S2-B4	S2-B5
	140	S2-C1	S2-C2	S2-C3	S2-C4	S2-C5
	180	S2-D1	S2-D2	S2-D3	S2-D4	S2-D5
	220	S2-E1	S2-E2	S2-E3	S2-E4	S2-E5

Appendix B3: Riser Configurations for Fatigue Analysis [SET3]

#	Angle	Net Buoyancy (tons)	Floater Length (m)	Top Length (m)	Total Length (m)	$D_B = D_H - D_S$ (m)	D_S (m)	Diff. (m)	TDP (m)	ID
		Variable	Variable	Variable		Constant				
1	8	70	275	2300	4375	66.7	119.4	0.0	1471	S3-A1
Base Case is Above										
2	8	74	275	2252	4327	66.7	162.2	42.8	1476	S3-A2
3	8	79	295	2197	4297	66.6	208.1	45.9	1486	S3-A3
4	8	84	320	2141	4261	66.5	254.1	46.0	1494	S3-A4
5	8	88	330	2088	4218	66.3	299.1	45.0	1491	S3-A5
6	8	79	281	2346	4427	100.7	119.9	0.0	1539	S3-B1
7	8	84	305	2294	4399	100.8	162.3	42.4	1554	S3-B2
8	8	88	310	2240	4350	100.3	208.4	46.1	1551	S3-B3
9	8	93	335	2184	4319	100.9	254.4	46.0	1558	S3-B4
10	8	97	350	2129	4279	100.2	299.5	45.1	1554	S3-B5
11	8	88	279	2396	4475	139.4	119.6	0	1600	S3-C1
12	8	93	304	2343	4447	140.1	162.4	42.8	1610	S3-C2
13	8	97	312	2288	4400	139.5	208.3	45.9	1606	S3-C3
14	8	102	336	2232	4368	140.9	254.4	46.1	1611	S3-C4
15	8	106	351	2177	4328	140.7	299.3	44.9	1605	S3-C5
16	8	97	277	2445	4522	179.9	119.6	0	1654	S3-D1
17	8	102	304	2390	4494	180.8	162.9	43.3	1663	S3-D2
18	8	106	312	2335	4447	180.8	208.8	45.9	1657	S3-D3
19	8	111	348	2275	4423	180.8	254.2	45.4	1663	S3-D4
20	8	115	363	2219	4382	180.7	299.7	45.5	1654	S3-D5
21	8	107	310	2483	4593	219.7	119.3	0.0	1721	S3-E1
22	8	111	326	2429	4555	219.1	162.1	42.8	1719	S3-E2
23	8	115	334	2374	4508	219.5	208.1	46.0	1711	S3-E3
24	8	120	370	2312	4482	219.7	254.8	46.7	1714	S3-E4
25	8	124	387	2256	4443	219.9	299.9	45.1	1707	S3-E5

		D_S (m)				
		120	162	208	254	300
D_B (m)	67	S3-A1 Base Case	S3-A2	S3-A3	S3-A4	S3-A5
	100	S3-B1	S3-B2	S3-B3	S3-B4	S3-B5
	140	S3-C1	S3-C2	S3-C3	S3-C4	S3-C5
	180	S3-D1	S3-D2	S3-D3	S3-D4	S3-D5
	220	S3-E1	S3-E2	S3-E3	S3-E4	S3-E5

Appendix B4: Riser Configurations for Fatigue Analysis [SET4]

#	Angle	Net Buoyancy (tons)	Floater Length (m)	Top Length (m)	Total Length (m)	$D_B=D_H-D_S$ (m)	D_S (m)	Diff. (m)	TDP (m)	ID
		Variable	Variable	Variable		Constant				
1	8	89.1	275	2300	4375	66.8	119.0	0.0	1471	S4-A1
2	8	94.2	275	2252	4327	66.8	161.8	42.8	1474	S4-A2
3	8	100.7	295	2197	4292	66.9	208.0	46.2	1483	S4-A3
4	8	107.1	320	2141	4261	66.9	254.1	46.1	1494	S4-A4
5	8	112.2	330	2088	4218	66.8	299.2	45.1	1489	S4-A5
6	8	100.5	281	2346	4427	100.6	119.4	0.0	1537	S4-B1
7	8	107.0	305	2294	4399	101.0	162.1	42.7	1552	S4-B2
8	8	112.2	310	2240	4350	100.7	208.5	46.4	1549	S4-B3
9	8	118.4	335	2184	4319	100.9	254.1	45.6	1556	S4-B4
10	8	123.6	350	2129	4279	100.4	299.4	45.3	1552	S4-B5
11	8	112.0	279	2396	4475	139.3	119.2	0	1598	S4-C1
12	8	118.5	304	2343	4447	140.3	162.3	43.1	1610	S4-C2
13	8	123.8	312	2288	4400	140.3	208.7	46.4	1605	S4-C3
14	8	129.9	336	2232	4368	141.0	254.1	45.4	1609	S4-C4
15	8	135.0	351	2177	4328	140.8	299.1	45	1603	S4-C5
16	8	123.5	277	2445	4522	179.9	119.2	0	1652	S4-D1
17	8	129.7	304	2390	4494	180.4	162.1	42.9	1661	S4-D2
18	8	134.8	312	2335	4447	180.3	208.0	45.9	1655	S4-D3
19	8	141.4	348	2275	4423	180.9	254.0	46	1661	S4-D4
20	8	146.4	363	2219	4382	180.6	299.3	45.3	1653	S4-D5
21	8	136.3	310	2483	4593	219.9	119.2	0.0	1718	S4-E1
22	8	141.5	326	2429	4555	219.6	162.2	43.0	1718	S4-E2
23	8	146.5	334	2374	4508	219.7	208.0	45.8	1709	S4-E3
24	8	152.9	370	2312	4482	219.9	254.7	46.7	1712	S4-E4
25	8	157.8	387	2256	4443	219.6	299.3	44.6	1703	S4-E5

		D_S (m)				
		120	162	208	254	300
D_B (m)	67	S4-A1	S4-A2	S4-A3	S4-A4	S4-A5
	100	S4-B1	S4-B2	S4-B3	S4-B4	S4-B5
	140	S4-C1	S4-C2	S4-C3	S4-C4	S4-C5
	180	S4-D1	S4-D2	S4-D3	S4-D4	S4-D5
	220	S4-E1	S4-E2	S4-E3	S4-E4	S4-E5

Appendix B5: Riser Configurations for Fatigue Analysis [SET5]

#	Angle	Net Buoyancy (tons)	Floater Length (m)	Top Length (m)	Total Length (m)	$D_B=D_H-D_S$ (m)	D_S (m)	Diff. (m)	TDP (m)	ID
		Variable	Variable	Variable		Constant				
1	8	76.7	288	2847	4935	66.3	120.0	0.0	1762	S5-A1
2	8	81.0	288	2792	4880	66.0	162.7	42.7	1770	S5-A2
3	8	86.5	308	2736	4844	66.1	209.0	46.3	1786	S5-A3
4	8	91.9	333	2683	4816	66.0	255.3	46.3	1800	S5-A4
5	8	96.3	343		2143	66.0	300.7	45.4	1804	S5-A5
				2946						
6	8	86.4	294	2894	4988	99.9	120.6	0.0	1837	S5-B1
7	8	91.7	318	2840	4958	99.7	162.9	42.3	1858	S5-B2
8	8	96.1	323	2784	4907	99.2	209.3	46.4	1859	S5-B3
9	8	101.4	348	2729	4877	99.5	255.3	46.0	1872	S5-B4
10	8	105.9	365		2165	99.1	300.6	45.3	1875	S5-B5
				3000						
11	8	96.6	298	2946	5044	139.2	120.6	0.0	1912	S5-C1
12	8	101.7	323	2893	5016	138.9	163.1	42.5	1929	S5-C2
13	8	106.2	331	2837	4968	139.2	208.8	45.7	1932	S5-C3
14	8	111.4	355	2781	4936	140.0	254.8	46.0	1940	S5-C4
15	8	115.6	370		2170	139.1	300.2	45.4	1941	S5-C5
				3050						
16	8	106.5	305	2995	5100	179.4	120.4	0.0	1981	S5-D1
17	8	111.8	335	2940	5075	179.7	163.2	42.8	1998	S5-D2
18	8	116.1	343	2880	5023	179.5	209.4	46.2	1997	S5-D3
19	8	121.4	378	2824	5002	179.3	255.3	45.9	2009	S5-D4
20	8	125.5	394		2194	179.2	301.1	45.8	2006	S5-D5
				3093						
21	8	116.7	330	3040	5170	219.2	120.2	0.0	2052	S5-E1
22	8	121.0	346	2985	5130	218.7	163.1	42.9	2056	S5-E2
23	8	125.3	354	2924	5078	219.0	209.4	46.3	2053	S5-E3
24	8	130.6	390	2868	5058	219.2	255.3	45.9	2065	S5-E4
25	8	134.8	407	3480	5687	219.0	300.3	45.0	2061	S5-E5

		D_S (m)				
		120	162	208	254	300
D_B (m)	67	S5-A1	S5-A2	S5-A3	S5-A4	S5-A5
	100	S5-B1	S5-B2	S5-B3	S5-B4	S5-B5
	140	S5-C1	S5-C2	S5-C3	S5-C4	S5-C5
	180	S5-D1	S5-D2	S5-D3	S5-D4	S5-D5
	220	S5-E1	S5-E2	S5-E3	S5-E4	S5-E5

Appendix B6: Riser Configurations for Fatigue Analysis [SET6]

#	Angle	Net Buoyancy (tons)	Floater Length (m)	Top Length (m)	Total Length (m)	$D_B=D_H-D_S$ (m)	D_S (m)	Diff. (m)	TDP (m)	ID
		Variable	Variable	Variable		Constant				
1	8	97.5	288	2895	4983	66.1	119.4	0.0	1759	S6-A1
2	8	103.2	288	2847	4935	66.2	162.5	43.1	1768	S6-A2
3	8	110.2	308	2792	4900	66.3	208.9	46.4	1786	S6-A3
4	8	117.0	333	2736	4869	66.0	254.9	46.0	1798	S6-A4
5	8	122.8	343	2683	4826	66.4	300.9	46.0	1802	S6-A5
6	8	110.2	294	2946	5040	100.3	120.7	0.0	1837	S6-B1
7	8	117.0	318	2894	5012	100.2	163.2	42.5	1855	S6-B2
8	8	122.3	323	2840	4963	99.1	208.7	45.5	1858	S6-B3
9	8	129.0	348	2784	4932	99.3	254.6	45.9	1871	S6-B4
10	8	135.0	365	2729	4894	99.5	300.7	46.1	1875	S6-B5
11	8	123.2	298	3000	5098	139.7	120.8	0.0	1912	S6-C1
12	8	129.7	323	2946	5069	139.4	163.2	42.4	1927	S6-C2
13	8	135.3	331	2893	5024	139.3	208.7	45.5	1930	S6-C3
14	8	141.8	355	2837	4992	139.8	254.3	45.6	1939	S6-C4
15	8	147.4	370	2781	4951	139.6	300.4	46.1	1939	S6-C5
16	8	135.7	305	3050	5155	179.6	120.2	0.0	1981	S6-D1
17	8	142.2	335	2995	5130	179.3	162.4	42.2	1995	S6-D2
18	8	147.7	343	2940	5083	179.2	208.7	46.3	1995	S6-D3
19	8	154.5	379	2880	5059	179.0	254.6	45.9	2006	S6-D4
20	8	160.2	394	2825	5018	179.6	300.8	46.2	2004	S6-D5
21	8	149.0	330	3093	5223	220.1	120.9	0.0	2051	S6-E1
22	8	154.2	346	3040	5185	218.9	163.1	42.2	2054	S6-E2
23	8	159.5	354	2985	5138	218.8	208.9	45.8	2052	S6-E3
24	8	166.3	390	2924	5114	219.1	254.9	46.0	2063	S6-E4
25	8	171.9	407	2868	5075	219.6	300.6	45.7	2060	S6-E5

		D_S (m)				
		120	162	208	254	300
D_B (m)	67	S6-A1	S6-A2	S6-A3	S6-A4	S6-A5
	100	S6-B1	S6-B2	S6-B3	S6-B4	S6-B5
	140	S6-C1	S6-C2	S6-C3	S6-C4	S6-C5
	180	S6-D1	S6-D2	S6-D3	S6-D4	S6-D5
	220	S6-E1	S6-E2	S6-E3	S6-E4	S6-E5

Appendix B7: Riser Configurations for Fatigue Analysis [SET7]

#	Angle	Net Buoyancy (tons)	Floater Length (m)		Top Length (m)	Total Length (m)	$D_B = D_H - D_S$ (m)	D_S (m)	Diff. (m)	TDP (m)	ID
		Variable	Variable		Variable		Constant				
1	8	83.0	300	0	3490	5590	66.8	120.0	0.0	2045	S7-A1
2	8	87.5	300	0	3442	5542	66.1	162.2	42.2	2057	S7-A2
3	8	93.5	320	20	3387	5507	66.4	209.2	47.0	2081	S7-A3
4	8	99.2	345	25	3331	5476	66.2	255.2	46.0	2099	S7-A4
5	8	103.8	355	10	3278	5433	65.9	300.6	45.4	2107	S7-A5
6	8	93.4	307	0	3545	5652	100.3	120.4	0.0	2130	S7-B1
7	8	98.9	331	24	3493	5624	99.7	162.4	42.0	2154	S7-B2
8	8	103.6	336	5	3439	5575	99.1	208.8	46.4	2162	S7-B3
9	8	109.3	361	25	3383	5544	99.5	255.2	46.4	2180	S7-B4
10	8	114.3	380	19	3328	5508	99.4	300.9	45.7	2189	S7-B5
11	8	104.5	317	0	3603	5720	139.6	119.6	0.0	2219	S7-C1
12	8	110.0	342	25	3549	5691	139.4	162.9	43.3	2239	S7-C2
13	8	114.9	350	8	3497	5647	140.1	208.2	45.3	2247	S7-C3
14	8	120.3	374	24	3441	5615	140.6	254.1	45.9	2262	S7-C4
15	8	124.8	389	15	3384	5573	139.6	300.4	46.3	2265	S7-C5
16	8	115.5	333	0	3655	5788	180.1	119.8	0.0	2302	S7-D1
17	8	121.2	366	33	3600	5766	180.2	162.4	42.6	2324	S7-D2
18	8	125.7	374	8	3545	5719	179.8	208.6	46.2	2327	S7-D3
19	8	131.3	409	35	3485	5694	179.5	254.9	46.3	2343	S7-D4
20	8	136.0	424	15	3430	5654	180.0	300.9	46.0	2346	S7-D5
21	8	126.0	350	0	3703	5853	220.4	120	0.0	2377	S7-E1
22	8	130.5	365	15	3650	5815	219.8	162.7	42.7	2383	S7-E2
23	8	134.8	373	8	3595	5768	219.3	208.4	45.7	2385	S7-E3
24	8	140.6	410	37	3536	5746	220.3	254.1	45.7	2402	S7-E4
25	8	145.1	427	17	3480	5707	220.2	299.5	45.4	2403	S7-E5

		D_S (m)				
		120	162	208	254	300
D_B (m)	67	S7-A1	S7-A2	S7-A3	S7-A4	S7-A5
	100	S7-B1	S7-B2	S7-B3	S7-B4	S7-B5
	140	S7-C1	S7-C2	S7-C3	S7-C4	S7-C5
	180	S7-D1	S7-D2	S7-D3	S7-D4	S7-D5
	220	S7-E1	S7-E2	S7-E3	S7-E4	S7-E5

Appendix B8: Riser Configurations for Fatigue Analysis [SET8]

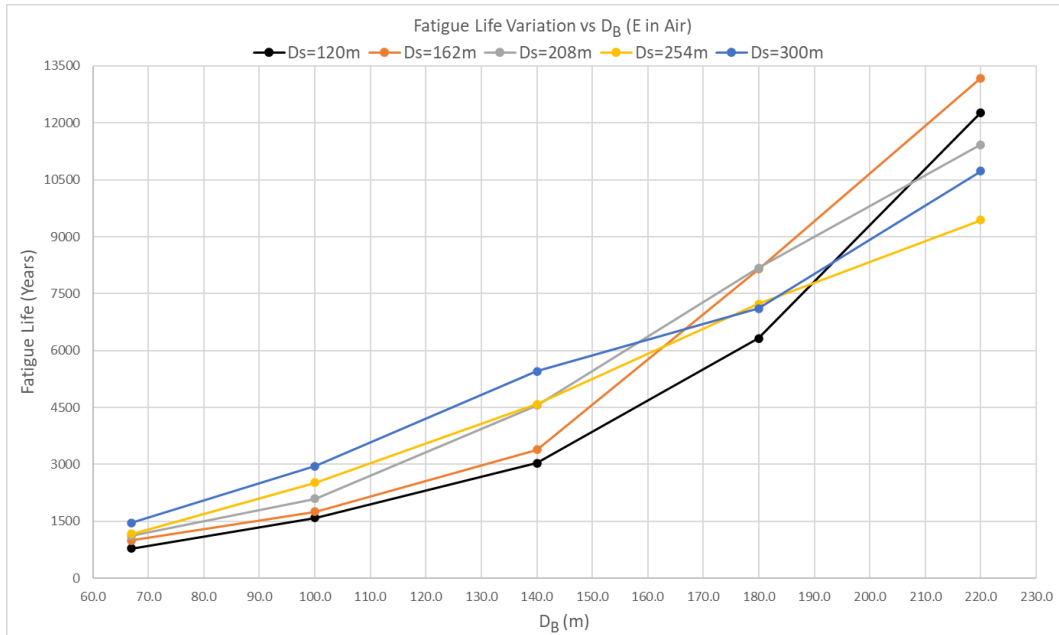
#	Angle	Net Buoyancy (tons)	Floater Length (m)	Top Length (m)	Total Length (m)	$D_B = D_H - D_S$ (m)	D_S (m)	Diff. (m)	TDP (m)	ID
		Variable	Variable	Variable		Constant				
1	8	105.5	300	3490	5590	66.5	119.2	0.0	2041	S8-A1
2	8	111.5	300	3442	5542	66.3	162	42.8	2055	S8-A2
3	8	119.0	320	3387	5507	66.3	208.6	46.6	2079	S8-A3
4	8	126.2	345	3331	5476	66.0	254.7	46.1	2097	S8-A4
5	8	132.3	355	3278	5433	66.2	300.5	45.8	2105	S8-A5
6	8	119.0	307	3545	5652	100.4	120.2	0.0	2130	S8-B1
7	8	126.0	331	3493	5624	99.8	162.1	41.9	2152	S8-B2
8	8	132.0	336	3439	5575	99.3	208.6	46.5	2162	S8-B3
9	8	139.2	361	3383	5544	99.6	254.9	46.3	2178	S8-B4
10	8	145.5	380	3328	5508	99.3	300.4	45.5	2189	S8-B5
11	8	133.3	317	3603	5720	140.1	119.8	0.0	2217	S8-C1
12	8	140.1	342	3549	5691	139.4	162.5	42.7	2237	S8-C2
13	8	146.5	350	3497	5647	140.6	208.3	45.8	2247	S8-C3
14	8	153.3	374	3441	5615	140.8	254	45.7	2260	S8-C4
15	8	159.2	389	3384	5573	140.2	300.8	46.8	2265	S8-C5
16	8	147.2	333	3655	5788	180.3	119.7	0.0	2300	S8-D1
17	8	154.5	366	3600	5766	180.6	162.4	42.7	2332	S8-D2
18	8	160.2	374	3545	5719	180.1	208.5	46.1	2327	S8-D3
19	8	167.4	409	3485	5694	179.9	254.9	46.4	2342	S8-D4
20	8	173.3	424	3430	5654	180.3	300.8	45.9	2346	S8-D5
21	8	160.5	350	3703	5853	220.5	119.7	0.0	2375	S8-E1
22	8	166.3	365	3650	5815	220.1	162.6	42.9	2383	S8-E2
23	8	171.9	373	3595	5768	219.8	208.6	46.0	2385	S8-E3
24	8	179.2	410	3536	5746	220.6	254.1	45.5	2402	S8-E4
25	8	185.0	427	3480	5707	220.7	299.7	45.6	2403	S8-E5

		D_S (m)				
		120	162	208	254	300
D_B (m)	67	S8-A1	S8-A2	S8-A3	S8-A4	S8-A5
	100	S8-B1	S8-B2	S8-B3	S8-B4	S8-B5
	140	S8-C1	S8-C2	S8-C3	S8-C4	S8-C5
	180	S8-D1	S8-D2	S8-D3	S8-D4	S8-D5
	220	S8-E1	S8-E2	S8-E3	S8-E4	S8-E5

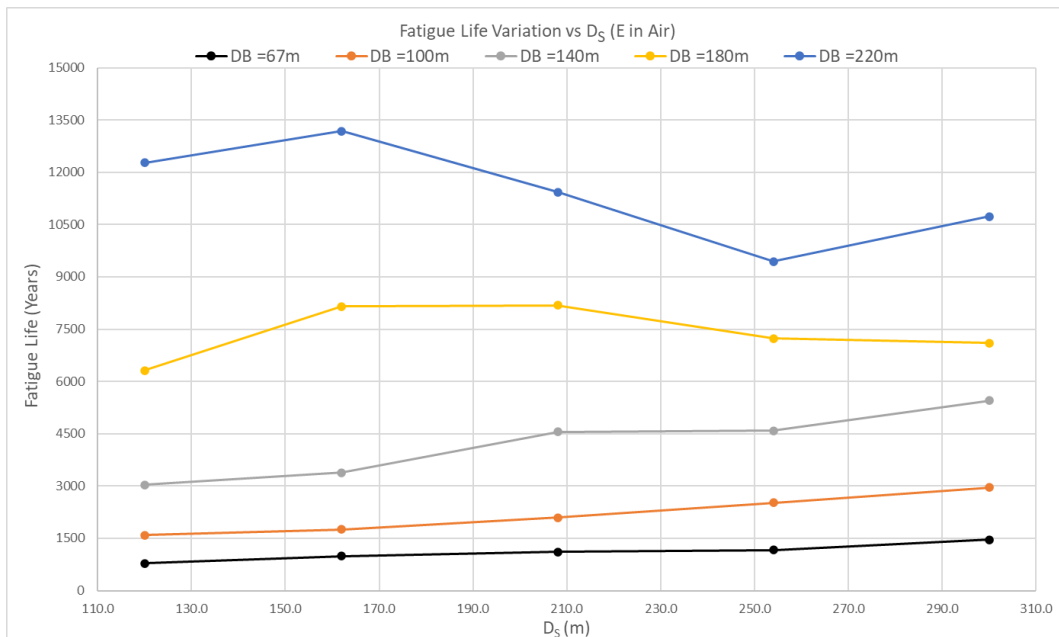
Appendix C: Fatigue Analysis Results (Inner Wall)

Appendix C1: Analysis Results [SET1]

- Variation of Fatigue Life at TDP against D_B



- Variation of Fatigue Life at TDP against D_S

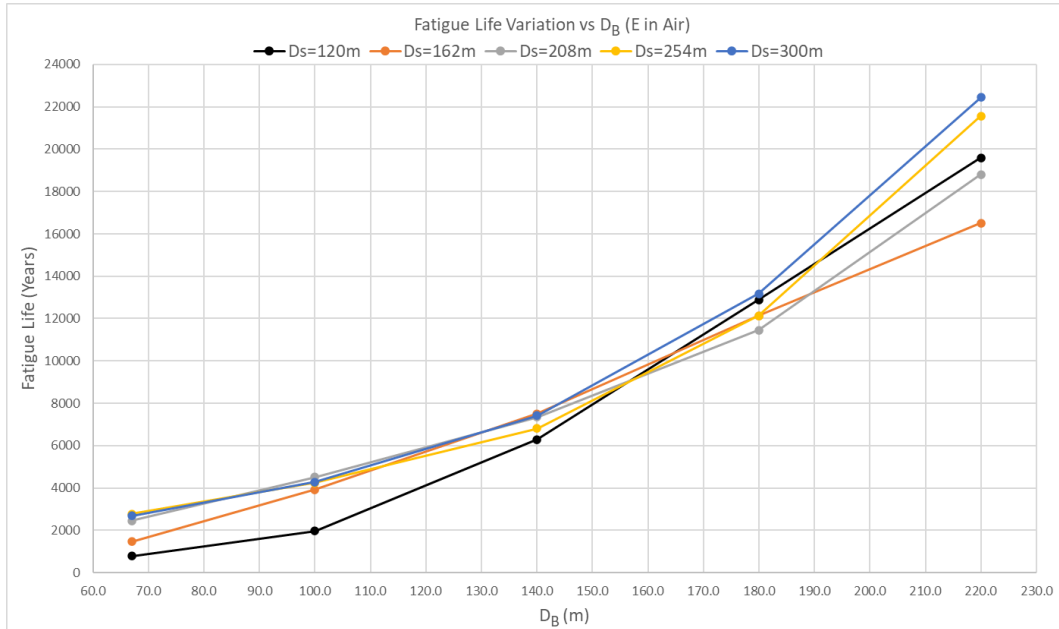


-
- Summary of fatigue life at TDP

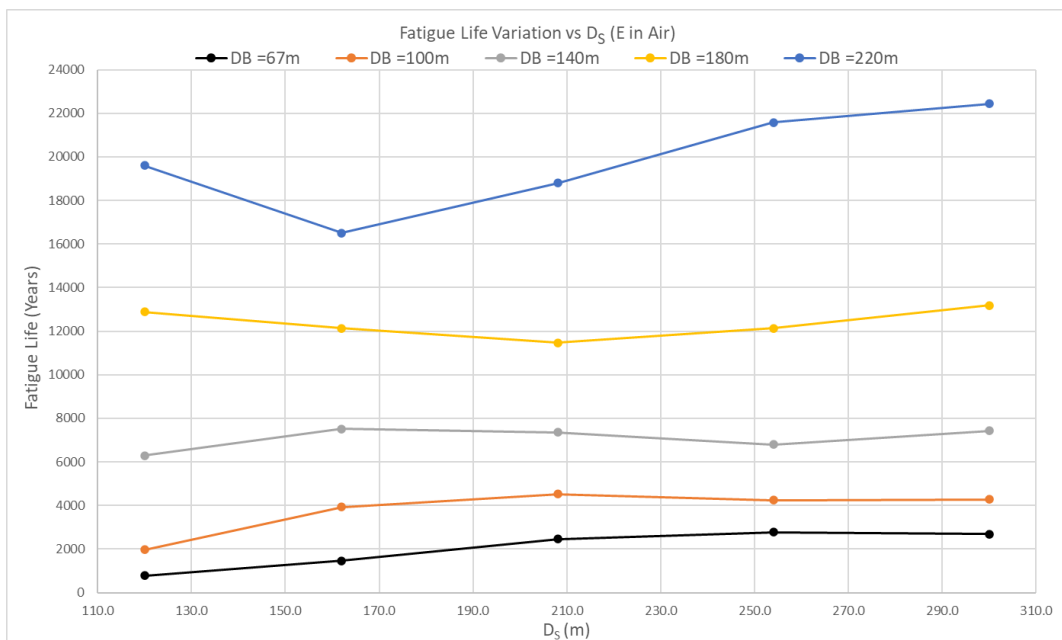
	Fatigue Life at TDP (Years)				
D_B (m)	D_S=120m	D_S =162m	D_S =208m	D_S =254m	D_S =300m
67.0	779	990	1114	1165	1457
100.0	1592	1751	2096	2517	2956
140.0	3029	3385	4553	4585	5456
180.0	6317	8151	8182	7233	7103
220.0	12273	13181	11429	9440	10734

Appendix C2: Analysis Results [SET2]

- Variation of Fatigue Life at TDP against D_B



- Variation of Fatigue Life at TDP against D_s

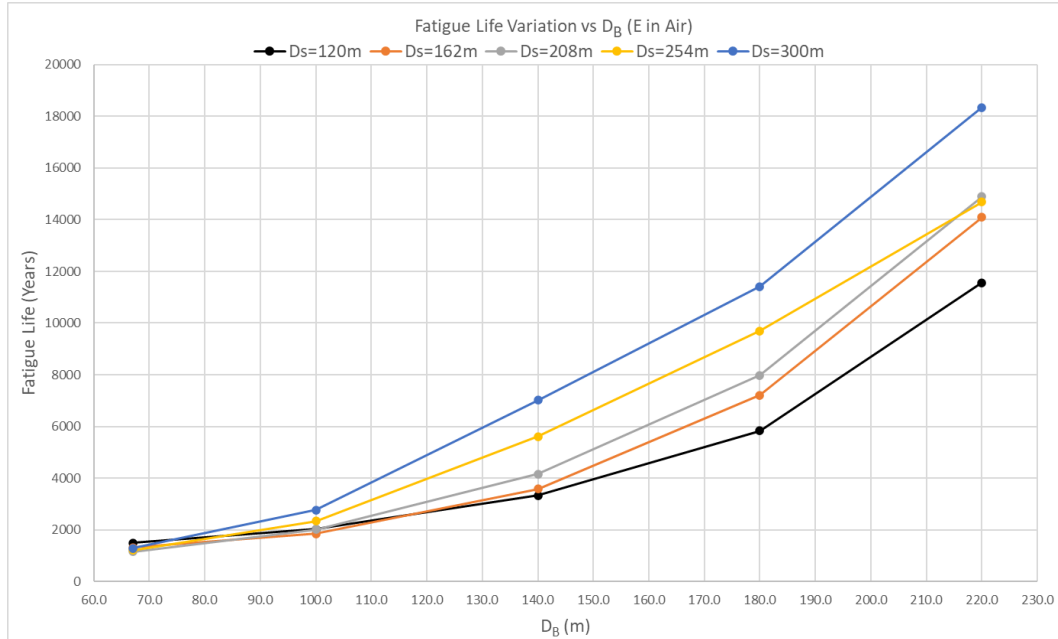


-
- Summary of fatigue life at TDP

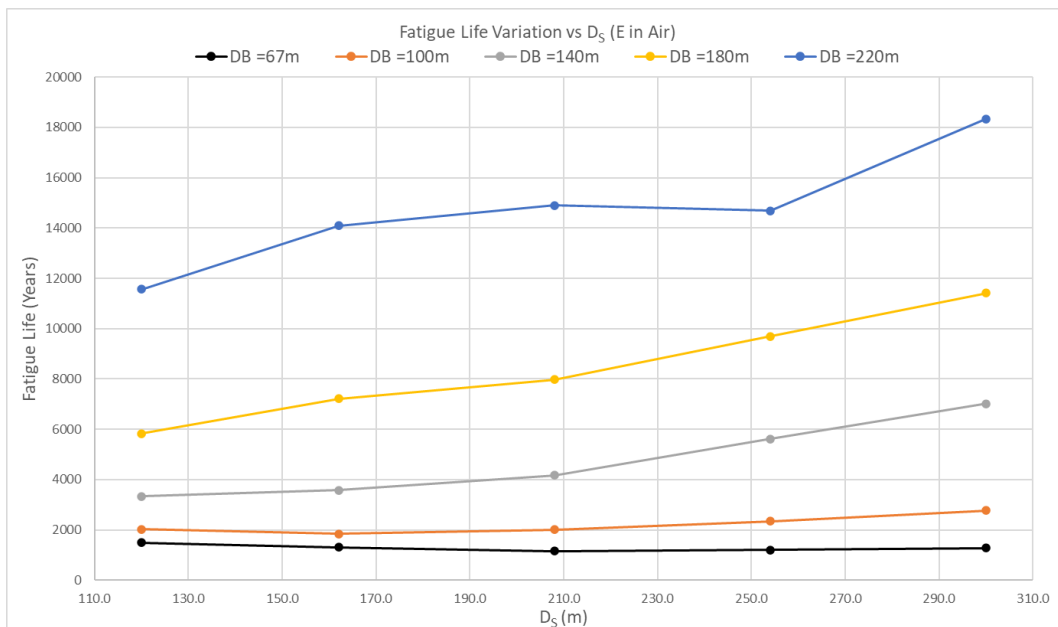
	Fatigue Life at TDP (Years)				
D_B (m)	D_S=120m	D_S =162m	D_S =208m	D_S =254m	D_S =300m
67.0	777	1463	2453	2776	2683
100.0	1965	3928	4520	4235	4287
140.0	6293	7516	7355	6800	7418
180.0	12885	12135	11461	12130	13174
220.0	19595	16512	18805	21574	22443

Appendix C3: Analysis Results [SET3]

- Variation of Fatigue Life at TDP against D_B



- Variation of Fatigue Life at TDP against D_s

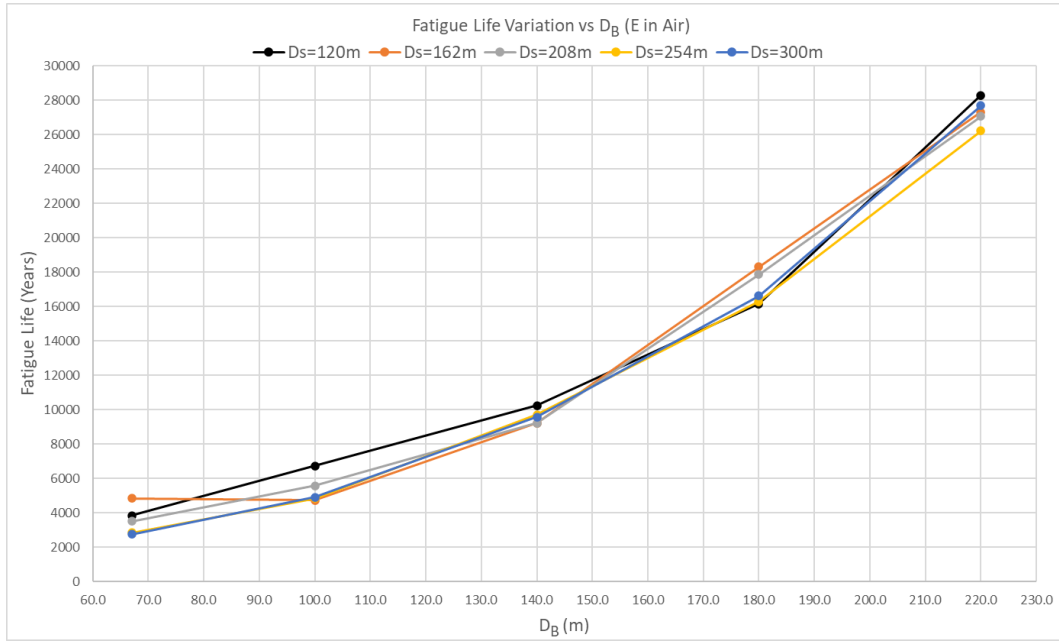


-
- Summary of fatigue life at TDP

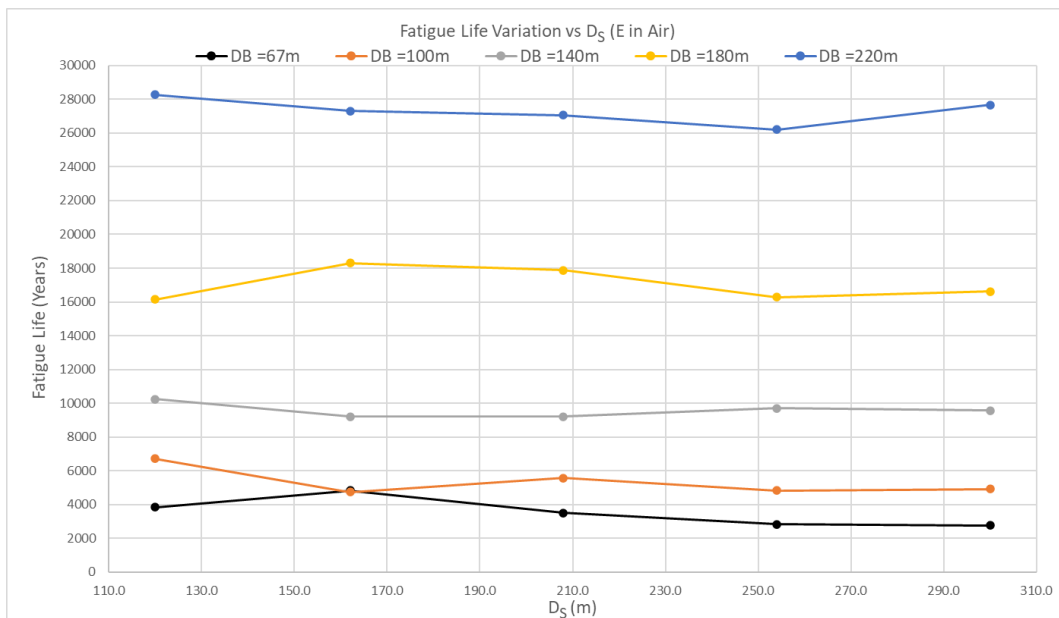
	Fatigue Life at TDP (Years)				
D_B (m)	D_S=120m	D_S =162m	D_S =208m	D_S =254m	D_S =300m
67.0	1491	1312	1153	1203	1284
100.0	2018	1843	2013	2337	2769
140.0	3325	3575	4164	5615	7012
180.0	5825	7212	7980	9700	11420
220.0	11567	14091	14900	14680	18339

Appendix C4: Analysis Results [SET4]

- Variation of Fatigue Life at TDP against D_B



- Variation of Fatigue Life at TDP against D_s

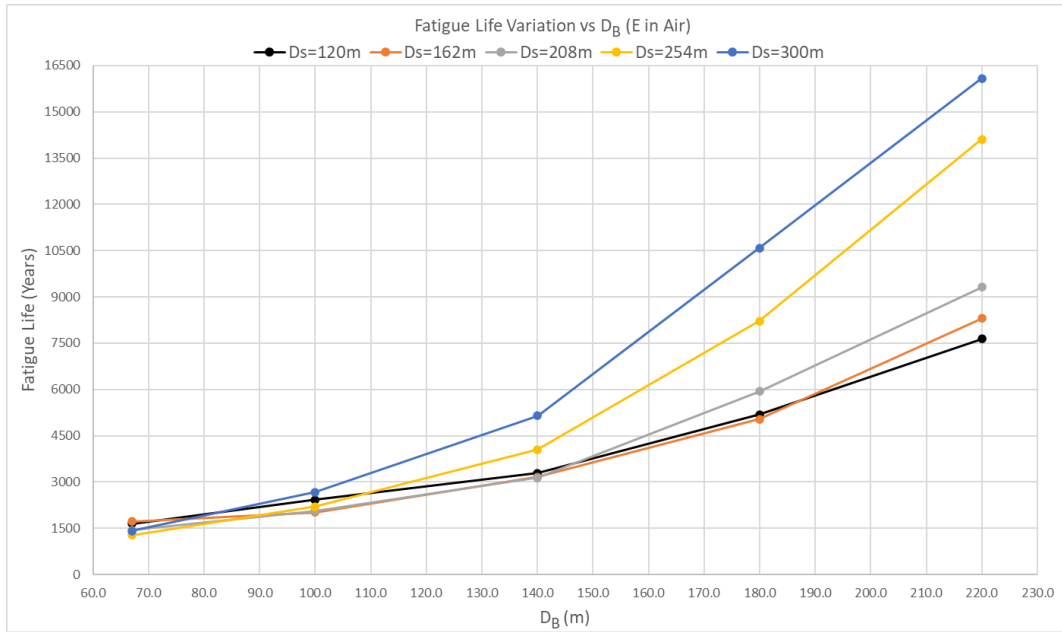


-
- Summary of fatigue life at TDP

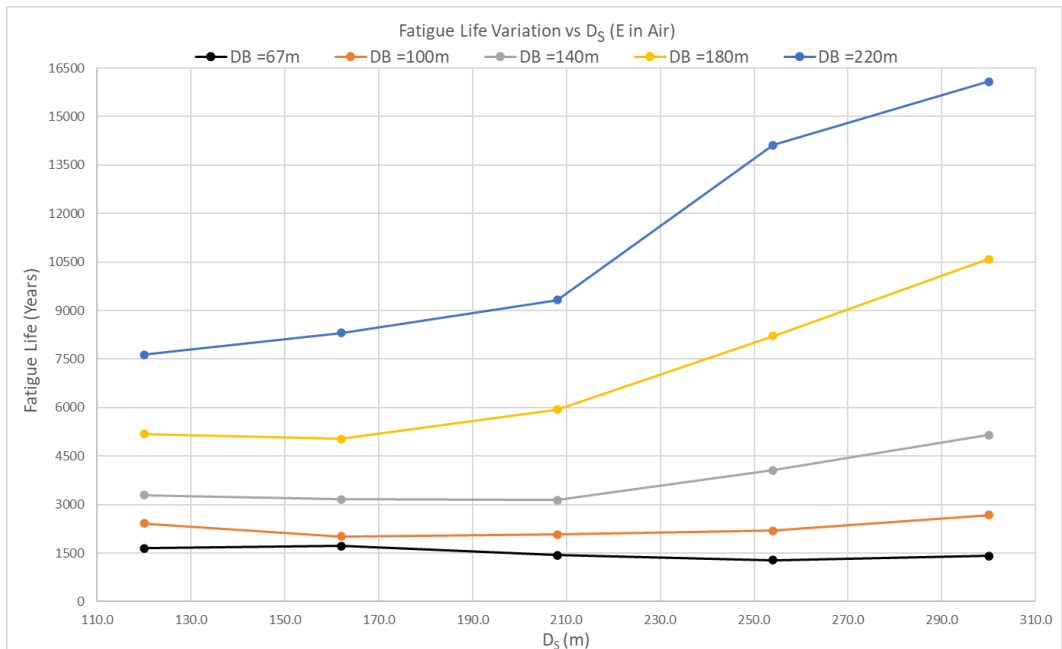
	Fatigue Life at TDP (Years)				
D_B (m)	D_S=120m	D_S =162m	D_S =208m	D_S =254m	D_S =300m
67.0	3844	4830	3499	2832	2757
100.0	6720	4731	5575	4836	4916
140.0	10238	9210	9218	9708	9563
180.0	16153	18299	17865	16275	16622
220.0	28277	27307	27049	26217	27671

Appendix C5: Analysis Results [SET5]

- Variation of Fatigue Life at TDP against D_B



- Variation of Fatigue Life at TDP against D_S

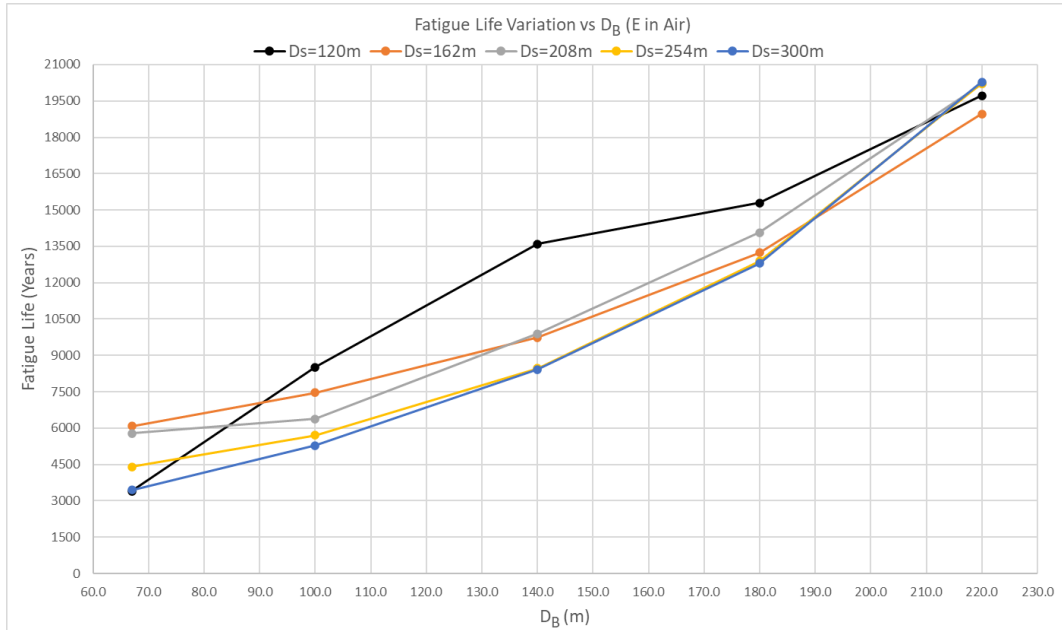


-
- Summary of fatigue life at TDP

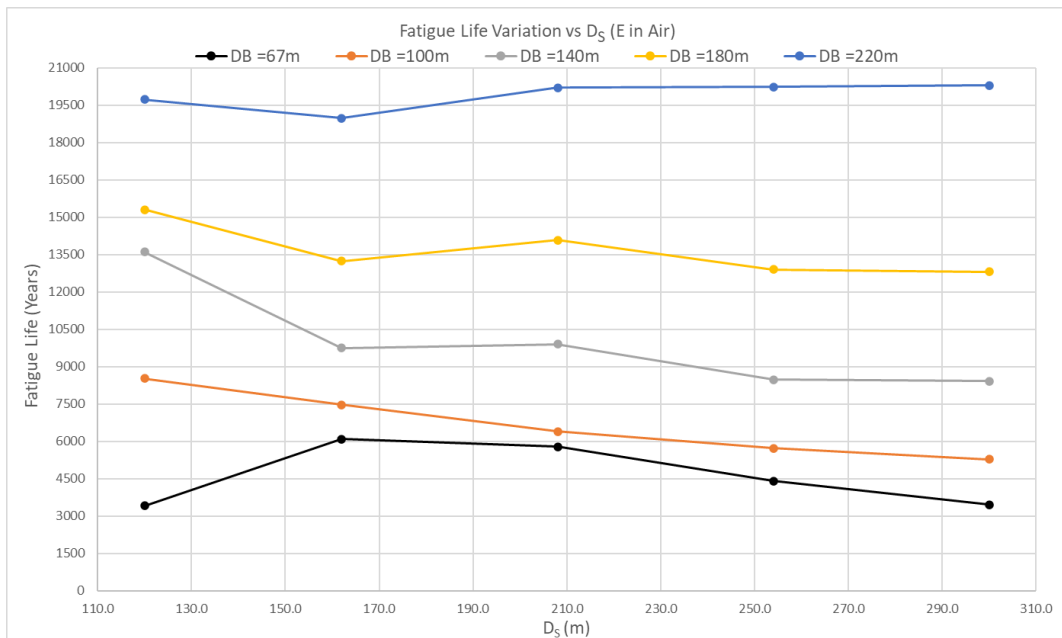
	Fatigue Life at TDP (Years)				
D_B (m)	D_S=120m	D_S =162m	D_S =208m	D_S =254m	D_S =300m
67.0	1647	1726	1435	1280	1416
100.0	2420	2018	2072	2199	2673
140.0	3293	3166	3137	4058	5149
180.0	5188	5034	5938	8217	10588
220.0	7634	8305	9322	14114	16079

Appendix C6: Analysis Results [SET6]

- Variation of Fatigue Life at TDP against D_B



- Variation of Fatigue Life at TDP against D_s

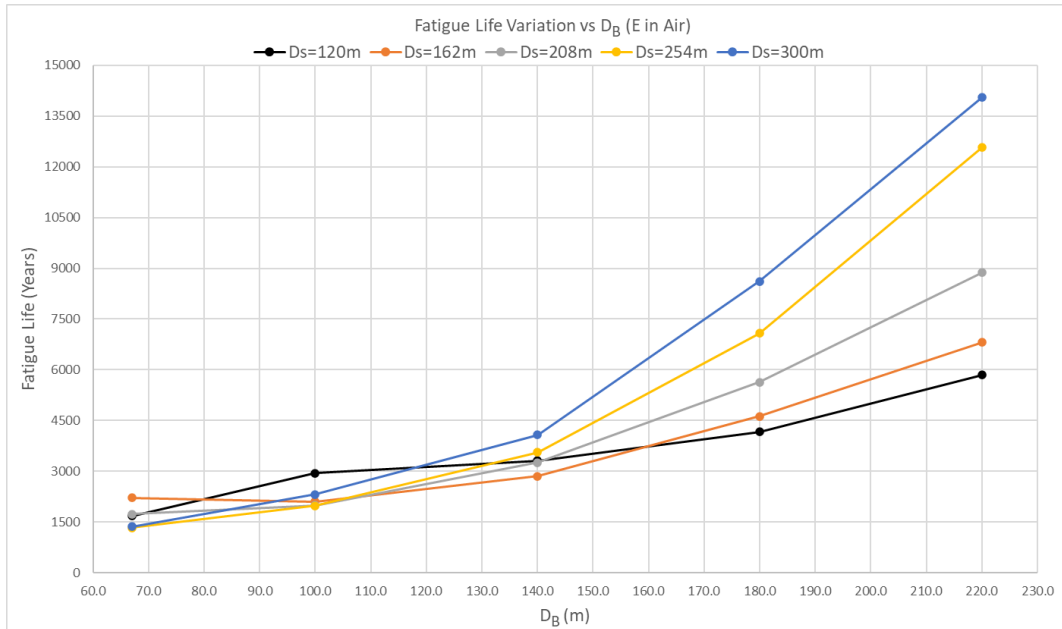


-
- Summary of fatigue life at TDP

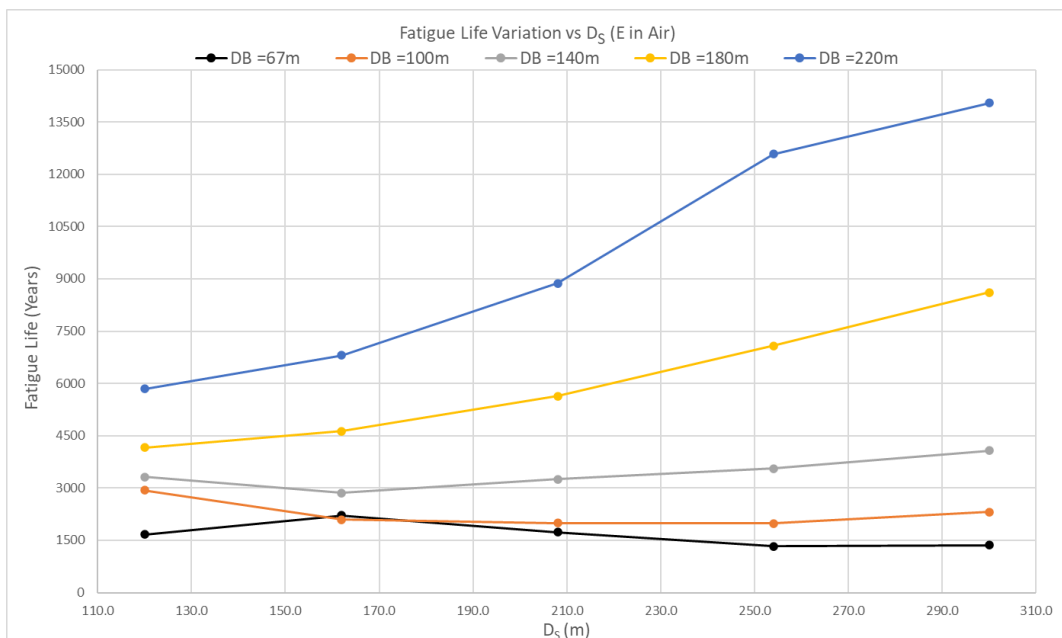
	Fatigue Life at TDP (Years)				
D_B (m)	D_S=120m	D_S =162m	D_S =208m	D_S =254m	D_S =300m
67.0	3407	6086	5781	4404	3448
100.0	8513	7459	6387	5712	5277
140.0	13603	9738	9901	8474	8415
180.0	15301	13235	14069	12894	12806
220.0	19723	18967	20199	20228	20286

Appendix C7: Analysis Results [SET7]

- Variation of Fatigue Life at TDP against D_B



- Variation of Fatigue Life at TDP against D_s

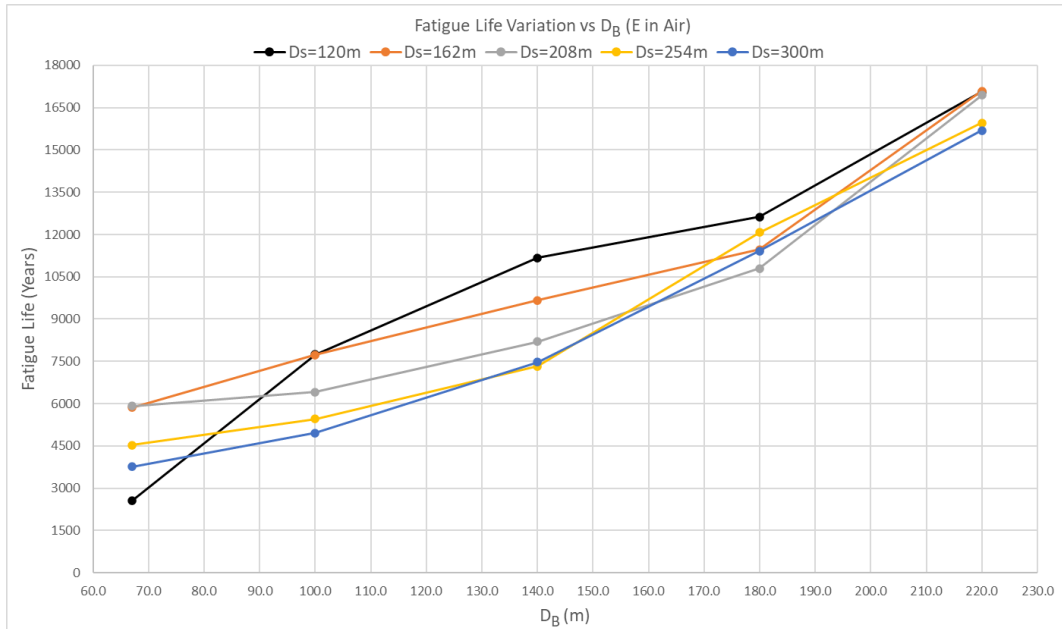


-
- Summary of fatigue life at TDP

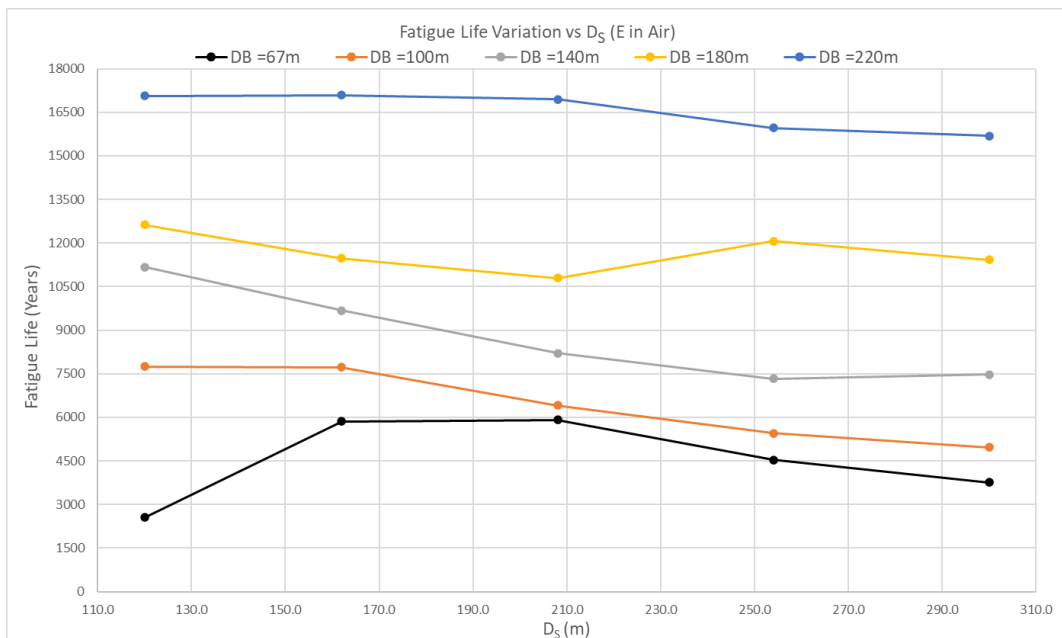
	Fatigue Life at TDP (Years)				
D_B(m)	D_S=120m	D_S =162m	D_S =208m	D_S =254m	D_S =300m
67.0	1673	2211	1730	1330	1362
100.0	2941	2098	1994	1984	2312
140.0	3318	2856	3257	3560	4073
180.0	4164	4627	5638	7081	8616
220.0	5846	6806	8878	12576	14047

Appendix C8: Analysis Results [SET8]

- Variation of Fatigue Life at TDP against D_B



- Variation of Fatigue Life at TDP against D_s

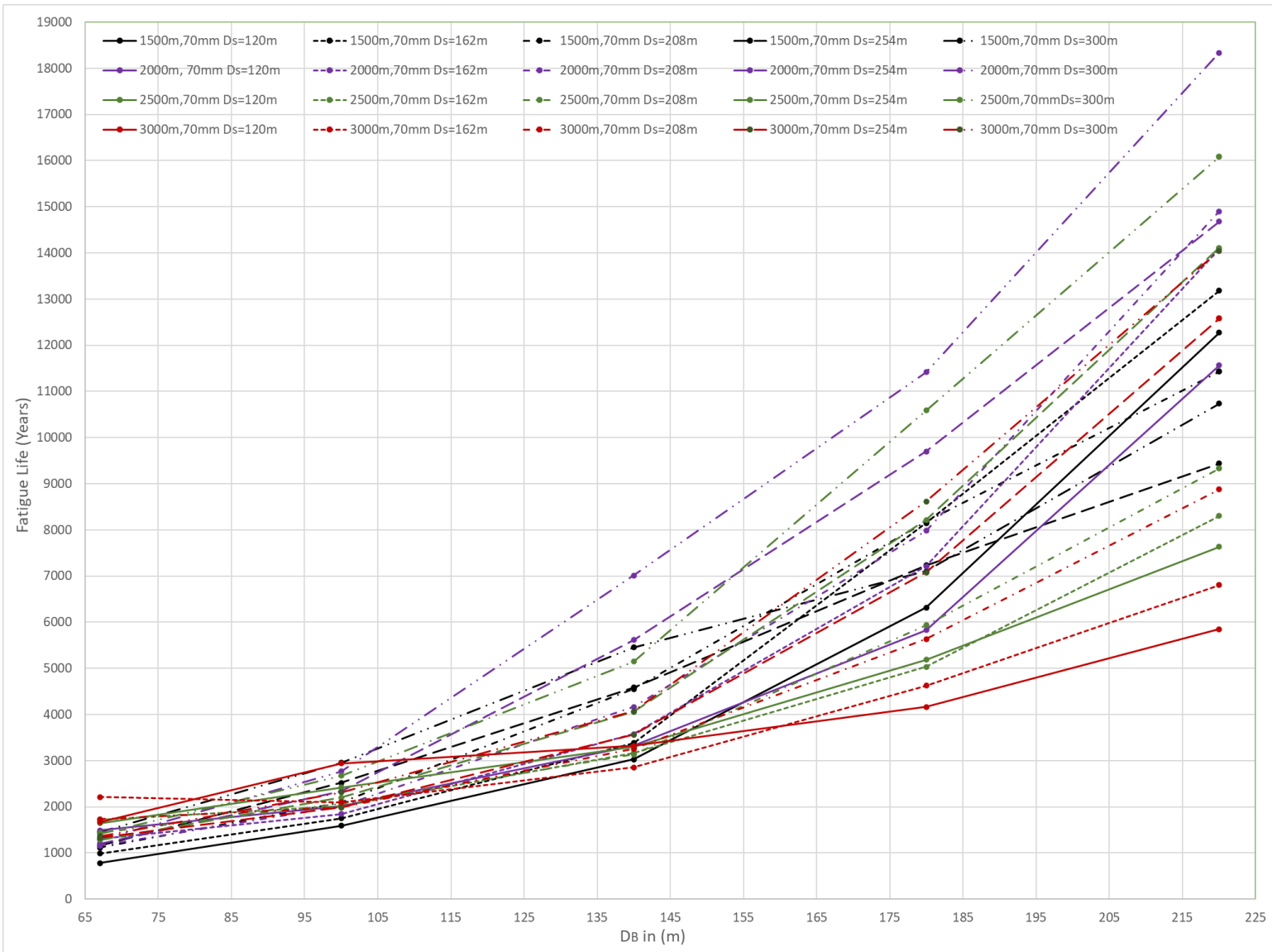


-
- Summary of fatigue life at TDP

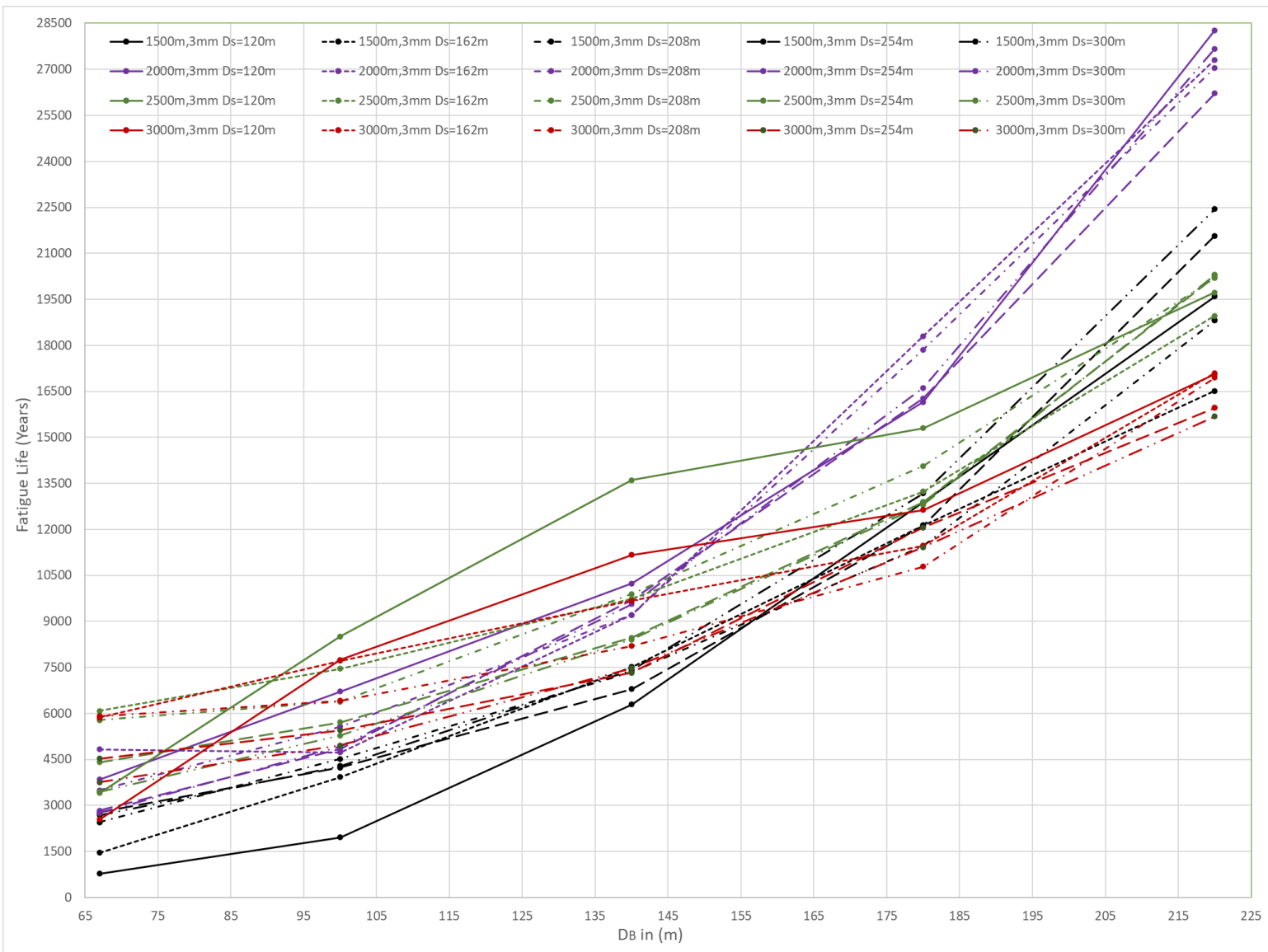
	Fatigue Life at TDP (Years)				
D_B (m)	D_S=120m	D_S =162m	D_S =208m	D_S =254m	D_S =300m
67.0	2546	5862	5914	4527	3761
100.0	7748	7722	6416	5456	4965
140.0	11169	9672	8202	7329	7474
180.0	12631	11469	10794	12068	11420
220.0	17061	17094	16947	15966	15689

Appendix D: Summary of Fatigue Life Variation near TDP (Inner Wall)

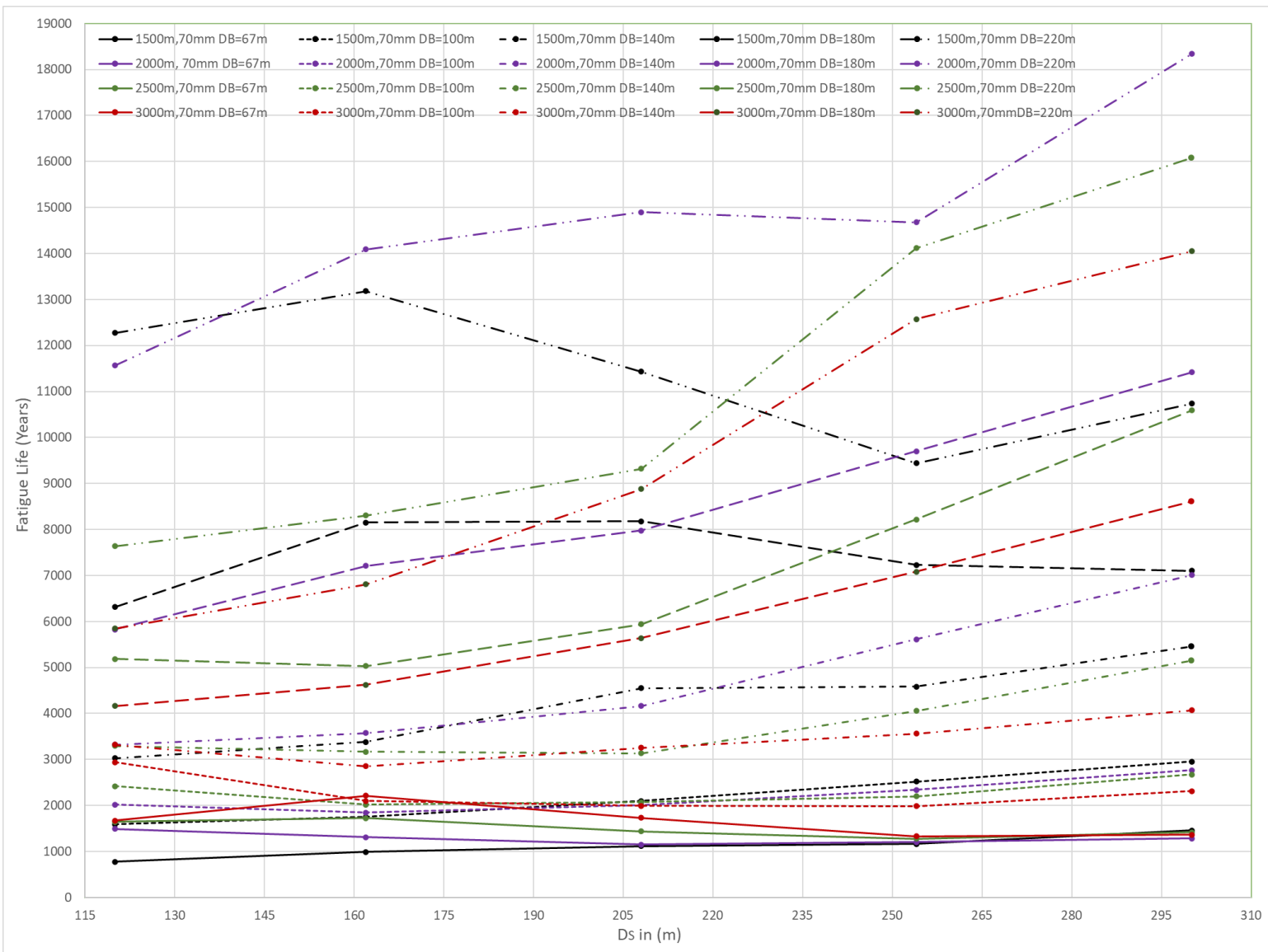
Appendix D1: Fatigue Life Variation Against D_B for 70mm Coating



Appendix D2: Fatigue Life Variation Against D_B for 3mm Coating



Appendix D3: Fatigue Life Variation Against D_s for 70mm Coating



Appendix D4: Fatigue Life Variation Against D_s for 3mm Coating

